Site Directed Immobilization of BMP-2: Two Approaches for the Production of Osteoinductive Scaffolds

Gerichtete Immobilisierung von BMP-2: Zwei Ansätze zur Herstellung osteogener Trägerstrukturen

Doctoral thesis for a doctoral degree
at the Graduate School of Life Sciences,
Julius-Maximilians-Universität Würzburg,
Section Biomedicine

submitted by

Barbara Tabisz

from Leżajsk

Chair of Tissue Engineering and Regenerative Medicine
University Hospital Würzburg

Würzburg 2016

Submitted on:

………………………………………………….……..

Members of the Promotionskomitee:

Chairperson: Prof. Dr. Alexander Buchberger

Primary Supervisor: Prof. Dr. Heike Walles
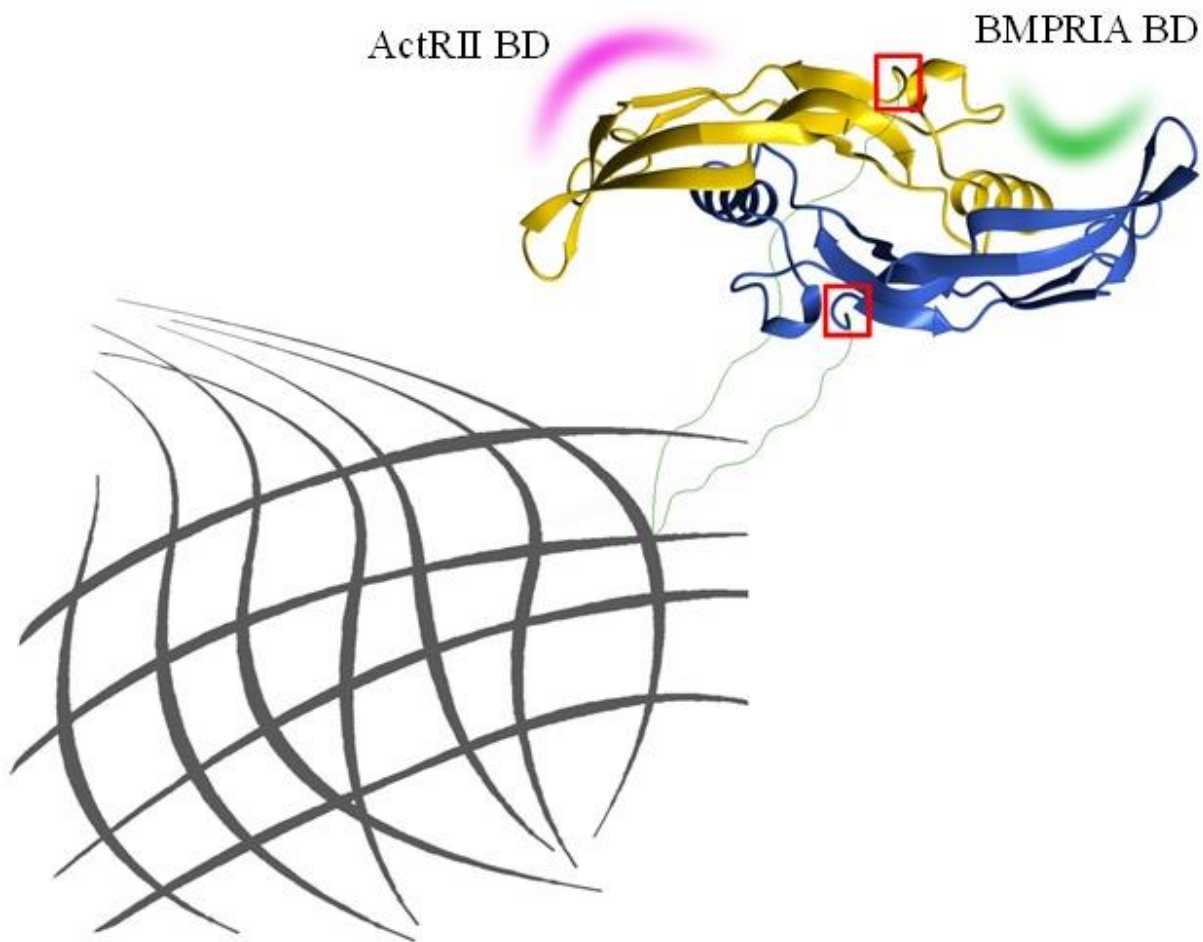
Supervisor (Second): Prof. Dr. Thomas Müller

Supervisor (Third): Dr. Kai Sohn

Supervisor (Fourth): Dr. Joachim Nickel

Date of Public Defence: …………………………………….…………

Date of Receipt of Certificates:

………………………………………….

ActRII BD

BMPRIA BD

List of figures

Abbreviations

AaRS/tRNA	aminoacyl-tRNA-synthetase/tRNA pair
ACDF	anterior cervical discectomy and fusion
ALP	alkaline phosphatase
amber stop codon	TAG stop codon
BCA	bicinchoinic acid
BISC	BMP-induced signaling complex
BMP2-A2C	BMP2 variant containing an extra N-terminal cysteine
BMP2-K3Plk	BMP2 variant containing plk in place of lysin at the 3rd amino acid position
BMP2-wt	wildtype BMP2
BMPRIA (Alk3)	bone morphogenetic protein receptor, type IA
BMPs	bone morphogenetic proteins
C2C12	mouse myoblast cell line
C3H10T1/2	line of C3H mouse embryo cells
CHAPS	3-[(3-Cholamidopropyl)dimethylammonio]-1-propanesulfonate
CHES	2-(Cyclohexylamino)ethanesulfonic acid
CSD	critical-size defect
CuAAC	copper(I)-catalyzed alkyne-azide cycloaddition
DCC	dicyclohexylcarbodiimide
Dlx5	homeobox protein DLX-5
DMEM	Dulbecco's Modified Eagle Medium
DMPA	2,2-Dimethoxy-2-phenylacetophenone
DTT	dithiothreitol
EC50	half maximal effective concentration
EDC	1-ethyl-3-(3-dimethylaminopropyl)carbodiimide hydrochloride
EDTA	ethylenediaminetetraacetic acid
EGF	epidermal growth factor
ESI-MS	elektrospray-Ionisation mass spectrometry
FCS	fetal calf serum

FDA	Food and Drug Administration
FGF-2	fibroblast growth factor 2
FPLC	fast protein liquid chromatography
GSH	glutathione
GSSG	glutathione disulfide
GuHCl	guanidinium chloride
HA	hyaluronic acid
Hey1	hairy/enhancer-of-split related with YRPW motif protein 1
HPLC	high-performance liquid chromatography
IBs	inclusion bodies
Id1-3	DNA-binding protein inhibitor ID-1-3
IEX	ion exchange chromatography
IL-11	interleukin 11
IPTG	isopropyl β-D-1-thiogalactopyranoside
KD	equilibrium dissociation constant
LB	lysogeny broth
MSCs	mesenchymal stem cell
Msx2	homeobox protein MSX-2
MWCO	molecular weight cut-off
NBT/BCIP	combination of nitro-blue tetrazolium chloride and 5-bromo-4-chloro-3'-indolyphosphate p-toluidine salt)
NMWL	Nominal Molecular Weight Limit
Notch	notch (DSL) proteins
OD	optical density
OSM	oncostatin M
Osx	osteoblast-specific transcription factor Osterix
p38/MAPK	mitogen-activated protein kinases
PBS	phosphate-buffered saline
PCL	poly-ε-caprolactone
PEEK	polyetheretherketone
Pen/Strep	penicillin/streptomycin
pET11a-pyrtRNA-BMP2-K3Plk	plamid construct encoding BMP2-K3Plk
PFC	preformed BMP complex

PGE2	prostaglandin E2
PLA	poly(DL-lactic acid)
PLGA	poly(lactic-co-glycolic) acid
Plk	propargyl-lysine
pNPP	para-Nitrophenylphosphate
Pox-cys	poly(2-oxazoline) polymer functionalized with a terminal cysteine
pRSFduet-pyrtRNAsynth	plasmid construct encoding pyrrolysyl tRNA synthetase
Prx2	paired mesoderm homeobox protein 2
PTHrP	parathyroid hormone-related protein
RANK	activator of Nuclear Factor κ B
RANKL	receptor activator of nuclear factor kappa-B ligand
RT	room temperature
RU	resonance units
SDS	sodium dodecyl sulfate
SDS-PAGE	sodium dodecyl sulfate polyacrylamide gel electrophoresis
Snail	zinc finger protein SNAI1
SP HP	sepharose strong cation exchange columns
T7 RNA polymerase	RNA polymerase from the T7 bacteriophage
TB	terrific broth
TCEP	tris(2-carboxyethyl)phosphine
Tcf7	transcription factor 7
TCP	tricalcium phosphate
TFA	trifluoroacetic acid
TGF- β	transforming growth factor β
THPTA	tris(3-hydroxypropyltriazolylmethyl)amine
Tris	tris(hydroxymethyl)aminomethane
VEGF	Vascular Endothelial Growth Factor
WB	Western blot

Abstract

Bone fractures typically heal without surgical intervention. However, pathological situations exist which impede the healing process resulting in so-called non-union fractures. Such fractures are nowadays treated with scaffold material being introduced into the defect area. These scaffolds can be doped with osteogenic factors, such as bone morphogenetic protein (BMP)2. BMP2 belongs to the most osteogenic growth factors known to date. Its medical use, efficiency and safety have been approved by FDA for certain applications. Currently, BMP2 is distributed with a stabilizing scaffold, which is simply soaked with the growth factor. Due to fast release kinetics supraphysiological high doses of BMP2 are required which are causally associated with severe side effects observed in certain applications being most harmful in the area of the cervical spine. These side-effects include inflammation, swelling and breathing problems, leading to disastrous consequences or secondary surgical interventions. Since it could be shown that a retardation of BMP2 release from the scaffold resulted in superior bone forming properties in vivo, it seems obvious to further reduce this release to a minimum. This can be achieved by covalent coupling which in the past was already elaborated using mainly classical EDC/NHS chemistry. Using this technique coupling of the protein occurs non-site-directedly leading mainly to an unpredictable product outcome with variable osteogenic activities. In order to improve the reproducibility of scaffold functionalization by BMP2 we created variants one of which contains a unique unnatural amino acid substitution within the mature polypeptide sequence (BMP2-K3Plk) and another, BMP2-A2C, in which an N-terminal alanine has been substituted by cysteine. These modifications enable site-specific and covalent immobilization of BMP2 e.g. onto polymeric beads. Both proteins were expressed in E. coli, renatured and purified by cation-exchange chromatography. Both variants were extensively analyzed in terms of purity and biological activity which was tested by in vitro interaction analyses as well as in cell based assays. Both proteins could be successfully coupled to polymeric beads. The different BMP2 functionalized beads were shown to interact with the ectodomain of the type I receptor BMPR-IA in vitro indicating that the biological activity of both BMP2 variants retained upon coupling. Both functionalized beads induced osteogenic differentiation C2C12 cells but only of those cells which have been in close contact to the particular beads. This strongly indicates that the BMP2 variant are indeed covalently coupled and not just adsorbed.

We claim that we have developed a system for a site-specific and covalent immobilization of BMP-2 onto solid scaffolds, potentially eliminating the necessity of high-dose scaffold loading. Since immobilized proteins are protected from removal by extracellular fluids, their activities now rely mainly on the half-life of the used scaffold and the rate of proteolytic degradation. Assuming that due to prolonged times much lower loading capacities might be required we propose that the immobilization strategy employed in this work may be further refined and optimized to replace the currently used BMP2-containing medical products.

Zusammenfassung

Knochenbrüche heilen typischerweise ohne die Notwendigkeit chirurgischer Eingriffe. Es gibt jedoch pathologische Situationen, in denen keine Heilung erfolgt was zur Ausbildung sogenannter non-union Frakturen führt. Solche Frakturen werden heutzutage mit Trägermaterialen versorgt, welche in die Defektzonen eingebracht werden. Diese Trägermaterialien können mit osteogen wirkenden Faktoren dotiert sein, z.B. mit bone morphogenetic protein (BMP)2. BMP2 gehört zu den am meisten osteogen wirkenden Faktoren, welche derzeit bekannt sind. Die Nutzung dieses Faktors als Medikament, wurde aufgrund seiner Effizienz und der Sicherheit in der Anwendung von der FDA für bestimmte Anwendungsgebiete zugelassen. Derzeit wird BMP2 mit einer stabilisierenden Trägerstruktur vertrieben, wobei diese einfach mit dem Wachstumsfaktor getränkt wird. Aufgrund schneller Freisetzungskinetiken werden unphysiologisch hohe Mengen von BMP2 gebraucht, welche in Beziehung zu extremen Nebeneffekten gebracht werden, die bei verschiedenen Anwendungen, speziell im Wirbelsäulenbereich, beobachtet werden konnten. Die Nebeneffekte umfassen Endzündungen, einhergehend mit Schwellungen und Atemprobleme, welche weitere Operationen nach sich ziehen können. Da bereits gezeigt werden konnte, dass eine Verzögerung der BMP2 Freisetzung aus der Trägerstruktur eine Verbesserung der osteogenen Wirkung mit sich bringt erscheint es offensichtlich, diese Freisetzung auf ein Minimum zu reduzieren. Dies kann durch kovalente Anbindung erreicht werden, was bereits in der Vergangenheit durch die Verwendung klassischer EDC/NHS Kopplungschemie versucht wurde. Bei dieser Art der Anbindung wird das Protein ungerichtet gekoppelt, was zu unvorhersagbaren Produktqualitäten mit variablen osteogenen Aktivitäten führt.

Um eine Reproduktion solcher Funktionalisierungen mit BMP2 zu ermöglichen wurden zwei BMP-2 Varianten erzeigt, wobei bei einer der Varianten eine Aminosäure im N-terminalen Teil des reifen Proteinteils gegen eine unnatürliche Aminosäure BMP2-Plk), bei der anderen ein Alanin gegen ein Cystein ausgetauscht wurde BMP2-A2C. Durch diesen Austausch wird es möglich, diese Varianten gerichtet an polymere Strukturen anzubinden. Beide Proteine wurden in E. coli exprimiert, renaturiert und mittels Kationenaustausch-Chromatographie aufgereinigt. Die resultierenden Proteinprodukte wurden intensiv bzgl. ihres Reinheitsgrades sowie ihrer biologischen Aktivität überprüft. Letzteres erfolgte sowohl durch In-vitro Interaktions-Analysen als auch durch zellbasierte Untersuchungen. Beide Proteine konnten erfolgreich an polymere Strukturen ("beads") gekoppelt werden. Es konnte gezeigt werden, dass die verschiedenen BMP2 funktionalisierten beads mit isolierten Ektodomänen des BMP

Typ I Rezeptors (BMPR-IA) interagieren. Dies belegt, dass die biologische Aktivität auch nach der Kopplung erhalten bleibt. Die funktionalisierten beads induzieren die osteogene Differenzierung von C2C12 Zellen. Die Differenzierung erfolgt aber nur in jenen Zellen die im direkten Kontakt zu den beads stehen. Dies legt nahe, dass beide BMP2 Varianten wirklich kovalent gekoppelt und nicht nur adsorbiert sind.

Es kann behauptet werden, dass im Rahmen dieser Arbeit ein System entwickelt wurde, durch das eine gerichtete Immobilisierung von BMP2 an solide Oberflächen möglich ist. Dadurch können möglicherweise die notwendigen BMP2 Mengen reduziert werden, da bereits Subnanogram Mengen der gekoppelten BMP2 Varianten Osteogenese auslösen können. Da gekoppelte Proteine nicht durch interstitielle Flüssigkeiten entfernt werden können unterliegt die Fortdauer ihrer biologischen Aktivität der Halbwertszeit des verwendeten Trägermaterials, was durch die verlängerten Wirkzeiten eine Verringerung der verwendeten Wachstumsfaktormenge ermöglicht. Es wird beabsichtigt diese Kopplungsstrategie weiterzuentwickeln um die derzeit am Markt befindlichen BMP2 beinhaltenden Medizinprodukte ersetzen zu können.

I.   Introduction

1. Bone morphology and physical properties

Healthy skeleton plays crucial anatomical and physiological roles in a human organism. It provides a protection for internal organs, support for surrounding tissues, such as muscles and tendons, and builds the scaffold supporting the whole body structure. Therefore mechanical stability and resilience are key features of a healthy skeleton. Bones are composed of trabecular and cortical bone. Trabecular bone, with 50–95% porosity, is present inside of the flat bones and at both apexes of a long bone in the region of the proximal and distal epiphysis, adjacent to articular cartilage. It is a spongy structure harboring red blood marrow, hematopoietic stem cells and blood vessels. On the other hand, cortical bone exhibiting 5-10% of porosity constitutes the outer part of the flat bones and the diaphysis of a long bone, with a medullary cavity in the center. The inner part of the compact cortical bone, as well as cancellous bone is lined with a membranous endosteum, with an outer surface of the cortical bone covered with a fibrous tissue rich in blood vessels, osteoblasts, osteoclasts and nerve fibers, called periosteum (*1*). Bone is also a reservoir for calcium and phosphate ions therefore playing an important role in calcium homeostasis. Mature calcified bone is composed of 70 % hydroxyapatite, 25 % organic matrix, and 5 % water. Bones are constantly exposed to high load and compression forces and are therefore susceptible to injuries and fractures, despite the intrinsic mechanical strength. Therefore, to maintain their stability, highly controlled processes of bone remodeling take place continuously throughout the lifespan of an organism.

2. Regulation of bone remodelling

Bone tissue constantly undergoes complex processes of tissue remodeling in order to remove microstructure damages and thereby maintain right resilience and compression resistance. A multitude of cross-signaling factors is involved in this process to assure the adequate response to internal as well as external stimuli, such as mechanical stimulation or immunological response. A complete cycle of bone remodeling comprising activation phase, bone resorption, matrix production and mineralization takes approximately 12 weeks (*2*). Within this time

osteoblasts, osteoclasts, and osteocytes act together by secreting cross-reactive modulators and chemoattractants. In the first phase of bone remodeling the damaged tissue needs to be resorbed, which is accomplished by osteoclasts, which are recruited from osteoclast precursor cells. (*3*).
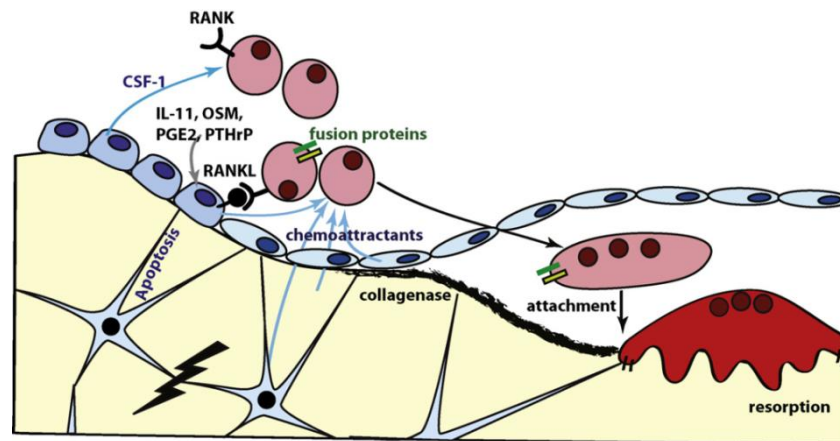
Figure 1: Schematic process of osteoclast formation (*3*)

Legend: cells from the osteoblastic lineage – shades of blue; cells from the osteoclastic lineage – shades of red; osteoclast precursors – round, pink cells, osteoblast – round dark blue cells, lining cells – flat blue cells; resorbing osteoclast – dark blue, osteocytes - star-shaped cells, fusion proteins –green bars; the lightning indicates a bone microdamage. The CSF-1 factor released from osteoblasts stimulates the osteoclast progenitors to proliferation, expression and presention of the RANK receptor on their cell surface. IL-11, OSM, PGE2 and PTHrP present in an extracellular space together with microdamage-triggered apoptotic signals lead to upregulated RANKL expression by osteoblasts. Interaction of RANK and RANKL induce formation of fusion proteins on the surface of osteoclast progenitors, which mediate the attachement of resorbing osteoclast into a bone remodeling unit.

During bone resorption osteoclasts secrete hydrochloric acid (in order to degrade hydroxyapatite crystals) and a range of proteases, such as cathepsin K to cleave collagen and other proteins building bone matrix. In the final step of bone remodeling osteoblasts migrate into the resorbed bone cavity. This process is not completely unraveled, but it is presumed to be triggered by a series of growth factors released from bone matrix that was degraded by osteoclasts in the previous stage. That might include bone morphogenetic proteins (BMPs), transforming growth factor β (TGF- β), or insulin-like growth factor (IGF)-II. After completing matrix deposition osteoblasts differentiate further into bone lining cells or osteocytes embedded within the bone matrix. Mineralization is the final stage of bone remodeling (*4*). Various types of cells participating in the process of bone remodeling are also involved in fracture healing, which is an emergency event, resembling to some extend *de novo* bone formation.

3. Critical-size bone defects

Apart from standard bone fractures that are relatively easily repaired by an organism itself, another group of bone defects, called critical-size (CSD), non-union or non-healing bone defects may occur. They can be defined as the smallest size defect that exhibits no potential for healing throughout the natural life of an individual without an external intervention (*5*) or rather in case of animal studies "the size of a defect that will not heal over the duration of the study". Such defect may arise from surgical procedures, high energy trauma, bone cancer, or osteoporotic deficiencies and fractures. (*6*). In general terms a critical size-defect can be divided into 2 groups: viable and non-viable. Viable defects are characterized by the sufficient blood supply and may arise from improper surgical procedure and weak stabilization of the wound site, resulting in excessive callus formation. Sometimes bone injuries involve striping of periosteum and surrounding tissue resulting in poor or non-existing blood supply. Such defects are called non-viable, and callus formation is not observed in such cases. In the current research several bone segments are mostly studied and they represent bones of the cranium: mandible and calvaria, as well as weight-bearing long bones, such as tibia, fibula and femur. For example calvarial defects have been studied in several animal models, e.g.: rat (4 and 8mm), rabbit (15mm), dog (17 and 20mm), sheep (18-20mm), and primates (15, 25mm) (*7*) 4mm defect was verified to be a critical size for a mouse long bone defect model (*8*). Because of such a great diversity it is of the highest importance to create a proper model of CSD that is standardized, and large enough to eliminate the possibility of any spontaneous healing (*9*).

4. Current clinical treatment of non-healing bone defects

Present treatment options for CSD are fairly limited and possess a considerable number of drawbacks and limitations. A method recognized as a gold standard in modern medicine is an autologous bone grafting, which relies on a resection of a fragment from a healthy bone, mainly from the iliac crest area, and introducing it into a bone-deficient segment. Despite excellent biological compatibility, plenty of disadvantages are related to this approach. The main one is the non-satisfactory success rate, ranging from 60 to 100%, and applicability is limited only to minor volume defects. Other disadvantages involve shortage of available bone

for transplantation, painful convalescence, and morbidity of a donor-site (*10–12*). Another successful technique used to treat large bone defects is called distraction osteogenesis, where 2 bone ends are clumped together to leave only a small gap in between. After the callus is formed within the gap, the space between the ends is stretched to make a place for further bone formation. The quality and vascularization of a newly formed bone is excellent. Nonetheless the procedure is painful, carries a risk of fixation-related infection and is extremely long, demanding from 40 to 50 days to heal a defect of 1 cm in length (*13*). Another alternative used in practical medicine is an allograft or xenograft replacement. Such procedures provide a scaffold and bone-stimulating mineral phase but their use is not completely safe. Bovine bone xenograft under the name CopiOs®Cancellous Particulate Xenograft is already available on the market for over 40 years. But in spite of a good availability of xenografts, a contamination with bacteria and viruses as well as high immunogenicity constitute a real risk, therefore special precautions including sterilization techniques must be obeyed. Nevertheless, even with keeping all the precautions and using acellularized scaffolds, satisfactory screening for viruses is not possible (*14*). As an alternative to biological bone material, synthetic materials, such as bone cement made of methyl methacrylate or tricalcium phosphate are used in surgical procedures. They have however insufficient mechanical or biological properties, such as high brittleness in case of TCA or nonresorbable nature in case of the latter (*13*). Therefore there is a high demand for engineered biocompatible scaffolds, able to induce bone formation without exerting considerable side effects. Here in place come the synthetic scaffolds populated with osteoblastic-like or mesenchymal stem cells as well as materials functionalized with osteogenic growth factors, such as bone morphogenetic protein 2.

5. Role of BMP2 in bone fracture repair

BMPs have been discovered by M. Urist in 1960s, who noticed that demineralized bone matrix was able to stimulate ectopic bone formation in a soft tissue, and he named this presumed active molecule 'bone morphogenetic protein' (*15*). Later it was understood that it was the whole BMP/TGF-β family, rather than only one specific molecule, that was responsible for osteoinductive properties of the demineralized matrix. BMP2 is one of the most studied representatives of the TGF-β family and has been extensively investigated in terms of bone regeneration and fraction repair. Data from multiple in vivo studies show

positive influence of BMP2 on fracture healing (*16–18*). It has been tested, that in C2C12 osteoprogenitor cells a huge range of genes involved in osteogenic differentiation is regulated upon treatment with BMP2. Among them signal transduction genes have been classified as immediate early response, including Smad6, Smad7, OASIS, TIEG, Prx2, Snail and Id1-3. On the other hand intermediate early and late early response genes were shown to be targeted in the process of osteoblastic differentiation. These included Hey1 and Tcf7 transcription factors associated with Notch and Wnt signaling (*19*). In vitro studies with cell lines representing different stages of osteoblastic differentiation showed that among the whole family, BMP-2, BMP-6, and BMP-9 are the most potent osteogenic factors, being the only ones able to induce differentiation in non-committed C3H10 pluripotent cells (*20*). Yet, regardless of the great success of in vivo studies, it is still not completely understood how BMP2 promotes bone regeneration in a mature organism. Tsuji et al (2006) investigated what happens at the fracture site in mice deficient in limb-specific BMP2. The results showed that mutated mice were not able to initiate the regenerative cascade, and periosteum activation did not take place at the fracture site, even when other BMPs, such as BMP4 and BMP7 were still expressed. In spite of available mesenchymal stem cells surrounding the wounded area, no healing events were observed. It shows that BMP2 is an indispensable element of a healing cascade, promoting callus formation and differentiation of certain MSCs species into chondrocyte and osteoblast lineages (*21*). BMPs are essential molecules not only controlling skeleton formation during mammalian development, but they also contribute to bone healing during postnatal life. They transmit their signal via two main mechanisms: the canonical SMAD and non-canonical p38/MAPK pathway, with the latter involved in alkaline phosphatase and osteocalcin expression in osteoblastic cells (*22*). It was shown that C3H10T1/2 cells transformed with an adenoviral vector carrying BMP2 gene promoted mineralization, increased alkaline phosphatase activity, and led to elevated expression levels of bone related markers, like collagen I, osteocalcin, and osteopontin (*23*).

6. BMP2 signaling

The secreted mature Bone morphogenetic protein 2 is a homodimeric protein consisting of 2 subunits of 114 amino acids each. Within its structure four regions have been identified that are responsible for interaction with BMP2 receptors. 2 wrist epitopes are created by both of the BMP2 subunits and show high affinity to BMP type I receptors. The second receptor binding site is called knuckle epitope, which appears within each of the BMP2 subunits, and binds to the so-called type II receptors (*24*). As already mentioned, proteins from a BMP family are paracrine mediators transducing the signal by interaction with two types of transmembrane serine/threonine kinase receptors: type I and type II. There are seven type I and five type II BMP receptors identified to date, out of which BMPRIA (Alk3), BMPRIB (Alk6), BMPRII and ActR-II are the target receptors for BMP2 signaling (*19, 25*). Both, type I and II receptors together are indispensable elements of BMP2 signaling. They possess an extracellular ligand binding domain and an intracellular kinase domain, which is constitutively active for the type II BMP receptor. Upon ligand binding the type II receptor transphosphorylates the type I receptor within its GS-box motif, which is a glycine/serine-rich region situated upstream of the kinase domain. As a result the kinase domain of the type I receptor (L45 loop) further phosphorylates signaling mediators, the so-calle SMAD proteins.(*26*). The mode of BMP receptor oligomerization is highly flexible. Pre-existing heteromeric complexes of BR-II/BR-Ia, BR-II/BR-Ib and BR-Ia/BR-Ib, as well as homomeric BR-II/BR-II, BR-Ia/ BR-Ia, BR-Ib/ BR-Ib have been detected in the absence of the BMP ligand (*27*). There is evidence that depending on the mode of receptor assembly different signaling pathways are addressed. There are at least two possibilities how BMP2 initiates the signaling cascade. In the first scenario BMP2 ligand interacts with a type I receptor, upon which type II receptor gets recruited into the complex and phosphorylates the type I receptor. In this event cascade the non-canonical pathway is activated resulting in the induction of ALP via p38/MAPK (*28*). In the second scenario already preformed heteromeric complexes of both type I and type II receptors capture the BMP2 ligand on the cell surface, which activates the complex by promoting its conformational changes leading to sequential phosphorylation events and the canonical smad-dependent signaling.
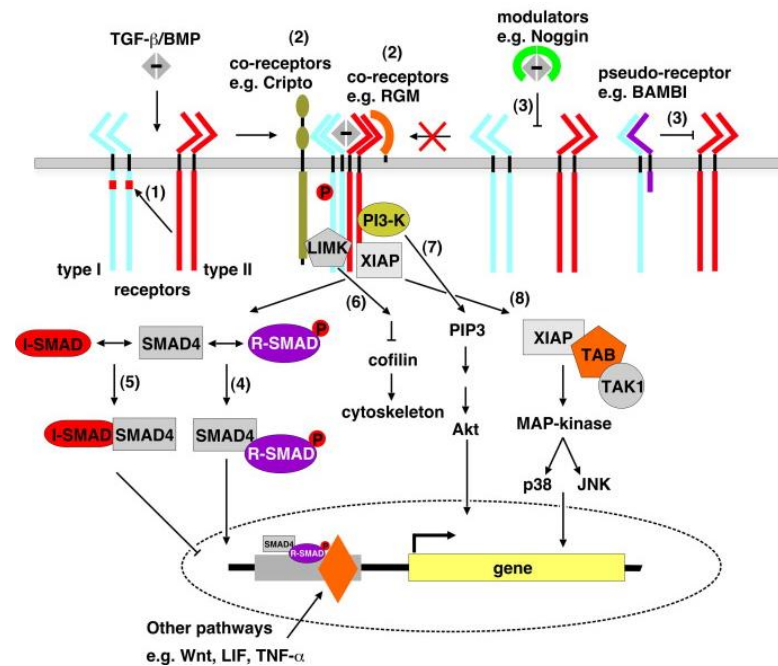
Figure 2: Signaling cascade of bone morphogenetic proteins. (*29*)

BMP2 binds to type I and type II receptors embedded in the cell membrane of responsive cells. Upon binding the type II receptor transphosphorylates the type I receptor thus activating the kinase activity of the type I receptor - marked by a red box (1). Other transmembrane receptors or proteins might modulate the BMP binding (2,3). The activated type I receptor further phosphorylates R-SMAD molecules which in complex with co-SMAD4 molecules are transported into the nucleus regulating the gene expression (4). Inhibitory SMADs negatively regulate BMP signaling by complex formation with co-SMAD4 (5). Apart from the described canonical SMAD-dependent BMP2 pathway members of other signaling cascades are also involved in binding to TGFb/BMP receptors (6,7,8).

Phosphorylated R-smads in complex with Co-smad (smad 4) are translocated into the nucleus, where they interact with series of transcription factors, such as Osterix (Osx), core binding factor alpha 1 (Runx2/Cbfa1), Homeobox protein (Msx2), and Homeobox protein DLX-5 (Dlx5) which in turn mediate the transcription of corresponding genes to induce osteogenesis (*24*). There are also differences in the way that these receptor complexes are internalized upon ligand binding. In case of the BMP-induced signaling complex (BISC) internalization via caveolae takes place, while oligomerization via preformed complexes (PFC) triggers Clathrin-dependent internalization (*26*).
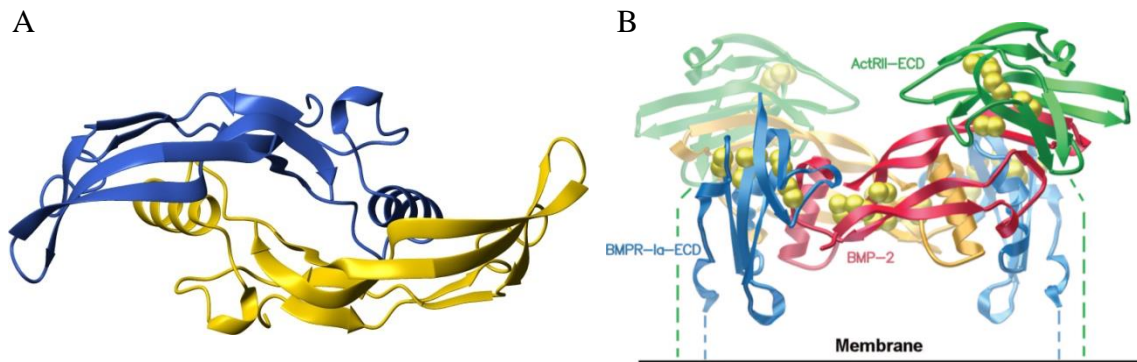
Figure 3: Ribbon representation of the BMP2 structure

(A) BMP2 dimer (each monomer depicted as blue or yellow), (B) ternary signaling complex of BMP2 (both subunits shown in orange and red), BMPRIA ectodomain (BMPR-Ia-ECD) shown in blue, and ActRII ectodomain (ActRII-EDC) shown in green. Cystine residues are presented as yellow spheres. C-termini connecting the receptors with the cell membrane are shown as dashed lines (*25*).

7. Clinical use of BMP2

Despite positive outcome from multiple animal trials that examined various BMP2 carriers to treat critical bone defects (*30–36*) there is only a limited choice of BMP2-functionalized constructs available for surgical procedures. Already in 2002 a construct comprising of titanium mesh and demineralized bone matrix reconstituted with naturally derived BMPs was implanted in segmental mandibular bone defects of 6 patients. In 2 out of 6 cases treated with the BMP2 device there was an evident bone formation examined by histological evaluation (*37*). Nevertheless positive clinical outcome was achieved only for collagen-based BMP2 devices. There is only one series of FDA-approved medical products containing BMP2 as an active agent for the use in surgical procedures. They all have been developed by Medtronic and are based on a scaffold manufactured of bovine collagen I soaked with recombinant hBMP2 at a concentration of 1.5 mg/mL. Induct Os® BMP2 bone grafts have been approved by the European Medicines Agency (EMEA) for single level lumbar interbody spine fusion and treatment of acute tibia fractures (*38*). Subtypes of bone grafts under the name 'INFUSE®' have been approved by the FDA for medical use in humans in 2002 for exclusive treatment of acute, open tibial shaft fractures, degenerative disc disease at single level L2-S1 in skeletally mature patients, as well as for sinus and alveolar ridge augmentations for defects associated with extraction sockets (*39*). Because safety of these products was approved only

for the use in the four cases described above, applications other than that are left to surgeons' discretion. There are several case reports showing adverse clinical consequences related to off-label use of INFUSE® Bone Graft devices. They mainly concern extensive swelling and edema developed at the implantation site. A Medtronic implant used in a 2-year-old boy in a bone defect created as a consequence of craniosynostosis-correcting surgery caused an ubnormal and progressive swelling extended across the patient's face till the anterior cervical region. This state was maintained until the implant was removed at day 10 after implantation (*40*). Another case of complications after an anterior cervical discectomy and fusion (ACDF) surgery was described by Perri et al (2007). After treatment with rhBMP2 a 54-year male patient developed massive neck swelling spreading to pharyngeal tissue and difficulty with swallowing at the 5th postoperative day (*41*). In an independent, retrospective clinical record review a cervical spine fusion procedure using a BMP2-soaked collagen sponge was investigated on 69 patients. 27.5% of the patients subjected to the surgery had significant swelling problems compared to 3.6% in the non-rhBMP-2 group (*42*). In response to multiple reports concerning severe complications after use of BMP-2 implants in the region of cervical spine, the FDA issued a warning note to healthcare practitioners about life-threatening complications, such as swelling of throat and neck tissues occurring mostly between 2nd and 14th day after implantation. Swelling is especially dangerous complication in the region of cervical spine because of proximity of an airway structures, and it has been reported to result in difficulty in swallowing, speaking and breathing (*43*). BMP2-soaked collagen sponge has also been used for treatment of continuous mandibular defects. In the study of Carter et al (2008) closing of the defect was observed in 3 out of 5 patients, with the longest follow-up of 22 months after the surgery. In 4 out 5 patients subjected to the procedure significantly more swelling was observed, compared to the standard reconstruction using autologous bone transplant (*44*). Some attempts were made to treat posterior cervical spine with BMP2 because it was suspected that anterior airway structures might not be affected by this procedure. A retrospective evaluation of 204 patients that underwent posterior spinal fusion augmentation indeed had a significantly increased fusion rate. However the highest rate of recurrent neck pain was also observed in patients treated with BMP2 (*45*). The study comparing BMP2 device versus autograft in Posterior Lumbar Interbody Fusion (PLIF) procedure showed heterotopic bone formation in the central canal in 20.8% of the patients treated with BMP-2 compared to 8.3% of patients undergoing and autograft procedure (*46*). The nature of the above side effects is not certainly known, but it might be assumed that the supraphysiological doses of BMP2 and its free diffusion to neighbour tissues might be a

reason for undesired reactions towards BMP2 implants used in all those procedures. There are areas in the body responding well to collagen BMP2 implants, as it is observed in lumbar spine fusion, tibia, or cleft reconstruction, however, there is also a need for new, more advanced and controllable BMP2 constructs that could be used in neuralgic structures of the body, eg. cervical spine.

8. BMP2 delivery strategies

As described before, present techniques applied in clinics for treatment of non-healing bone defects do not bring satisfactory results. Auto- or xenograft replacements carry certain side effects that restrict their safe use in patients. Therefore new polymer materials functionalized with osteoinductive growth factors are being constantly developed to support orthopedic surgeons. The most promising osteoinductive growth factor seems to be BMP2. Considering limited applicability of BMP2 implants available on the market, more efficient and safer delivery strategies need to be developed. A proper implantation material and sustained delivery into a resected bone area are the main challenges in treatment of critical size bone defects, as BMP2 directly injected into the blood stream is rapidly cleared from the body within minutes (6.7 min. in non-human primates) (*47*). Modern carrier materials need to be able to capture BMP2 molecules for a long period of time without affecting its biological activity, and at the same time without promoting an initial burst release, which is a commonly encountered phenomenon. Therefore, various immobilization strategies, composites, polymers and biological scaffolds have been developed during the last years in order to optimize the healing process of bone.

8.1 Physical adsorption

A frequently used BMP2 delivery approach in vivo is physical adsorption onto natural or synthetic scaffolds. Such technique is easy to perform, does not require any special scaffold functionalization or protein modification. Yet, a major disadvantage of this approach is random protein immobilization compromising its biological activity. One of the main concerns in case of adsorption is the uncontrolled protein release rate, with a high initial burst release occurring in vast majority of cases (*48–51*). Initial burst release is considered an undesired phenomenon, because bone requires long time to regenerate and therefore extended

exposure towards osteoinductive growth factors is preferred. High doses of applied BMP2 entail also a series of side effects which are detrimental for the healing process and in certain cases for well-being and life of patients. Various scaffold materials have been tested as BMP2 carriers with hydroxyapatite/β-tricalcium phosphate (*52*) being well accepted in clinical environment. It has been shown in a small clinical evaluation that grafts composed only of combined hydroxyapatite and β-tricalcium phosphate effectively support regeneration of intrabony periodontal defects (*53*).
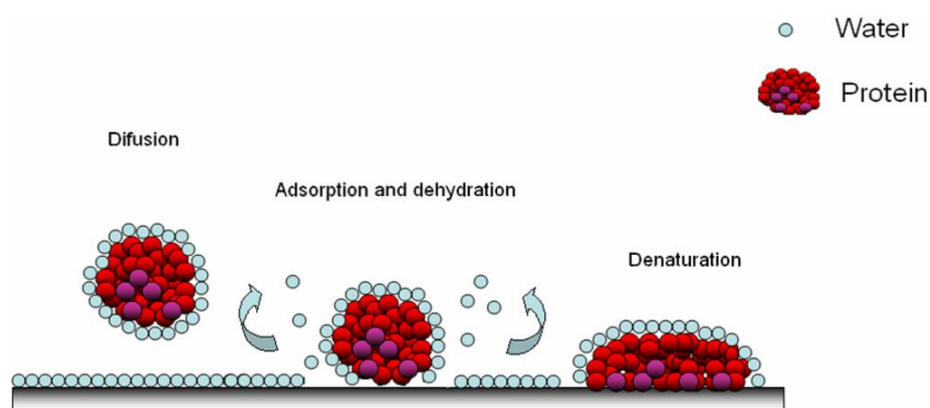
Figure 4: Adsorption of biomolecules to a polymeric material (*54*)
Proteins may interact with surfaces through hydrophilic or hydrophobic residues depending on the characteristics of the surface. While interacting with hydrophobic surfaces a protein undergoes unfolding by release of the water molecules and spreading the hydrophobic residues onto the surface. This process minimizes the area of the hydrophobic core of the protein in the solvent. On the other hand hydrophilic surfaces interact with proteins via polar residues. In this scenario the tendency of irreversible protein unfolding is lower as the hydration of both components is favorable.

A study of Maus et al showed that addition of BMP2 to tricalcium phosphate scaffold in the bovine distal femoral epiphysis led to healing efficiency comparable to autologous graft, whereas remodeling rate was even higher for TCP-BMP2 scaffolds than for the autograft (*55*). In this approach BMP2 was added to TCP during the mixing process instead of soaking, thereby authors speculated that the protein was evenly distributed and slowly released in the course of scaffold degradation. Delivery of BMP2 on titanium implants coated with graphene oxide was proposed for treatment of calvarial defects. In the animal study the implant was introduced into mouse calvaria and showed an improved healing in comparison to uncoated titanium implants. Nonetheless, again a burst release in first several days was observed in uncoated and, to a lesser extent, coated scaffold. BMP2 has also been delivered to cells in vitro on nanodiamonds particles. Coated nanodiamonds were able to induce differentiation of C2C12 cells, but a burst release was observed within the first 2 hours in buffers of different

pH (*56*). Adsorption of BMP2 on poly-ε-caprolactone (PCL) surfaces also resulted in successful differentiation of C2C12 cells and ectopic bone formation when implanted subcutaneously into a mouse back.
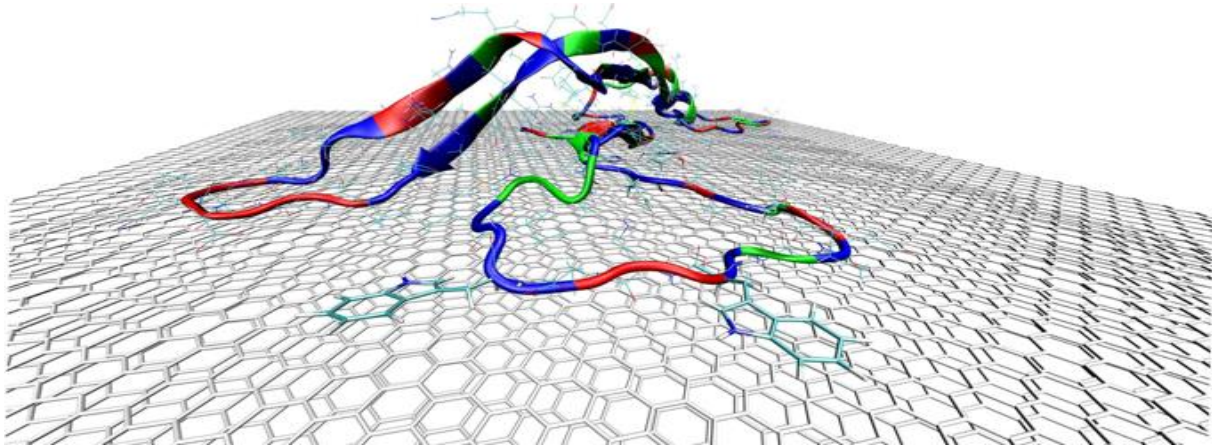
Figure 5: Adsorption of BMP-2 to a hydrophobic graphite surface (*57*)
Nonpolar residues are shown in blue, neutral residues in green and polar residues in red. The N-terminus is shown in yellow and C-terminus in orange.

As in previously described examples, also here a high initial release was observed within the first 3 days. On the other hand PCL scaffolds functionalized with BMP2 by chemical crosslinking showed no alkaline phosphatase induction, which means that the covalently and randomly immobilized BMP2 lost its biological activity or its bioavailability was greatly reduced (*58*). Adsorption of recombinant BMP2 on collagen sponges is widely accepted among clinicians, as it has been approved by drug-controlling agencies in Europe and USA. It has been shown already in late 90' that BMP2 adsorbed on a collagen sponge triggered superior healing scores in a goat tibia compared to all control groups, which was characterized by increased in torsional toughness, significantly tougher callus and increased total callus new bone volume (*59*). Yet, it has been demonstrated later, that collagen sponge also promotes high release rates within several first days after adsorption (*60*). One of the most successful release kinetics has been achieved by physisorption of BMP2 to surfaces coated with oxygen-terminated nanocrystalline diamond particles. In this approach BMP2 was shown to be desorbed with stable exponential kinetics with fully preserved bioactivity (*61*). BMP2 immobilized on these crystalline nanodiamonds triggered differentiation of human mesenchymal stem cells and showed good results in the in vivo experiment. Titanium dental implants coated with nanodiamonds and BMP2 were shown to achieve good osseointegration when implanted into sheep calvaria. Along with these results new bone formation was

detected 4 weeks after surgery, however bone formation was also achieved in all control groups (*62*). BMP2 has also been immobilized by electrostatic interactions between the protein and the scaffold. For instance polycaprolactone (PCL) fibers were modified with poly-acrylic acid using a γ-ray irradiation technique. In this approach positively charged BMP-2 molecules formed a complex with the highly negative poly-acrylic acid. Such functionalized scaffolds showed sustained BMP-2 release over 28-days and were able to induce osteogenic differentiation of MG-63 cells (*63*). The crosslinking and irradiation of PCL fibers were performed before complexation with BMP2, therefore the authors claimed that the bioactivity of BMP2 should not be affected by this process.

8.2 Encapsulation

Encapsulation of growth factors within a polymeric matrix or microspheres is a popular alternative for drug delivery because of the manufacture ease, high loading capacity, and responsiveness to environmental conditions, such as temperature or pH. The release kinetic of encapsulated drugs depends strongly on the properties of a polymer, its porosity and degradability. The release might be achieved either by the diffusion from a porous structure or as a result of partial scaffold degradation (*64*). The disadvantages of this approach are harsh conditions used for the polymer manufacture, which may lead to loss of protein bioactivity. Lots of different polymers have been tested as a carrier system for BMP2, such as PLGA microspheres (*65*), poly(DL-lactic acid) (PLA) scaffold (*66*), gelatin microspheres (*67*), chitosan/chondrotin sulfate nanoparticles (CHI/CS NPs) (*68*). When BMP-2 has been encapsulated within a poly(DL-lactic acid) (PLA) scaffold, the mix of the protein and the PLA polymer was subjected to hight pressure and 35°C in order to achieve a porous structure. No experiment was performed in order to estimate how the manufacture process influenced BMP2 bioactivity. BMP2 release from gelatin microspheres strongly depends on activity of matrix metalloproteinases and is minimal in absence of collagenase. On the other hand addition of gelatin-degrading enzymes leads again to high initial burst releases (*67*).

8.3 Affinity interactions

In order to improve release kinetics of BMP2 physically adsorbed on biological implants, various surface functionalization techniques have been utilized. Interaction of BMP2 with

glycosaminoglycans, mainly heparin, is studied at most. The N-terminal region of the mature part of BMP2 is rich in lysines and arginines which constitute a heparin binding site that is responsible for affinity interaction between BMP2 and heparin/heparan sulfates (*69*). Because affinity interactions are stronger than physical adsorption it has been proposed that scaffolds functionalized with heparin would assure controlled continuous release of BMP2. When osteoblast cells were exposed to heparinized-chitosan scaffolds, expression of osteopontin and osteocalcin was upregulated, and ALP activity as well as calcium deposition where significantly increased, but BMP2 release curves revealed a profile characteristic for the initial bulk release within the first 5 days (*70*). Tricalcium phosphate/hydroxyapatite granules have also been coated with heparin-functionalized collagen in order to provide long-term BMP2 delivery (*71*). However, when 10μg BMP2 was delivered in collagen sponges filled with heparin-conjugated fibrin there was no bone formation observed in response to posterolateral lumbar fusion in rabbits (*72*). These results are in contrast to previous investigation, where 50μg of BMP2 was used (*73*). Another example of heparin use is a biohybrid hydrogel consisting of star-shaped poly(ethylene-glycol) (starPEG) and heparin. Here, the starPEG polymer provides the mechanical stability of the scaffold, whereas heparin guarantees immobilization of growth factors via affinity interactions (*74*). Also, polycaprolactone/poly(lactic-co-glycolic acid) (PCL/PLGA) scaffolds functionalized with heparin–dopamine and conjugated with bone morphogenic protein-2 (BMP-2) were shown to promote differentiation of osteoblast-like MG-63 cells as well as in vivo bone formation in rat femur defect (*75*). Apart from polymer materials, also titanium implants have been modified, by covalent conjugation of heparin. In the study of Kim et al (2014) titanium implants were first functionalized with propargyl groups, then by click reaction with 2-azidoethanamine reactive amine groups were attached, and heparin was conjugated by condensation reaction with formation of amide bonds (*76*). Conjugation of BMP2 can also be achieved using the strong affinity interaction between avidin and biotin. In the study of Hauff et al biotinylated BMP2 has been immobilized onto microcontact printed biotinylated fibronectin via a NeutrAvidin cross-linker. Fibronectin, which is a component of the extracellular matrix, interacts with cells via a RGD peptide motif. According to the authors, a combination of immobilized BMP2 with matrix proteins could provide a suitable tool to study the signaling pathways and crosstalks involved in cellular behaviour, such as migration and adhesion. Along with predictions, immobilized BMP2 was able to induce SMAD 1/5/8-dependent signaling in C2C12 cells, which means that its bioactivity in an immobilized state has been preserved (*77*). Another option to couple growth factors is introduction of fusion affinity tags

at the N or C terminus of the protein sequence. However, such modification might lower the bioactivity of a growth factor when the tag is introduced in the proximity of the active sites, or in case of proteins containing cysteine bridges a tag might hinder their refolding capability. Jennissen et al (2007) introduced a poly-tyrosine tag at the N-terminus of BMP2. Terminal tyrosines might be then chemically transformed into dihydroxy phenylalanine (DOPA) which can be bound with a high affinity to titanium dioxide surface. Nevertheless, the modified BMP2 showed lower bioactivity in cell-based alkaline phosphatase assays in comparison to the wild type protein, even without further chemical modification of the tyrosines (*78*).

8.4 Covalent coupling: site-directed vs random immobilization

Proteins and peptides are composed of amino acids that are joined together by the amide bonds. Whereas each amino acid contains at least one carboxylic group and an amine group they all participate in the condensation reaction forming intermolecular peptide bonds (except for the N-terminal amine group and C-terminal carboxylic group). Therefore, reactivity of the protein is determined mainly by the chemical composition of its side chains. A lysine residue carries a free primary amine group, whereas acidic amino acids, such as aspartic acid and glutamic acid contain a free carboxylic group. Another functional group present within a cysteine residue is a sulfhydryl (-SH) group. These functional moieties are largely exploited in protein crosslinking or immobilization strategies.
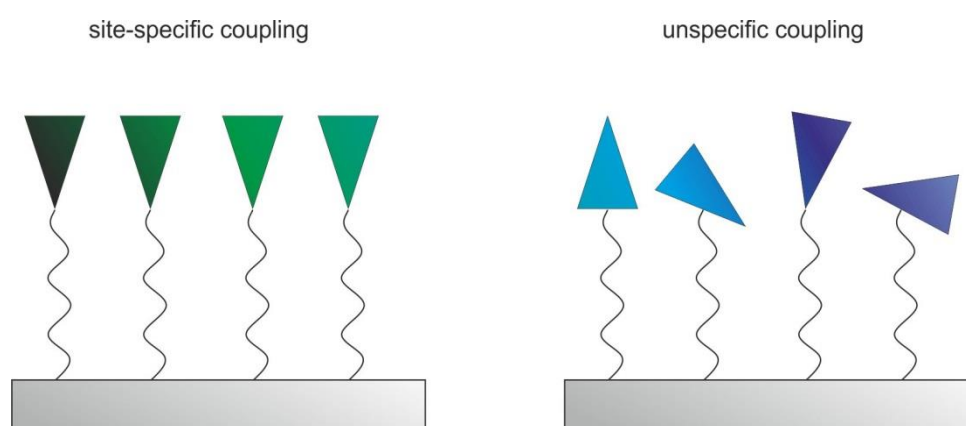
Figure 6: Schematic illustration of site-specific versus unspecific covalent coupling

Site-specific covalent coupling allows targeting of selected residues resulting in homogenous conformation of protein within the scaffold. Unspecific coupling results in random protein distribution within the scaffold and may affect accessibility of the biomolecule towards cognate receptors. Legend: grey rectangulars represent a scaffold, a grey wavy line represents a linker, and green and blue triangles represent biomolecules in different configurations.

Crosslinking using N-Hydroxysuccinimide esters (NHS reagent) is an efficient and robust strategy for protein immobilization by reacting with the protein primary amines in slightly alkaline conditions. The disadvantage of this approach is however the fact, that the reaction may decrease the biological activity of a protein, e.g. by targeting moieties involved in receptor- or ligand- binding sites. One of the most common reagents used for non-specific protein immobilization on carboxylated surfaces are EDC (1-ethyl-3-(3-dimethylaminopropyl)carbodiimide hydrochloride) or DCC (dicyclohexylcarbodiimide), depending on the solubility preferences. These reagents catalyze spontaneous condensation reaction with the primary amines, without being incorporated in the final amide bond. The disadvantage of this reaction is the susceptibility of a protein to form polymeric structures, as protein primary amines start to react spontaneously not only with the scaffold, but also with carboxylic groups present within the same macromolecule. Such an approach was employed for immobilization of BMP2 on hyaluronic acid-modified poly(ε-caprolactone) (HA-PCL) scaffolds or covalent linking to antibacterial carboxymethyl chitosan-coated titanium implants. (*79*), where immobilized BMP2 was able to enhance calcium mineralization and alkaline phosphatase activity in human bone marrow mesenchymal stem cells. Similarly, using NHS/EDC chemistry BMP2 was immobilized on collagen-coated polyetheretherketone (PEEK) implants for prospective spinal surgery applications (*80*) and BMP4 on titanium implants previously functionalized with carboxyl or amine reactive groups (*81*).

It has to be noted, that no site-specific covalent coupling has been achieved to date for bone morphogenetic proteins. Most of the strategies used for immobilization of BMP2 base on non-specific covalent coupling or physical adsorption. Recent discoveries in the field of genetic code expansion opened a ground for introducing orthogonal and specific chemistry into a BMP2 structure providing a possibility of controlled site-specific and covalent immobilization. Here into play comes a range of chemically synthetized artificial amino acids, which can be directly incorporated into a polypeptide sequence by genetic codon expansion.

9. Aim of the study

Based on a common observation made in a vast number of studies we conclude, that BMPs need to be presented to surrounding tissues over a longer period of time in sufficiently high concentrations which is difficult to achieve with the known application methods. One of the strategies that may provide a sustained presentation of BMP2 is its covalent immobilization. Currently, there is no medical device containing covalently immobilized BMP2 available on the market. Therefore in herein work we aimed to establish the BMP2-A2C variant containing an extra N-terminal cysteine and the BMP2-K3Plk variant generated by genetic codon expansion that would be site-specifically and covalently immobilized on a solid scaffold. We hypothesize that covalent binding would overcome the side effects associated with physical adsorption by eliminating the initial burst release. Additionally, site-specific binding achieved through introduction of orthogonal chemical groups within an unnatural amino acid would enable highly controllable and directed saturation of an implant.

II.   Material and methods

1.   BMP2-A2C

1.1   Expression of the BMP2-A2C variant

JM109(DE3) competent bacteria were transformed with pET28-A2C plasmid (kindly provided by Prof. Dr. Thomas Müller) and incubated overnight at 37°C. A single colony was transferred to LB medium supplemented with 50µg/ml kanamycin, incubated for 8 h, and transferred into an overnight LB culture (50µg/ml kanamycin). On the next day bacteria were split 1:20 into a fresh TB medium supplemented with 30µg/ml kanamycin and incubated till OD 0.7 was reached. At OD 0.7 cultures were induced by addition of 1mM IPTG and incubated for 3 hours with shaking (200rpm). Cultures were centrifuged, supernatant discarded and pellets were frozen at -20°C for further procedures.

1.2   Purification of BMP2-A2C monomers from inclusion bodies

Bacterial pellets were subjected to 3 cycles of sonication (10min. with: 40sec. Puls,20sec. break and 30% amplitude) in STE buffer (10mM Tris pH=8.0; 150mM NaCL; 1mM EDTA; 375mM Saccarose; freshly added 1/1000 β-mercaptoethanol) using Branson Digital Sonifier 250 and 3 cycles of centrifugation in order to obtain inclusion bodies. IBs were resuspended with benzonase buffer (100mM Tris pH=7.1; 1mM EDTA; 3mM MgCL$_2$ 80U/mL benzonase) and incubated for 1h at RT with stirring. 0.5 volume part of triton buffer (60mMEDTA pH=7.0; 6% (v/v) Triton X-100; 1.5M NaCL) was added and the suspension was further incubated for 20min. at 4°C with stirring. The suspension was further centrifuged for 20min. with 6000rpm at 10°C, pellet resuspended again in TE buffer (100mM Tris pH=7.0; 20mM EDTA), and centrifuged. The pellet was finally resuspended in an extraction buffer (25mM NaAc pH=5.0; 3M GuCl; 1mM DTT) and incubated overnight at 4°C with stirring. Extracts were centrifuged at 25000rpm and concentrated to 20 OD/ml with an Amicon® concentrating cell and 3kDa MWCO membrane.

1.3 Refolding of BMP2-A2C monomers

The concentrated BMP2-A2C monomers were applied dropwise to the refolding buffer (50mM Tris-HCl pH 8.5, 1 M NaCl, 5 mM EDTA, 0.5 M GuHCl, 0.75 M CHES, 2 mM GSH, 1 mM GSSG) with stirring and incubated at RT for 5 days in dark.

1.4 Purification of refolded BMP2-A2C

After 5 days of refolding BMP2-A2C was concentrated in Amicon® Concentrating Cell with Ultrafiltration regenerated cellulose Discs, 10 kDa NMWL (Millipore), and dialyzed to urea buffer (100mM Tris pH 5.5, 300mM NaCl, 5mM EDTA, 6M Urea). The solution was filtered, degassed, and purified by cation-exchange chromatography (BioLogic Duo-Flow Protein Purification System, BIO-RAD) in urea buffer using 5ml SP HP column (GE Healthcare) and linear gradient elution up to 2M NaCl. 2ml IEX fractions were collected and analyzed by SDS-PAGE. Fractions containing dimeric BMP2-K3Plk were combined and dialyzed to 1mM HCl. Dialyzed solution was concentrated in an Amicon® Concentrating Cell with Ultrafiltration regenerated cellulose Discs, 10 kDa NMWL (Millipore), aliquoted, lyophilized, and frozen at -80°C.

1.5 Separation of BMP2-A2C homodimers

1mg of the BMP2-A2C variant in 1mM HCl was supplemented with TFA to a final TFA concentration of 0.1%. Protein was separated on a 4ml Jupiter C4 column (250x4.6mm, 5μm, 300Å) (Phenomenex) using a linear gradient elution up to 100% acetonitril. Fractions of 1ml were collected and analyzed by SDS-PAGE. Buffer A and buffer B were composed of 0.1% TFA in H_2O and 100% acetonitril respectively.

1.6 Western blot analysis of BMP2-A2C

1μg of BMP2-A2C was separated by SDS-PAGE and transferred onto a nitrocellulose membrane using a semi-dry western blot system (Semi-Dry Electroblotter Sedec™,Peqlab). The membrane was blocked with 5% milk, washed with TBST (2.5mM Tris base pH=7.6; 15mM NaCl; 0.1% Tween), and incubated overnight with a primary anti-BMP2 antibody

(Anti-BMP2 antibody - Differentiation marker ab 17885, ABCAM) at a dilution of 1:20 000 at 4°C on a roller mixer. On the following day the membrane was incubated for 1h at RT with a secondary antibody (goat polyclonal secondary antibody to rabbit IgG - H&L HRP ab97051, ABCAM) at a dilution of 1:50 000. Bands were developed using Amersham[TM] ECL[TM] Prime Western Blotting Detection Reagent (GE healthcare). Chemiluminescence was captured with FluorChemQ (Biozym Scientific GmbH) and AlphaView FluorChemQ software.

1.7   Evaluation of biological activity of BMP2-A2C

Myoblast progenitor C2C12 cells were used for osteogenic differentiation. Cells were seeded onto a 96-well plate at a concentration of 10 000 cells/well. Cells were cultured in 100µl of DMEM medium containing 10% FCS and 1% of Pen/Strep. After 12 hours of incubation the medium was replaced with DMEM medium containing 2%FCS and 1% Pen/Strep. BMP2-A2C and BMP2-wt were applied in duplicates at a concentration of 200nM and diluted using log-2 serial dilution. The plate was incubated for 3 days. After incubation the medium was removed, cells lysed with 100µl of lysis buffer (0.1 M Glycin pH 8.5, 1% TritonX-100, 1 mM $MgCl_2$, 1 mM $ZnCl_2$) an incubated at RT on an orbital shaker for 2h. After incubation 100µl of a paranitrophenyl-phosphate solution at a concentration of 2mg/ml in a reaction buffer (0.1 M Glycin pH 8.5, 1 mM $MgCl_2$, 1 mM $ZnCl_2$) was added to all wells and the absorption at 405nm was measured every 5 min. for 0.5h using a Tecan infinite M200 (Tecan Deutschland GmbH) multiplate reader. Dose response curves and the EC50 values were generated in OriginPro9.1G using a logistic model y = A2 + (A1-A2)/(1 + (x/x0)^p).

1.8   Immobilization of BMP2-A2C to iodoacetyl-functionalized acrylamide beads

250µg of BMP2-A2C was dissolved in 20µl of water and reduced with 2 molar eq of TCEP (tris(2-carboxyethyl)phosphine) for 1.5h at RT. UltraLink iodoacetyl resin beads (Thermoscientific) were washed with the reaction buffer. Upon reduction BMP2-A2C was transferred to 470µl of the reaction buffer (50mM Tris pH 8.5, 5mM EDTA, 6M urea), and 10µl of iodoacetyl-activated acrylamide beads were added. The mixture was incubated for 1h at RT. The beads were centrifuged, washed 3 times with the reaction buffer, and blocked with 50mM cysteine solution for 30 min. at RT. The supernatant was discarded, and beads were

thoroughly washed 5 times with HBS_{500} buffer, 5 times with 4M $MgCl_2$, and 5 times with PBS. The supernatant and all washing steps were analyzed by SDS-PAGE. Beads were stored in PBS.

1.9 Visualization of BMP2-A2C coupled to iodoacetyl-functionalized beads

Iodoacetyl-functionalized beads coupled to BMP2-A2C were blocked with 5% milk in TBST buffer for 1h at 4°C, and incubated with a BMP2 specific primary antibody (Anti-BMP2 antibody - Differentiation marker ab 17885, Abcam) (1:20 000) overnight at 4°C. Beads were washed 3 times with TBST (0.1% Tween) and incubated with Donkey Anti-Rabbit IgG H&L (Alexa Fluor® 488) antibody (Abcam, ab150061) (1:1000) for 1h at RT. Beads were washed 3 times with TBST (0.1% Tween) and fluorescence was detected by fluorescence microscopy (Keyence).

1.10 Quantification of BMP2-A2C immobilized to iodoacetyl-functionalized beads

For the quantification of BMP2-A2C covalently immobilized to the iodoacetyl-functionalized acrylamide beads the Pierce™ BCA Protein Assay Kit was used. The BCA assay exploits the reaction between bicinchoninic acid and cuprous cations (Cu+1) that are formed by contact of cupric sulfate with proteins. The coupling reaction was performed in a 2ml reaction volume. The beads were separated using poly-prep® chromatography columns (BioRad) and resuspended with 400µl water prior to measurement. 100µl of beads was transferred to 300µl of the BCA working reagent. The assay was performed in triplicates. Tubes were incubated at 60°C according to the manufacturer's protocol. To calculate the amount of protein coupled to a single bead, the UV/VIS absorption of non-coupled beads at 280nm was subtracted, and normalized to the number of beads applied to the reaction.

1.11 Fluorescent labelling of BMPRIA receptor ectodomain

100µg of BMPRIA receptor ectodomain was incubated with a NHS-activated fluorescent dye Texas Red (lifetechnologies) in a 1:5 molar ratio. Reaction was performed in HBS_{150} buffer (10mM HEPES pH 7.4, 150mM NaCl) at 4°C overnight. Receptor was further dialyzed 5 times against HBS_{150} buffer, 2 times with 4M $MgCl_2$, and 5 times with HBS_{500} buffer.

1.12 Interaction of BMP2-A2C coupled to iodoacetyl-functionalized beads with BMPRIA receptor ectodomain

10µl of beads coupled to BMP2-A2C were incubated with 1µM fluorescent BRIA receptor ectodomain in HBS$_{500}$ buffer for 1h at RT. Beads were washed 5 times with the reaction buffer and visualized using fluorescent microscopy (Keyence).

1.13 Evaluation of osteogenic potential of beads coupled to BMP2-A2C

C2C12 cells were seeded and treated as for verification of BMP2-A2C activity except for cell lysis and pNPP treatment. Additionally, iodoacetyl-activated acrylamide beads coupled to BMP2-A2C were applied to the wells and overlaid with 0.4% of low melting agarose (dissolved in DMEM medium, supplemented with 2%FCS and 1% Pen/Strep after cooling to 37°C) in order to prevent movement of the beads. Upon agarose gelling wells were covered with 50µl of DMEM medium (2% FCS, 1% Pen/Strep). Plates were incubated for 3 days. Medium was removed, 100µl of 1-Step™ NBT/BCIP substrate solution (Thermoscientific) was transferred to all wells, and the plate was incubated in dark at RT for 15 min. Upon colour development the staining solution was removed, replaced with PBS, and plates were analyzed microscopically (Keyence).

2. BMP2-K3Plk

2.1 Cloning of the BMP2-K3Plk variant

Human mature BMP2 (hmBMP2) sequence was amplified from p25N_hmBMP2 vector with a forward primer (5'GA CCA GGA CAT ATG GCT CAA GCC TAG CAC AAA CAG C3') introducing an NdeI restriction site and an amber stop codon (TAG) at the position of the first lysine, and a reversed primer (5'CCA GGA GGA TCC TTA GCG ACA CCC ACA ACC CT3') converting a naturally existing 3' TAG stop codon into TAA stop codon. Pfu polymerase was used for the amplification. Amplification was performed by initial denaturation for 5 min. at 95°C; 30 cycles of denaturation at 95°C for 1 min, 1 min. annealing at 60°C, 1 min. elongation at 72°C, and final extension for 10 min. at 72°C. The PCR product

was purified with Wizard® SV Gel and PCR Clean-Up System (Promega), and digested with the restriction enzyme NdeI (Fermentas) for 45 min. at 37°C. Enzyme was heat inactivated and the reaction was purified with Qiagen PCR purification kit. In the second step PCR product was digested with the restriction enzyme BamHI (Fast Digest, Fermentas) for 1h at 37°C and purified.

pET11a-pyrtRNA vector was double-digested with NdeI and BahmHI enzymes. In the first step the vector was digested with NdeI enzyme for 2h 45min. at 37°C. NdeI enzyme was inactivated for 20min. at 65°C and the vector was purified with Qiagen PCR purification kit. In the second step pET11a vector was digested with BamHI restriction enzyme (Fermentas Fast Digest) for 1h at 37°C and the enzyme was heat inactivated for 5 min. at 80°C. The product was dephosphorylated with Antarctic phosphatase (New England Biolabs), and the enzyme inactivated at 65°C for 10 min. Finally the digested vector was separated by agarose electrophoresis and purified using Promega wizard SV gel and PCR clean-up system.

Digested BMP2-K3TAG was ligated into digested pET11a-pyrtRNA vector using T4 DNA Ligase (ThermoScientific) for 2h at 22°C to generate the final construct pET11a-pyrtRNA-BMP2-K3Plk. Chemically competent NovaBlue cells (Novagen) were transformed with the ligation reaction according to the standard protocol, seeded on ampicillin agar plates (100μg/ml ampicillin), and incubated overnight at 37°C. Transformants were isolated, propagated, and plasmids were isolated using Wizard® Plus SV Minipreps DNA Purification kit (Promega) according to the manufacturer's protocol. Positive clones were identified by restriction digestion, colony PCR, and sequencing. NovaBlue cells were transformed with a plasmid verified by sequencing and propagated. High purity plasmid was isolated using QIAGEN®Plasmid Purification kit.

2.2 Optimization of BMP2-K3Plk protein expression

BL21(DE3)pLysS E.coli strain was initially used as an expression host for BMP2-K3Plk. BL21(DE3)pLysS cells were double transformed with pET11a-pyrtRNA-BMP2-K3Plk and pRSFduet-pyrtRNAsynth (coding for pyrrolysyl-tRNA synthetase), seeded on kanamycin (50μg/ml) /ampicillin (100μg/ml)/chloramphenicol (50μg/ml) plates. Expression efficiency was tested in presence of 1mM propargyl-lysine (Plk) after 3h and overnight in TB medium at 37°C and overnight in LB medium at 27°C. In parallel the amber codon mutation in the final

vector was reversed to the original lysine codon (AAA) by site-directed mutagenesis (QuikChange II Site-Directed Mutagenesis Kit, Agilent) with a forward 5'ATGGCTCAAGCCAAA CACAAACAGCGGAAAC3' and a reversed 5'GTTTCCGCTGTTTGTG TTTGGCTTGAGCCAT3' primer. Expression under standard conditions (3h, 37°C and 1mM IPTG) was performed. In another set-up BL21(DE3) strain was used to test BMP2-K3Plk expression. BL21(DE3) was double transformed with pET11a-pyrtRNA-BMP2-K3Plk and pRSFduet-pyrtRNAsynth (coding for pyrrolysyl-tRNA synthetase), seeded on kanamycin (50µg/ml) /ampicillin (100µg/ml) plates and incubated overnight at 37°C. On the next day several colonies were selected and propagated overnight at 37°C in a LB liquid culture supplemented with antibiotics. On the next day, cultures were transferred into TB liquid medium (1:20) supplemented with pH buffer and antibiotics, and grown till OD_{600} 0.7. To validate optimal concentrations of propargyl-lysine, final concentrations of 1mM, 2mM, 3mM, 4mM, 5mM, 7mM and 10mM of propargyl-lysine in the medium were used. Cultures were induced with 1mM IPTG within the next 30 min. Protein was expressed overnight at 37°C. For large scale expression the same procedure was applied in TB medium with a propargyl-lysine concentration of 10mM. Propargyl-lysine, as well as pET11a-pyrtRNA and pRSFduet-pyrtRNAsynth were kindly provided by prof. Lorenz Meinel from the Chair for Pharmaceutics and Biopharmacy, Institute for Pharmacy and Food Chemistry, University of Würzburg.

2.3 Purification of BMP2-K3Plk from inclusion bodies

Inclusion bodies were prepared as described for the BMP2-A2C variant in section 1.2.

2.4 Purification of BMP2-K3Plk according to Wessel and Flügge

Monomers purified from inclusion bodies were precipitated according to Wessel and Flügge (1984). Briefly, 100µl of the sample was mixed with 400µl of methanol and vortexed. 100µl of chloroform was added and vortexed again. Finally 300 µl of dH_2O deionized water was added, vortexed and centrifuged at 14 000rpm for 5min. Top aqueous phase was discarded, the mixture was supplemented with 800µl of methanol and centrifuged for 10min. at 14 000rpm. The supernatant was removed, and the pellet was air dried, and dissolved in 1mM HCl.

2.5   Evaluation of BMP2-K3Plk by mass spectrometry

To determine the mass of BMP2-K3Plk, monomers purified from inclusion bodies were precipitated according to Wessel and Flügge (1984) and analyzed with electrospray mass spectrometry analysis (ESI-MS). Refolded BMP2 dimers were purified by IEX chromatography and dialyzed to Millipore water prior to measurement. ESI-MS was performed using an APEX-II FT-ICR (Bruker Daltonic GmbH, Bremen) equipped with a 7.4 T magnet and an Apollo ESI ion source in positive mode. Desalted proteins were dissolved in MeOH/H2O/HAc (49.5/49.5/1) at a concentration range of 1 - 5µM. 2µL/min of sample were injected using a Hamilton syringe. Detection range was typically set to 750 - 3000 m/z according to earlier measurements with other BMP variants. The detection range was optimized to the signal containing area afterwards. 256 scans were recorded at a resolution of 256K.

2.6   Verification of BMP2-K3Plk refolding

The protein solution obtained from inclusion bodies was concentrated to 28OD/ml in an Amicon® concentrating cell. Half of the solution was used for the refolding with GSSG:GSH ratio 1:2. The other half was used for the refolding with GSSG:GSH ratio 1:4. The refolding buffer consisted of 50 mM Tris pH 8.0 - 8.2; 2M LiCl; 5 mM EDTA; 25 mM CHAPS; 2 or 4 mM glutathione (GSH), and 1 mM glutathione disulfide (GSSG). Monomers were applied dropwise, and incubated at RT for 5 days in dark. The small scale refolding experiment was performed according to the same procedure, using 1mM GSSG and 2mM GSH.

2.7   Purification of refolded BMP2-K3Plk by cation-exchange chromatography

The pH of the refolding buffer was adjusted to 3.0 using concentrated HCl and proteins were dialyzed to 1mM HCl and concentrated using a QuickStand Benchtop System (Hollow Fiber Cartridge, 5000 NMWC, surface 650cm^2) and further concentrated in an Amicon concentrating cell. The refolding buffer with GSSG to GSH ratio 1: 2 was centrifuged for 0.5 h at 5000 rpm and its composition was adjusted to buffer A (20mM NaAcl; 30% isopropanol), centrifuged for 10 min. at 5000 rpm and applied to the column.

The composition of the refolding buffer with GSSG to GSH ratio 1: 4 was directly adjusted to buffer A, centrifuged for 10 min. at 5000 rpm and loaded on the column. Fractions were eluted using a linear gradient of buffer B (20mM NaAc; 30% isopropanol, 2M NaCl), analyzed by SDS-PAGE, pooled and dialyzed to 1mM HCl.

2.8   Evaluation of BMP2-K3Plk biological activity

Myoblast progenitor C2C12 cells were used as BMP2-responsive cell line. Cells were seeded onto a 96-well plate at a concentration of 10 000 cells/well. Cells were cultured in 100µl of DMEM medium containing 10% FCS and 1% of Pen/Strep. After 12 hours of incubation the medium was replaced with DMEM medium containing 2%FCS and 1% Pen/Strep. BMP2-K3Plk and BMP2-wt were applied in 4 replicates at a concentration of 200nM and diluted using log-2 serial dilution. The plate was incubated for 3 days. After incubation the medium was removed, cells lysed with 100µl of lysis buffer (0,1 M Glycin pH 8.5, 1% TritonX-100, 1 mM $MgCl_2$, 1 mM $ZnCl_2$), and incubated at RT on an orbital shaker for 2h. After incubation 100µl of a paranitrophenyl-phosphate solution at a concentration of 2mg/ml in a reaction buffer (0.1 M Glycin pH 8.5, 1 mM $MgCl_2$, 1 mM $ZnCl_2$) was added to all wells and the absorption at 405nm was measured every 5 min. for 0.5h using a Tecan infinite M200 (Tecan Deutschland GmbH) multiplate reader. Dose response curves and the EC50 values were generated in OriginPro9.1G using a logistic model $y = A2 + (A1-A2)/(1 + (x/x0)^p)$.

2.9   Separation of BMP2-K3Plk using a heparin column

600µg of BMP2-K3Plk and BMP2-wt were loaded onto a FPLC (Akta avant, GE healthcare) heparin column (1ml heparin column HP, GE Healthcare) in buffer A (6M urea, 20mM NaAc, pH 4.5). Fractions were obtained using linear NaCl gradient elution from 0 to 2M.

2.10 SPR analysis using BMPRIA and ActRIIB receptor ectodomains

The ProteOn XPR36 biosensor system (Bio-Rad) was used for all biosensor experiments. Receptor ectodomains were N-biotinylated by incubation with equimolar concentrations of sulfo-NHS-LC-biotin (Pierce, Thermo Scientific, Rockford, IL, USA). The biotinylated receptor ectodomains were immobilized at ~500 resonance units (RU) to streptavidin coated

matrices of biosensor chips. Sensorgrams of ligand receptor interactions were recorded at a flow rate of 25 µl min^{-1} at 25°C. The association and dissociation time was set to 3 min. After each cycle the chips were regenerated with 4M MgCl$_2$ for 1 min. The binding affinities were calculated by fitting the kinetic data to a 1:1 Langmuir binding model. All binding constants were determined from two or more independent experiments using at least six different analyte concentrations. Standard deviations for the obtained affinities are less than 50%.

2.11 Optimization of click reaction conditions

2.11.1 Coupling of BMP2-K3Plk catalyzed by UV irradiation

Poly(2-oxazoline) polymer functionalized terminally with a sulfhydryl group (pox-cys) (0.6 mg, 6 eq) (kindly provided by prof. Jürgen Groll, Department for functional materials in medicine and dentistry University of Würzburg) was dissolved in 100ul 1mM HCl and mixed with BMP2-K3Plk (0.5 mg, 1 eq). Argon was passed through the solution to prevent oxidation of the pox-cys. Then 4,2mg DMPA (2,2-Dimethoxy-2-phenylacetophenone - radical starter) was solved in 10ml MeOH and 10ul of this solution (0.8 eq.) was added to the peptide/polymer solution. The solution was split into 3 parts and treated with UV light of 365nm for: 5 min, 15 min and 30 min. In parallel 0,5mg BMP2-K3Plk was dissolved in 50 µL instead of 100µL of the pox-cys solution, processed as described before and irradiated for 20min. with UV light of 365nm (*82*).

2.11.2 Coupling of BMP2-K3Plk using copper(I)-catalyzed alkyne-azide cycloaddition

2.11.2.1 Coupling of BMP2-K3Plk to azylated poly(2-oxazoline)

BMP2-K3Plk was reacted with a 2.5kDa poly(2-oxazoline) terminally functionalized with an azide group (pox-azide) (kindly provided by prof. Jürgen Groll, Department for functional materials in medicine and dentistry University of Würzburg). Reaction was performed overnight in Millipore water using final BMP2-K3Plk concentration of 76.9µM (1 eq), 2.4 eq pox-azide, 0.5 eq sodium ascorbate, and 0.3 eq CuSO$_4$.

2.11.2.2 Effect of sodium ascorbate and copper(II) sulfate on BMP2-wt

20 µM BMP2-wt in 45µL was incubated overnight at RT in Millipore water with varying ratios of sodium ascorbate to CuSO$_4$. Final concentration of 5mM NaAscorabte was used in

the experiment. Tested ratios of NaAscrobate to $CuSO_4$ were: (50:1); (40:1); (30:1); (20:1); (10:1); (1.7: 1) and (1:1). Samples were analyzed by SDS-PAGE and Coomassie Brilliant Blue staining.

2.11.2.3 Analysis of protective role of THPTA in CuAAC reaction

Reaction was performed in Millipore water for 24h in presence of 5mM NaAscrorbate, 0.10mM $CuSO_4$ and 200µM 3-Azido-7-hydroxycoumarin (baseclick). As a positive control propargyl alcohol, as model alkyne, was used. As negative control the same reaction was performed using wildtype BMP2. Tested ratios of $CuSO_4$ to THPTA were: (1:7); (1:10); (1:12); (1:15); (1:20); (1:10 reaction performed in H2O/tert-BuOH 2 eq : 1 eq). Samples were separated by SDS-PAGE and analyzed by Coomassie brilliant blue staining and fluorescent imaging (excitation 365nm).

2.11.2.4 Coupling of BMP2-K3Plk to biotinylated PEG-linker

Several conditions were tested for the optimal site-specific biotinylation of BMP2-K3Plk. 26µg (20 µM) BMP2-K3Plk was incubated with 200 µM PEG4-carboxamide-6-Azidohexanyl-Biotin (Lifetechnologies) at $37^{\circ}C$ for 15, 30, 45, and 60min. in 50µl of reaction buffer: 0.1M HEPES pH 7.0, 3.7M urea, 50µM $CuSO_4$, 250µM THPTA, 5mM NaAscorbate. As negative control reaction was performed with wildtype BMP2 for 1h. Above reaction conditions were additionally tested at $23^{\circ}C$ for 1, 2, 5, 10, and 15 min. Negative control reaction was performed for 15 min. and Millipore water instead of CuSO4 was used. Reaction was stopped by addition of EDTA to a final concentration of 5mM. Samples were separated by SDS-PAGE and blotted with Semi-Dry Electroblotter Sedec™ (Peqlab). Membrane was incubated with Streptavidin- Alexa Fluor® 488 Conjugate (lifetechnologies) in TBST buffer with 0.1% SDS for 1h at RT, and washed with TBST. The fluorescence was measured with FluorChemQ (Biozym Scientific GmbH).

2.12 Evaluation of CuAAC reaction efficiency

To evaluate the efficiency of the coupling reaction between BMP2-K3Plk and PEG4-carboxamide-6-Azidohexanyl-Biotin biotinylated BMP2-K3Plk was separated from non-biotinylated BMP2-K3Plk by reversed phase HPLC (Hitachi LaCHromUltraTM HPLC system) using the RP C4 column (4.0 mm x 125 mm, Machery-Nagel, Düren, Germany).

Buffer A 0.1% TFA in H_2O, and buffer B 0.1% TFA in 95% acetonitrile were used as a liquid phase. For protein elution a linear gradient from 20% to 100% buffer B was used.

In parallel BMP2-K3Plk was coupled to a fluorescent dye. 260µg of BMP2-K3Plk (20 µM) were incubated with 200 µM of Alexa Fluor® 488 Azide (Thermo Fisher Scientific) in 500µl of reaction buffer (0.1M HEPES pH 7.0, 3.7M Urea, 50µM $CuSO_4$, 250µM THPTA, 5mM NaAscorbate) for 15 min. at RT. Reaction was stopped by addition of EDTA to a final concentration of 5mM. The protein was dialyzed to 6M GuCl using a 10kDa MCWO membrane. The sample was divided into 3 parts and the fluorescence was measured in triplicates. The mean fluorescence values of the dialysis flowthrough were subtracted from the values of experimental samples. The excitation/emission parameters for the fluorescence measurement were set to 495/519nm. For the standard curve a log-2 dilutions of Alexa Fluor® 488 Azide were performed in triplicates starting from 10µM. The standard curve was generated in OriginPro 9.1 using a logistic model y = A2 + (A1-A2)/(1 + (x/x0)^p).

2.13 Immobilization of BMP2-K3Plk to neutravidin-agarose beads

260µg of BMP2-K3Plk (20 µM) were incubated with 200 µM PEG4-carboxamide-6-Azidohexanyl-Biotin (Lifetechnologies) in 500µl of reaction buffer (0.1M HEPES pH 7.0, 3.7M Urea, 50µM $CuSO_4$, 250µM THPTA, 5mM NaAscorbate) for 15 min. at RT with shaking. Reaction was stopped by addition of EDTA to a final concentration of 5mM. As negative control BMP2-wt was used. Biotinylated BMP2-K3Plk and the negative control were dialyzed to 1mM HCl, concentrated, and incubated for 1.5h at RT in 8ml HBS500 buffer (10mM HEPES pH 7.4, 500mM NaCl) with 50ul NeutrAvidin agarose beads (Thermoscientific) previously washed with reaction buffer. After incubation beads were thoroughly washed 5 times with HBS_{500} buffer, 5 times with 4M $MgCl_2$, 5 times with PBS, and stored in 500µl of PBS.

2.14 Direct immobilization of BMP2-K3Plk to azide-functionalized beads

260µg of BMP2-K3Plk (20µM) were incubated with 20µl of azide-functionalized agarose beads (Jena biosciences) in a reaction buffer (0.1M HEPES pH 7.0, 3.9M Urea, 50µM $CuSO_4$, 250µM THPTA, 5mM NaAscorbate) for 2h and 15min. at RT. Reaction was stopped by

addition of EDTA to a final concentration of 5mM. Beads were thoroughly washed 5 times with HBS_{500} buffer, 5 times with 4M $MgCl_2$, 5times with PBS and stored in PBS.

In order to couple BMP2-K3Plk to azide-functionalized silica particles the same conditions as for the agarose beads were used. For that 20mg of azide-functionalized silica particles were resuspended with 194,3µl of Millipore water and 4µl of the beads were used for the 100µl reaction.

2.15 Verification of BMP2-K3Plk immobilized to functionalized beads

In order to visualize BMP2-K3Plk immobilized to azide-functionalized beads and neutravidin agarose beads the beads were blocked with 5% milk in TBST buffer for 1h at 4^oC, and incubated with a BMP2 specific primary antibody (Anti-BMP2 antibody - Differentiation marker ab 17885, Abcam) (1:20 000) overnight at 4^oC. Beads were washed 3 times with TBST (0.1% Tween) and incubated with Donkey Anti-Rabbit IgG H&L (Alexa Fluor® 488) antibody (Abcam, ab150061) (1:1000) for 1h at RT. Beads were washed 3 times with TBST (0.1% Tween) and fluorescence was detected by fluorescence microscopy (Keyence).

2.16 Quantification of BMP2-K3Plk immobilized to neutravidin agarose beads

To evaluate the quantity of BMP2-K3Plk immobilized to NeutrAvidin agarose beads the coupling of BMP2-K3Plk to PEG4-carboxamide-6-Azidohexanyl-Biotin (Lifetechnologies) was performed in the 1,5ml reaction volume, stopped with addition of EDTA to a final concentration of 5mM, dialyzed to 1mM HCl and incubated with 150µl of neutravidin beads (ThermoScientific) in 24ml HBS500 buffer for 1,5h at RT. Beads were washed thoroughly as described previously, separated using poly-prep® chromatography columns (BioRad) and resuspended with water in 400µl final volume prior to measurement. Beads were boiled at 95^oC in 2% SDS solution in order to break the interaction between neutravidin and BMP2-K3Plk and centrifuged to recover the protein containing supernatant. 100µl of the supernatant was transferred to 300µl of the working reagent in triplicates. The assay was developed following the manufacturer's protocol. To calculate the amount of protein coupled to a single bead, absorption for non-coupled beads was subtracted, and normalized to the number of beads applied to the reaction.

2.17 Quantification of BMP2-K3Plk immobilized to azide agarose beads

The amount of BMP2-K3Plk immobilized to azide-functionalized agarose beads was measured with BCA Protein Assay Reagent (Thermoscientific). The coupling reaction was performed in a 2ml reaction volume. Beads were thoroughly washed as described before, separated using poly-prep® chromatography columns (BioRad) and resuspended with 400µl of water. 120µl suspension was added to 300µl of a working reagent in triplicates. Tubes were incubated at 60°C according to the manufacturer's protocol. To calculate the amount of the protein coupled to a single bead, absorption for non-coupled beads was subtracted, and normalized to the number of beads applied to the reaction.

2.18 Interaction of immobilized BMP2-K3Plk with BMPRIA ectodomain

Interaction of BMP2-K3Plk immobilized to azide-activated beads and neutravidin agarose beads with BRIA receptor ectodomain was determined by incubation with 1µM fluorescent BRIA receptor ectodomain in HBS_{500} buffer for 1h at RT. Beads were washed 5 times with the reaction buffer and visualized using fluorescent microscopy (Keyence).

2.19 Evaluation of osteogenic potential of beads coupled to BMP2-K3Plk

Osteoinductive potential of azide-functionalized and neutravidin-agarose beads coupled to site-specifically biotinylated BMP2-K3Plk was performed as described in section 1.13.

III. Results

1. BMP2-A2C

1.1 Evaluation of BMP2-A2C protein expression

In order to achieve site specific immobilization of BMP2 to a suitable scaffold two BMP2 variants were created. The first variant, named BMP2-A2C containing an extra N-terminal cysteine residue, was successfully expressed in JM109(DE3) bacteria. The expression was initially validated by SDS-PAGE and coomassie brilliant blue staining (Figure 7). The lanes corresponding to induced cultures show a band between 10kDa and 15kDa indicated by an arrow and match the electrophoretic mobility of the positive control (wildtype BMP-2). The predicted molecular weight of BMP2-A2C monomers is 13kDa. Leaky expression from the T7 promotor may be observed in lanes corresponding to uninduced BMP2-A2C cultures.
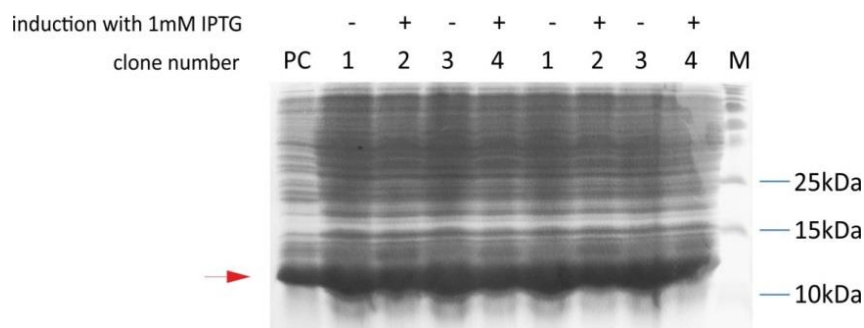
Figure 7: Expression of the BMP2-A2C variant

The figure shows SDS-PAGE separation and coomassie brilliant blue staining of BMP2-A2C expressed in *E.coli* strain JM109(DE3). Lanes: PC - wt BMP2, M - protein marker. The bands indicated with an arrow represent expressed BMP2-A2C monomers. Leaky BMP2-A2C expression can be also observed in uninduced clones (indicated by '-'). Induced clones are indicated with '+'.

1.2 Purification of the BMP2-A2C variant

BMP2-A2C variant was accumulated in bacterial inclusion bodies which required a stepwise isolation procedure. After isolation monomeric BMP2-A2C from inclusion the protein was refolded and purified by cation exchange chromatography in order to separate the wanted BMP2-A2C dimers (Figure 8).

A
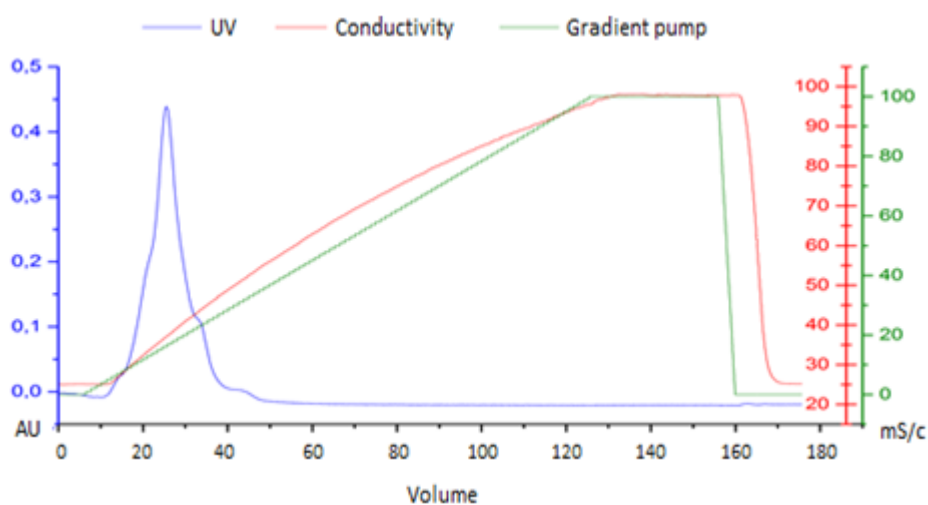
B
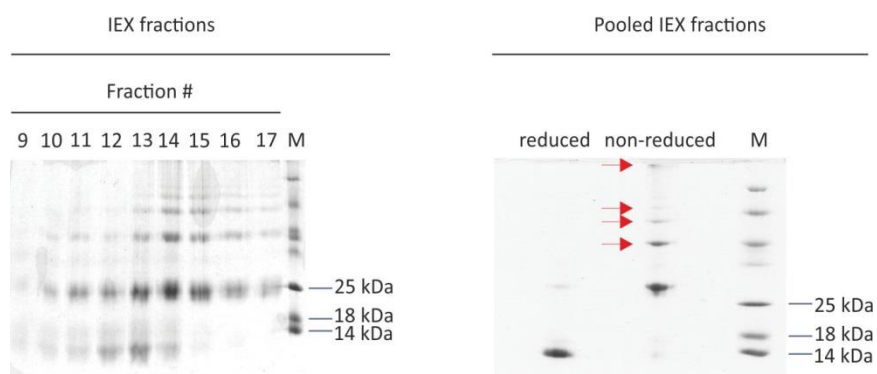
Figure 8: Purification of refolded BMP2-A2C by IEX chromatography

(A) Refolded BMP2-A2C was purified by cation-exchange chromatography in order to separate BMP2-A2C dimers. The protein was eluted within one sharp peak with a small shoulder indicating non-homogenous population of eluted protein; (B) Eluted BMP2-A2C fractions were analyzed by SDS-PAGE and Coomassie Brilliant Blue staining (left picture). Heterogenous population of BMP2-A2C monomers, dimers, and multimers was detected. Fractions containing BMP2-A2C dimers were pooled and analyzed by SDS-PAGE under reducing and non-reducing conditions in order to estimate the ratio of multimers to dimers in the final sample (right picture). Bands representing BMP2-A2C multimers are indicated with arrows (right picture). Legend: M – protein marker.

As shown in the Figure 8A the protein was eluted within one sharp peak with a small shoulder at a conductivity equal to 37.11 mS/cm. All protein containing fractions were analyzed by SDS-PAGE and Coomassie Brilliant Blue staining. Chromatography fractions containing dimeric BMP2-A2C were pooled and dialyzed to 1mM HCl. Approx. 1.3 mg of purified BMP2-A2C was obtained per 1g of inclusion bodies. The overall yield of produced BMP2-A2C was approx. 2mg per 1L of bacterial culture. Due to the additional cysteine introduced within the N-terminal region of the BMP2 mature polypeptide a heterogenous population of dimers and multimers varying in molecular weight was generated upon the refolding process, with the most prominent being a dimeric protein. Pooled fractions were analyzed by SDS-PAGE and coomassie staining under reducing and non-reducing conditions. Under reducing conditions only one band corresponding to BMP2-A2C monomers could be observed (Figure 8B). However, under non-reducing conditions (Figure 8B) multiple bands could be detected thus it seemed not feasible to separate properly folded BMP2-A2C dimers from multimeric structures. A further purification step appeared necessary. The IEX-purified fractions were therefore subjected to a secondary purification by reversed phase chromatography (Figure 9). In order to verify, whether this purification procedure would eliminate multimeric BMP2-A2C fractions an analytical amount of 1mg of BMP2-A2C variant was further purified using a C4 column.

A

B
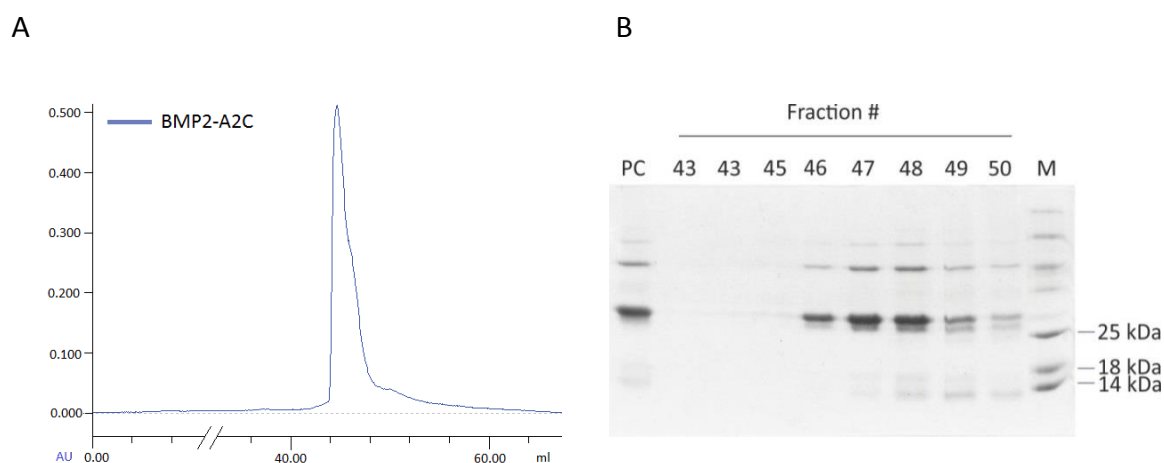
Figure 9: Purification of BMP2-A2C by reversed-phase chromatography

(A) Chromatogram of BMP2-A2C purified by reversed-phase chromatography. As BMP2-A2C dimers were not successfully separated by IEX chromatography, a second purification step using reversed-phase chromatography was used; (B) Analysis of reversed-phase chromatography fractions. Protein containing BMP2-A2C fractions were analyzed by SDS-PAGE and Coomassie Brilliant Blue staining. Legend: PC – BMP2-A2C purified by IEX chromatography; M – protein marker.

However, a separation of the BMP2-A2C dimers could not be achieved with this method. Because of similar hydrophobic properties between BMP2-A2C dimers and its multimers a satisfactory separation of dimers was not feasible. The fractions were analyzed by SDS-PAGE and Coomassie Brilliant Blue staining. Dimeric and multimeric bands of varying molecular weight were still present in all protein-containing fractions (Figure 9B).

1.3 Evaluation of BMP2-A2C by Western blot

In order to prove the identity of the purified protein sample, especially of the bands corresponding to high molecular weight structures SDS-PAGE, followed by Western blot analysis, was performed (Figure 10). Separation was performed under both, reducing and non-reducing conditions because of the dimeric nature of BMP2 (monomers coupled via disulfide bridges). WB was performed using an anti-BMP2 antibody raised against the mature polypeptide.
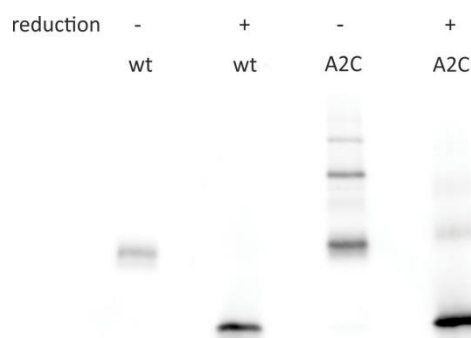
Figure 10: Western blot analysis of refolded BMP2-A2C

Purified BMP2-A2C was analyzed by Western blot to confirm the identity of the protein, especially the multimeric fraction visible in the Coomassie Brilliant Blue staining. Legend: wt - BMP2-wt; A2C – BMP2-A2C. Samples reduced with β-mercaptoethanol are indicated with '+' and non-reduced samples with '-'.

Non-reduced BMP2-A2C appeared in the Western blot as a mixture of dimers and multimers of varying molecular weight (Figure 10) as visualized previously with Coomassie Brilliant Blue staining (Figure 9B). The reduced BMP2-A2C appeared as 3 bands. The lowest band showed the same electrophoretic mobility as reduced BMP2-wt. The higher band migrated with a similar, though slower, electrophoretic mobility as non-reduced BMP2 dimers, and the highest band appeared as a multimeric protein with the electrophoretic mobility different than

the multimeric bands present in non-reduced BMP2-A2C. The 2 bands of higher molecular weight might therefore be a result of partial reduction of high molecular structures present in non-reduced BMP2-A2C. Possibly, not all disulfide bridges in multimeric BMP2-A2C were reduced upon β-mercaptoethanol treatment because of their limited accessibility. Incomplete reduction of BMP2-A2C might indicate that a fraction of the protein formed disulfide bridges between different cysteine residues than that in the BMP2-wt. Therefore, stronger reducing conditions may be required for their complete reduction. The results of the Western blot confirm that the dimeric bands as well as bands of higher molecular weight represent BMP2. However, the presence of multimers could affect the affinity of BMP2-A2C to main BMP2 receptors. Therefore, in the next step the interaction of BMP2-A2C with type I and type II BMP receptor ectodomains was investigated.

1.4   Interaction of BMP2-A2C with BMP2 receptor ectodomains

In order to validate the binding of the BMP2-A2C variant with type I and type II BMP receptors biotinylated BMPRIA and ActRIIB receptor ectodomains were individually immobilized to channels of a streptavidin coated surface plasmon resonance chip. BMP2-A2C variant was used as an analyte. The apparent KD for the BMP2-A2C applied to BMPRIA-decorated chip was approx. 0.6nM whereas BMP2-wt showed KD value equal approx. 0.7nM. For interaction with the ActRIIB receptor ectodomain immobilized on the SPR chip KD for the BMP2-A2C was equal approx. 1.7nM and 0.9nM for the BMP2-wt (Figure 11). These values show that the binding of BMP2-A2C to the main BMP2 receptor ectodomains is comparable to the wildtype BMP2, meaning that the BMP2-A2C multimers have the same binding to individual BMP2 receptor ectodomains as the wildtype protein.   The measured values are in agreement with the values published for wildtype BMP2 (*83*). However, BMP2 protein applied in vivo interacts simultaneously with both of the receptor ectodomains forming thereby a signaling complex. Therefore, even though BMP2-A2C showed similar binding constants to individual BMP2 receptor ectodomains, in the next step a cell-based assay was performed in order to validate the capability of simultaneous binding of BMP2-A2C to both receptors which are embedded within the cell membrane.
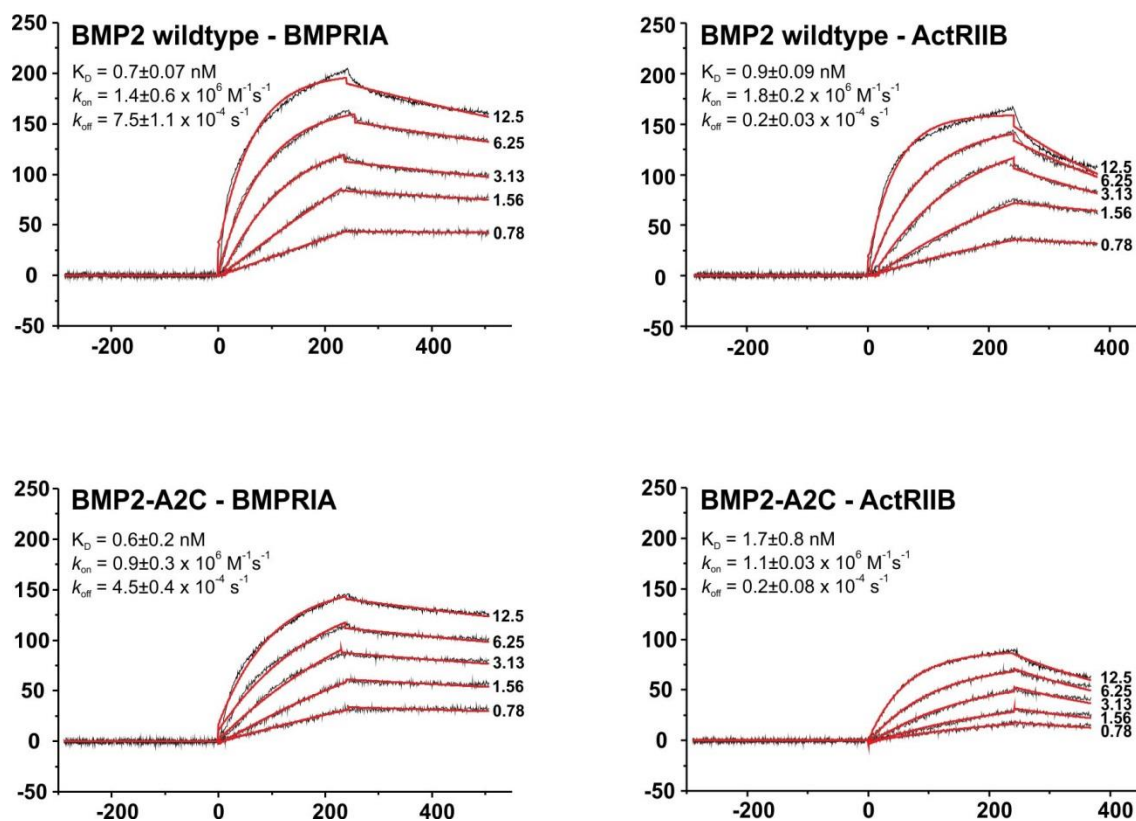
Figure 11: Binding of BMP2-A2C variant to BMPRIA and ActRIIB BMP2 receptor ectodomains

Interaction of BMP2-A2C variant and BMP2-wt with BMPRIA and ActRIIB BMP2 receptor ectodomains was measured by surface plasmon resonance. The measured KD values were in the same range for both measured proteins indicating similar affinity for both receptor ectodomains. The binding constants were determined from two or more independent experiments using at least six different analyte concentrations.

1.5 Evaluation of biological activity of BMP2-A2C

In order to evaluate the biological activity of the BMP2-A2C variant a cell-based assay using C2C12 cells was used. C2C12 myogenic progenitor cells differentiate towards osteoblastic lineage upon exposure to serum starvation conditions and BMP2, therefore they are reliable cells for testing of BMP2 bioactivity. Upon exposure to BMP2 C2C12 cells start to express alkaline phosphatase, which is an early marker for osteoblastic differentiation. The expression of alkaline phosphatase is dependent on the concentration of BMP2 applied to the cells. To calculate an EC50 values (the half maximal effective concentration) of BMP2-wt and BMP2-A2C a colorimetric assay with p-nitrophenyl phosphate was used. The p-nitrophenyl phosphate solution turns yellow upon cleavage of phosphate by alkaline phosphatase. For this purpose the cells were seeded onto 96-well plate and treated with serial dilutions of BMP2-wt

or the BMP2-A2C variant in medium supplemented with 2% FCS. After 3-days of incubation cells were lysed and the absorbance at 405nm was measured spectrophotometrically. The results were fitted in OriginPro9.1 using a Logistic model y = A2 + (A1-A2)/(1 + (x/x0)^p).
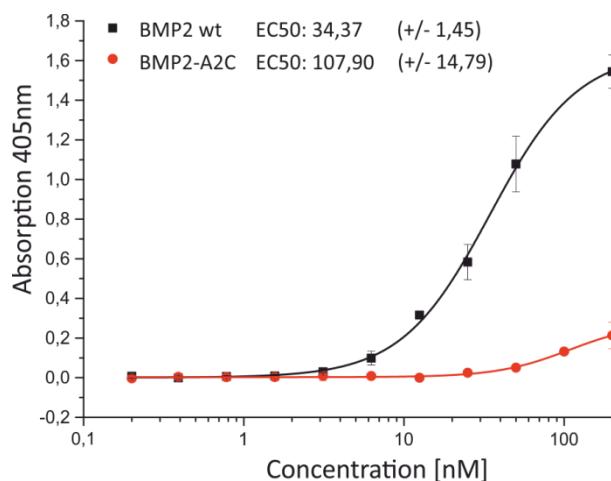
Figure 12: Validation of BMP2-A2C bioactivity

Biological activity of the BMP2-A2C variant was validated in a cell-based assay usingBMP2-responsive cell line C2C12. Bioactivity was determined based on the expression of alkaline phosphatase by C2C12 cells upon exposure to increasing concentrations of BMP2-A2C. BMP2-wt was used as a reference. The EC50 values were generated using logistic model y = A2 + (A1-A2)/(1 + (x/x0)^p). Each data point represents the mean absorption value from 2 biological replicates ± SD.

The calculated EC50 value was approx. 34nM for the wildtype BMP2 and approx. 108nM for the BMP2-A2C variant (Figure 12). Also the maximum absorption value was lower for the BMP-A2C mutant compared to wildtype BMP2. The mutation substituting alanine into cysteine in the BMP2-A2C mutant was located at the N-terminus of the polypeptide chain which, according to the present knowledge, is not involved in binding to any BMP2 cofactors, or receptors (except for the heparan sulfate). Hence, the difference in the dose response curve is most probably not related to the position of the mutation, but rather to structural and conformational changes of BMP2, being a consequence of introducing the additional cysteine. As shown in the Western Blot (Figure 10) the presence of extra cysteine residues led to formation of multimers, which could not be completely reduced to monomers, in contrast to wildtype BMP2. This fact led to a conclusion that in case of at least a portion of BMP2-A2C the disulfide bridges were formed differently than in the wildtype protein. Therefore, the discrepancy in the dose response curve between the wildtype and the mutant might originate

from the multimeric species present in the BMP2-A2C as well as from improperly folded dimers. It was shown in SPR evaluation (Figure 11) that BMP2-A2C has the same binding affinity towards BMPRIA and ActRIIB receptor ectodomains as wildtype BMP2. However, increased EC50 value and decreased efficacy of BMP-A2C manifested by the shift to the right on the dose response curve was observed in the cell based assay. This might indicate a presence of an internal competitive antagonist attenuating the signal transduction. If the BMP2-A2C multimeric molecules were unable to bind the type I BMP2 receptors one would expect a decreased potency (change in the EC50 value) but no change in the protein efficacy. However, the cell-based assay showed that both of these values changed for BMP2-A2C compared to BMP2-wt. Another hypothesis would be that BMP2-A2C can bind the type I receptor with the same affinity but the recruitment of the type II receptor is hindered. In this scenario the number of available BMP2 receptor complexes present in the cellular membrane would be decreased, though lower efficacy of the protein should be expected. As bioactive concentration of the BMP2-A2C would differ from the protein concentration measured by the UV-VIS spectrometry also the EC50 value should be increased. This scenario suits very well the dose response curve measured for the BMP2-A2C variant. The precise mechanism by which multimeric or improperly folded dimers act in the cellular assay as BMP2 inhibitors is not absolutely clear, as their binding affinity to main BMP2 receptors participating in signal transduction in C2C12 cells is similar to wildtype BMP2, as shown previously in SPR measurement (Figure 11). One could speculate that although the affinity to individual BMP2 receptors is the same for BMP2-A2C as it is for BMP2-wt, the proximity of both, type I and type II, receptors distributed on the cell surface prevents correct binding to the type II receptor by the bulky BMP2-A2C multimers.

1.6 Immobilization of BMP2-A2C to iodoacetyl-functionalized acrylamide beads

After detailed analysis, the BMP2-A2C variant was covalently coupled to iodoacetyl-functionalized acrylamide beads. Additional cysteine residues introduced within the N-terminus of BMP2-A2C allowed a partial reduction of the protein enabling a covalent coupling by thioether formation between the SH group of the protein and iodoacetamide group present on crosslinked acrylamide beads. Following partial reduction and the coupling procedure, the beads were thoroughly washed and stored in PBS. Samples of the reaction supernatant and the washing steps were collected and analyzed by SDS-PAGE and Coomassie

Brilliant Blue staining (Appendix). Uncoupled BMP2-A2C remained in the reaction supernatant, however no protein was detected in further washing steps as analyzed by SDS-PAGE. As negative control the same coupling procedure was applied to BMP2-wt. The uncoupled protein also here remained in the supernatant. The beads were washed according to the same scheme as for the BMP2-A2C variant. Upon reduction some monomers were generated in both, BMP2-wt and the BMP2-A2C variant. More BMP2-A2C monomers relative to dimers were visible in SDS-PAGE compared to BMP2-wt. It may be explained by the fact that a greater amount of BMP2-wt monomers was generated by the reduction procedure compared to BMP2-A2C. Consequently, higher monomer concentration of BMP2-wt compared to BMP2-A2C would lead to more efficient coupling of BMP2-wt monomers to the beads. Such scenario would be in agreement with the results shown in Figure 10 where β-mercaptoethanol reduction was more efficient for wildtype BMP2 than for the BMP2-A2C variant. In order to verify whether the coupling reaction between BMP2-A2C and iodoacetyl-functionalized acrylamide beads was successful and specific, BMP2-A2C-coupled beads as well as beads incubated with BMP2-wt under the same conditions were fluorescently stained. Beads were initially blocked and incubated with a primary BMP2 antibody, followed by subsequent staining with secondary fluorescent antibody conjugated to Alexafluor488 (Figure 13).
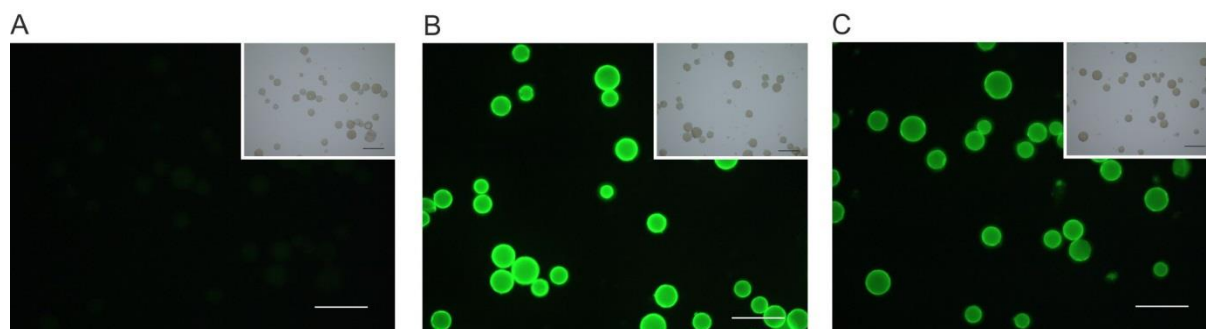
Figure 13: Detection of BMP2-A2C immobilized to iodoacetyl-functionalized beads
BMP2-A2C variant was covalently coupled to iodoacetyl-functionalized beads via cysteine residues. Uncoupled beads and beads reacted with BMP2-wt were used as negative control. Upon thorough washing steps the presence of BMP2 on the beads was verified by incubation with the primary BMP2 antibody and secondary fluorescent antibody. The scale bars represent 200nm. (A) non-coupled beads, (B) beads coupled to BMP2-wt, (C) beads coupled to BMP2-A2C.

Fluorescent analysis revealed prominent staining for beads coupled to both: BMP2-wt, as well as BMP2-A2C variant. Considering the harsh washing steps, the prominent staining indicates

that both proteins were successfully covalently coupled to the beads. Even though all cysteine residues of the dimeric BMP2-wt participate in the formation of the disulfide bridges, the reducing step and subsequent covalent coupling must have occurred between the cysteines naturally present in the BMP2-wt sequence and iodoacetyl groups on the beads. Therefore, it implies that the coupling reaction between the BMP2-wt and the iodoacetyl-functionalized beads was either not site-specific or not covalent, which should also account at least partially for BMP2-A2C. Nevertheless after excessive washing of beads with strong buffers non-covalent interaction with beads might be excluded. In contrast to these observations there was no fluorescent signal detected for non-coupled iodoacetyl-functionalized beads. Stronger staining visible for the beads coupled to BMP2-wt in comparison to BMP2-A2C would indicate that a higher quantity of wildtype BMP2 was coupled to the beads. However, it might also be explained by the presence of multimers in the BMP2-A2C population, which might shield other dimeric BMP2-A2C molecules and hinder their accessibility by the antibodies. Assuming that the monomer formation upon reducing step was greater in the BMP2-wt sample (Figure 10), the accessibility of the BMP2 antibody should be higher for immobilized BMP2-wt than for the immobilized BMP2-A2C species.

1.7   Quantification of BMP2-A2C immobilized to iodoacetyl acrylamide beads

To confirm the assumption from the previous experiment that a higher quantity of BMP2-wt compared to BMP2-A2C was immobilized per one iodoacetyl-functionalized acrylamide bead a colorometric protein assay was used. Because the protein was coupled to an insoluble acrylamide material a direct spectroscopic protein measurement could not be applied here.Therefore the BCA (bicinchoinic acid) protein assay was used. The assay was developed within a 2-step reaction. In the first step a light blue complex of a protein and copper^{2+} ions was formed at basic pH. In the second step reduced cuprous cations resulting from the first step reacted with bicinchoinic acid to form an intense purple reaction product. The absorbance of the resulting BCA/copper complex was measured at 562nm.
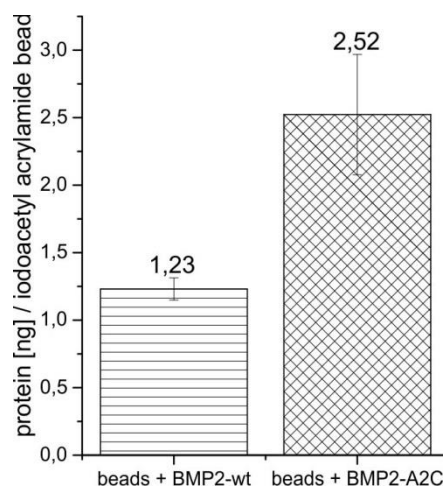
Figure 14: Quantification of BMP2-A2C coupled to iodoacetyl-functionalized beads

The amount of BMP2-A2C and BMP2-wt coupled to iodoacetyl-functionalized acrylamide beads was quantified by BCA protein assay. The mean absorption for the uncoupled beads was subtracted from the experimental samples. Bars represent the mean values ± SD of 3 replicates.

As shown in Figure 14 approximately double amount of the BMP2-A2C variant (2.5ng/bead) was coupled to the iodoacetyl-functionalized beads compared to wildtype BMP-2 (1.2ng/bead). This data confirm the results from the fluorescent staining (Figure 13), in terms of a successful immobilization of both BMP variants to the beads . As shown in Figure 14, more BMP2-A2C protein have been covalently bound to iodoacetyl-functionalized groups present on the surface of the beads. The more efficient coupling of BMP2-A2C may be a result of the additional cysteine residues available for the reaction. However, these results are in clear contradiction to the fluorescent staining shown in Figure 13 where a stronger staining was observed for beads coupled to BMP2-wt. Since the BCA assay measures the protein peptide bonds, it is a more reliable method to evaluate the number of immobilized molecules than the fluorescent staining using a BMP2 antibody. The antibody can bind only to its recognized epitopes within BMP2-A2C which are accessible. Multiple epitopes of BMP2-A2C forming conglomerates could be masked, as they could be shielded by other BMP2-A2C molecules. In this case the antibody would recognize only the external, exposed BMP2-A2C molecules. Additionally, strong fluorescent staining of the beads coupled to wildtype BMP2 might indicate substantial coupling of BMP2-wt monomers, which are easily accessible by the BMP2 antibody.

According to the information provided by the manufacturer of the iodoacetyl-functionalized acrylamide beads 6mg of reduced IgG (approx. mw: 75000 g/mole) might be coupled to 1ml of the settled resin. Considering that reduced IgG molecules are approx. 3 times larger than

BMP2-A2C dimers and that only 10µl of the beads were used for the reaction, the maximum binding for BMP2-A2C should be approx. 1,2 nmoles. Therefore, it can be estimated that approx. 8.3 times excess of BMP2-A2C compared to the binding capacity of the beads was used for the reaction. Therefore, the parameter limiting the saturation of BMP2-A2C on the surface of the beads should be in this case the number of the reactive iodoacetyl groups and efficiency of the reducing step.

After validating the quantity of immobilized BMP2-A2C per one bead it was verified in the next step whether covalently coupled BMP2-A2C is still able to bind the type I BMP2 receptor which is a prerequisite for the downstream signal transduction.

1.8 Interaction of immobilized BMP2-A2C with BMPRIA receptor ectodomain

BMP2 transmits the signal via interaction with the extracellular domains of type I and type II BMP receptors. The strongest affinity of BMP2-wt has been measured towards the BMPRIA receptor (*83*), and thus this receptor was chosen for the binding experiments. It was shown in Figure 11 that the affinity of soluble BMP2-A2C to BMPRIA receptor ectodomain was almost identical to wildtype BMP2. However, it was not known whether the BMP2-A2C variant covalently immobilized to iodoacetyl-functionalized beads is still able to bind to BMPRIA receptors and thus retains its structural integrity being essential for the ligand´s biological activity. To answer this question beads coupled to BMP2-A2C and wildtype BMP2 were incubated with fluorescently labelled BMPRIA receptor ectodomain, washed and visualized by fluorescent microscopy.
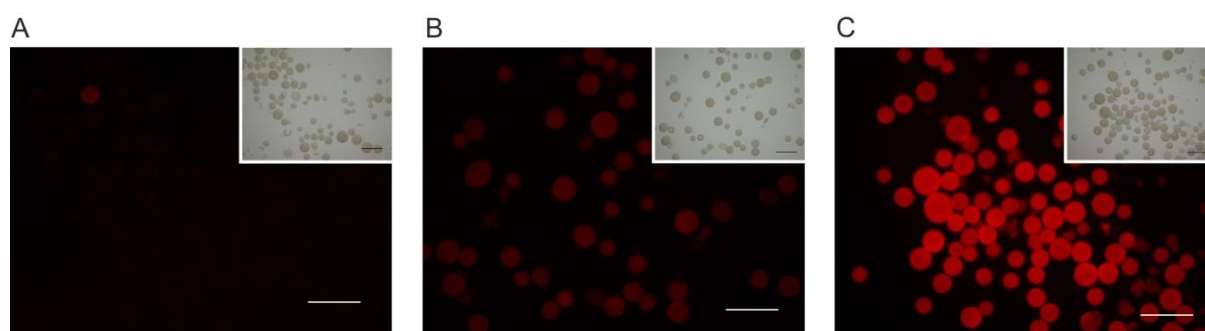
Figure 15: Interaction of iodoacetyl-functionalized beads coupled to BMP2-A2C with BMPRIA receptor ectodomain
The iodoacetyl-functionalized acrylamide beads coupled to BMP2-A2C were incubated with fluorescently-labelled BMPRIA ectodomain. The beads were washed and visualized by the fluorescent microscopy. As control uncoupled beads and beads reacted with BMP2-wt were used. The scale bars represent 200nm. (A). non-coupled beads; (B) beads coupled to BMP2-wt; (C) beads coupled to BMP2-A2C.

The images showed fluorescent signal for both BMP2-wt- and BMP2-A2C-coupled beads. Nonetheless, the fluorescence of beads coupled to BMP2-A2C was significantly stronger than that of the beads coupled to BMP2-wt. This might indicate that random reduction of cystine residues in BMP2-wt followed by interaction with the iodoacetyl-functionalized beads resulted in structural or orientational changes that hindered proper interaction with the main BMP2 receptor ectodomain. Nevertheless, according to the data from the protein quantification (Figure 14) approx. double amount of BMP2-A2C over BMP2-wt has been immobilized to the beads, which would also partially explain weaker fluorescence of the beads coupled to wildtype BMP2. The results from the previous experiments, including fluorescent staining with BMP2 antibody (Figure 13) and analysis of the supernatants from the coupling procedure (Appendix), indicate that higher number of partly unfolded and reduced BMP2-wt participated in the coupling reaction compared to BMP2-A2C. Since both BMP2 subunits are involved in formation of the wrist epitope responsible for binding of type I receptor weaker fluorescence of the beads coupled to BMP2-wt should also be expected. No staining was observed for the non-coupled iodoacetyl-functionalized beads, as there was no protein immobilized therein and the non-coupled beads showed low autofluorescence (Figure 15).

1.9   Differentiation of C2C12 cells upon exposure to BMP2-A2C-coupled beads

To finally verify the osteogenic potential of iodoacetyl-functionalized beads covalently coupled to BMP2-A2C variant C2C12 myoblast progenitor cells were used as a BMP2-responsive osteogenic differentiation model. Beads were applied onto the cell monolayer and embedded with agarose to prevent them from translocation. Over 3 days in serum starvation conditions the differentiation of premyoblastic cells towards osteoblastic lineage was examined. In wells treated with non-coupled beads there was no staining for alkaline phosphatase detected hence there differentiation of C2C12 was not influenced by the material, nor was it triggered by the chemical functionalization of acrylamide beads. In contrast, strong localized osteogenic differentiation was observed in wells supplemented with beads coupled to BMP2-A2C as well as BMP2-wt (Figure 17B,C). In both cases the staining was restricted only to the close proximity of the beads.
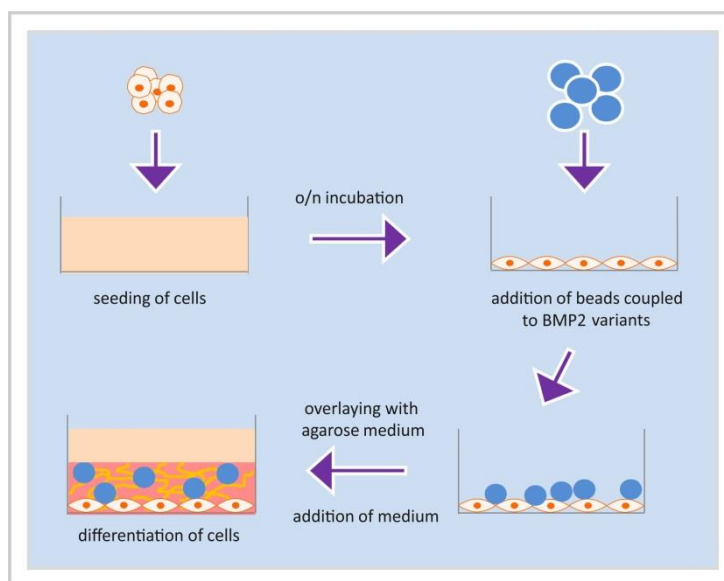
Figure 16: Scheme presenting application of functionalized beads to C2C12 myoblast progenitor cells
C2C12 were seeded onto a 96-well plate and incubated overnight. On the next day the iodoacetyl-functionalized beads covalently coupled to BMP2-A2C and BMP2-wt were applied to the wells and the beads were overlaid with low melting agarose. Upon gelling the agarose immobilized the acrylamide beads in place.

Based on the previous results showing high binding of beads coupled to BMP2-A2C to fluorescently labelled BMPRIA receptor ectodomain one would expect that the beads would also trigger the differentiation of BMP2-responsive C2C12 cells. However, activity studies (Figure 12) of uncoupled BMP2-A2C showed markedly reduced efficacy in comparison to wildtype BMP2, which was most probably caused by the presence of the multimeric structures that played a role of an internal inhibitor. BMP2-A2C immobilized to the beads consisted therefore not only of active BMP2-A2C dimers but also of multimeric structures acting as an inhibitor of BMP2 signaling. The question was whether a further decrease of the efficacy generated by the reduction step would block the signaling activity of BMP2-A2C. However, as shown in Figure 17C the beads covalently coupled to the BMP2-A2C variant triggered prominent differentiation of C2C12 cells that were precisely at that position where the beads were localized. Also, strong differentiation of C2C12 cells upon treatment with coupled BMP2-wt was remarkable considering the results from the previous experiments, which revealed that wildtype BMP2 covalently coupled to iodoacetyl-functionalized acrylamide beads showed highly reduced binding to BMPRIA receptor in comparison to the BMP2-A2C variant (Figure 15), and the amount of immobilized BMP2-wt was 2-times lower than for BMP2-A2C (Figure 14).
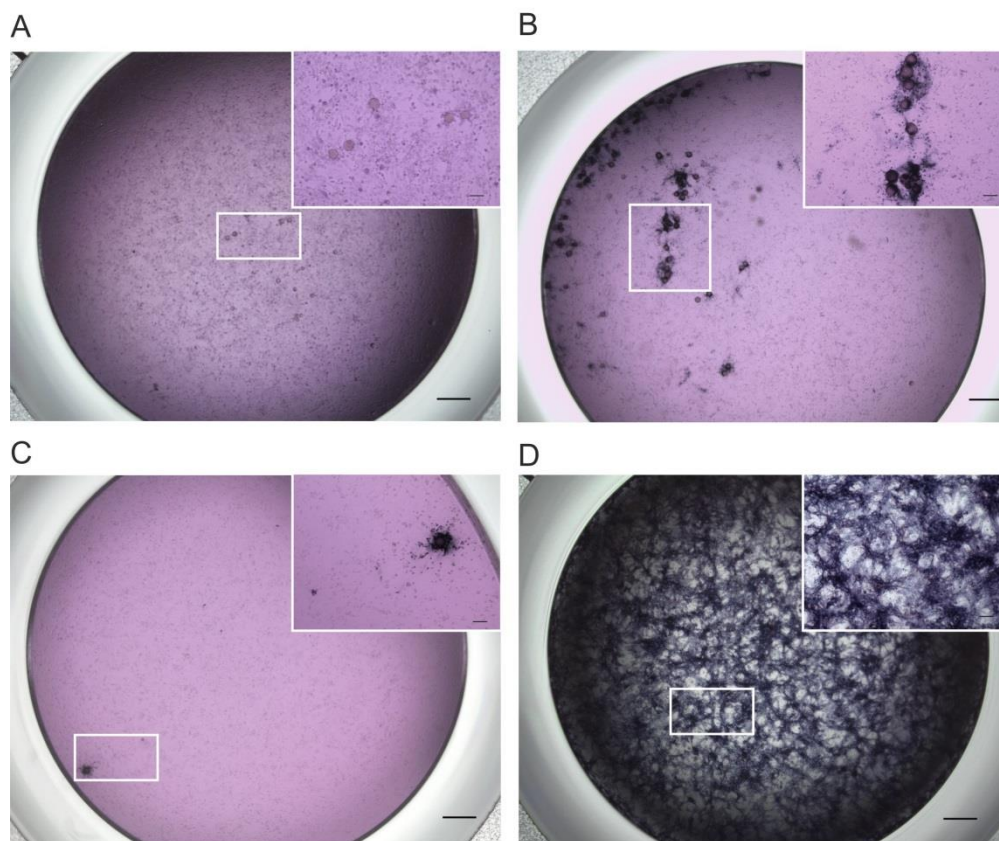
Figure 17: Alkaline phosphatase expression of C2C12 upon exposure to iodoacetyl-functionalized acrylamide beads.
Iodoacetyl-functionalized acrylamide beads covalently coupled to BMP2-A2C were applied to C2C12 monolayer culture and overlaid with low melting agarose. Differentiation of C2C12 cell was visualized by dark blue staining of alkaline phosphatase. As negative control uncoupled beads and beads reacted with BMP2-wt were used. As positive control 25nM of soluble BMP2-wt was used. The scale bars represent 500nm in the main pictures and 100nm in the enlargement. (A) uncoupled beads, (B) beads coupled to BMP2-wt, (C) beads coupled to BMP2-A2C, (D) 25nM soluble BMP2-wt.

Considering the inactive monomeric BMP2-wt immobilized to the beads (resulting from the reducing step prior to immobilization) one could speculate that much lower than ~1ng/bead of active BMP2-wt was immobilized on the beads. This indicates that the coupling of BMP2 to a scaffold could be performed at much lower density than the one currently tested while still preserving the differentiating potential of the beads. Lowering the dose of BMP2 immobilized on the scaffold while preserving its signaling capabilities would have a great economical and therapeutic benefits for the potential implant. The results of this experiment also confirm the hypothesis that BMP2 is still active in an immobilized state and that the BMP2-dependent signaling cascade leading to induction of ALP is triggered independently of the ligand internalization.

2. BMP2-K3Plk

2.1 Cloning of BMP2-K3Plk

The backbone of pET11-a vector carrying a sequence encoding pyrrolysyl-tRNA was double-digested with BamHI and NdeI enzymes. The backbone of the vector was purified by agarose gel electrophoresis (Figure 18A), excised from the gel and further purified. The BMP2 sequence was amplified by PCR. NdeI and BamHI restriction sites were introduced into the forward and the reversed primer respectively. An amber stop codon mutation was introduced within the forward primer. The reversed primer contained a mutation substituting the original amber TAG stop codon at the 3' terminus of the native BMP2-wt sequence into a TAA stop codon. Changing the stop codon at the 3' terminus was necessary, because otherwise expression would exceed the native translational stop if the loaded propargyl lysine-tRNA was present.
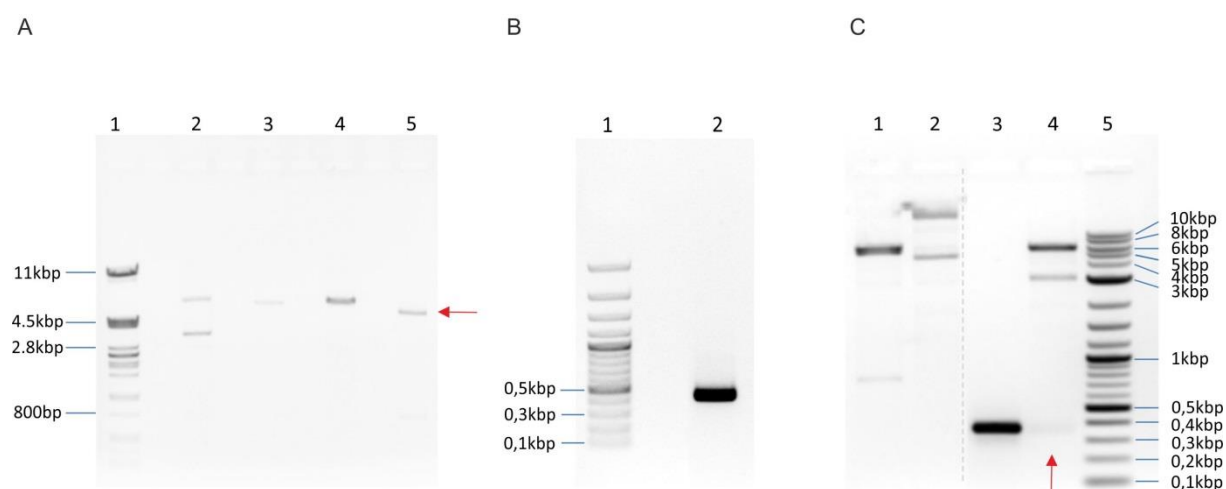
Figure 18: Cloning strategy of BMP2-K3Plk

(A) Restriction digestion of the pET11a vector. The pET11a-pyrtRNA vector carrying a gene for pyrrolysine tRNA synthetase was digested with restriction enzymes BamHI and Nde. The pET11a-pyrtRNA vector backbone is marked with a red arrow. Lanes: M. DNA ladder; 1. Non-digested pET11a; 2. pET11a digested only with NdeI; 3. pET11a digested only with BamHI; 4. pET11a double digested with NdeI and BamHi; (B) PCR amplification of BMP2-K3Plk sequence. BMP2-K3Plk cDNA carrying an amber TAG codon mutation was amplified using primers containing NdeI and BamHI restriction sites; Lanes: 1 - DNA ladder, 2. Amplified BMP2-K3Plk cDNA; (C) Verification of the positive clones. Amplified BMP2-K3Plk cDNA was ligated with the backbone of pET11-pyrtRNA vector and the positive clones were selected using the restriction digestion and colony PCR; lanes: 1. Double digested pET11-a; 2. pET11-a-pyrtRNA non-digested; 3. Product of the colony PCR; 4. Ligated pET11-a_BMP2-K3Plk digested with BahmHI and NdeI; 5. DNA ladder. The BMP2-K3Plk insert is marked with an arrow.

The expected PCR product of 360bp is visualized in Figure 18B. The BMP2-K3Plk insert was ligated with the backbone of the pET11-a vector, amplified in NovaBlue (Novagen) bacteria and analyzed by colony PCR and the restriction digestion with NdeI and BamHI enzymes. The digestion and colony PCR product of 353bp are depicted in Figure 18C. The vector was finally analyzed by sequencing.

2.2 Optimization of BMP2-K3Plk protein expression

The constructed vector coding BMP2-K3Plk was initially expressed in the E.coli strain BL21(DE3)plysS. The construct was co-transformed with pRSFduet-pyrtRNAsynth containing the gene coding pyrrolysyl tRNA synthetase. Varying expression conditions were used, including different temperatures, medium, and time (Figure 19A,B,C). Additionally, in order to verify, whether the newly formed construct was able to express wildtype BMP2 the amber codon mutation was reversed back to the original AAA codon which encodes a lysine residue (Figure 19D). As depicted in Figure 19A,B,C expression of BMP2-K3Plk could not be achieved under any of the tested conditions in the strain BL21(DE3)plysS. However, it was shown, that the construct in which the amber codon was reversed back to the original AAA codon expressed BMP2-wt within 3h after IPTG induction (Figure 19D). Therefore the main transcription elements in the expression vector, including the cDNA sequence of BMP2-K3Plk, promoter and the ribosome binding site seemed to be correctly operational. These results indicate also that the lack of BMP2-K3Plk expression in BL21(DE3)pLysS bacteria is directly associated with the presence of the stop codon introduced at the position of the third lysine residue in the mature BMP2-wt sequence. Because expression of wildtype BMP2 was successful, the vector sequence was not further optimized. Instead, different expression conditions were tested. Varying temperatures, expression duration and the used media did not show any improvement in terms of the protein yield. Perhaps other expression parameters, such as the moment of induction and different propargyl-lysine concentrations could be tested as well. However, the choice of the bacterial strain seemed to be the key parameter. BL21(DE3)pLysS strain enables a tight control of the recombinant protein expression by the presence of the T7 lysozyme gene derivative. Lysozyme forms a complex with T7 RNA polymerase and inhibits the basal transcription of target genes, which may be detrimental for expression of challenging proteins. The plasmid coding for lysozyme is maintained within the cell by conferring the resistance to chloramphenicol, which can downregulate the

transcription of recombinant proteins. In case of BMP2-K3Plk BL21(DE3)pLysS bacteria were transformed with 3 plasmids, which maintenance could lead to a substantial consumption of cellular resources. Another hypothesis explaining the lack of BMP2-K3Plk expression in the BL21(DE3)pLysS strain might be a degradation of propargyl-lysine by the cellular lysozyme. Even though the most recognized substrate for lysozyme are components of the bacterial cell wall, such as peptidoglycan (containing $\beta(1 \rightarrow 4)$ linkages between N-acetyl-muraminic acid and N-acetyl-D-glucosamine residues) a number of other, also synthetic, low molecular weight molecules have been identified as lysozyme substrates (*84*).
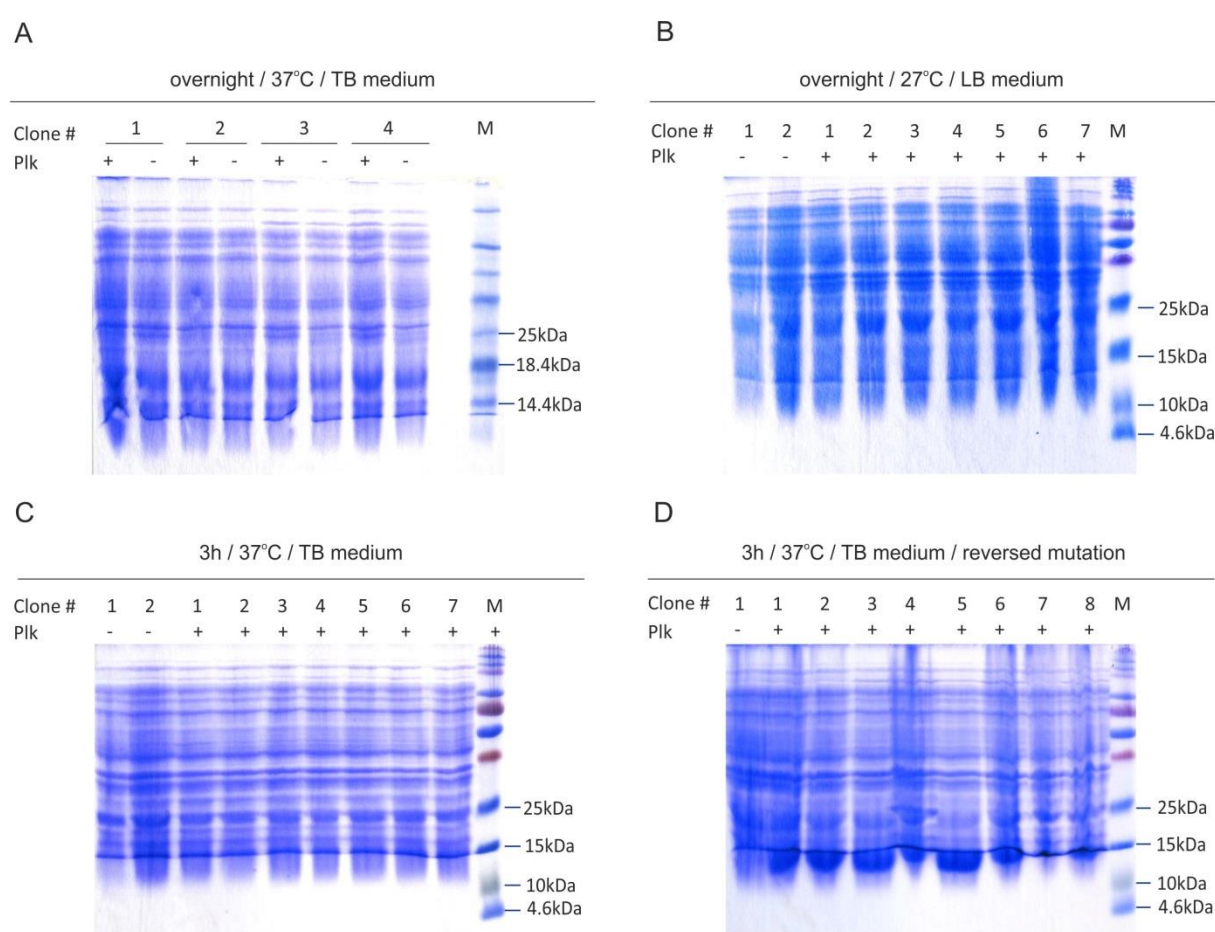
Figure 19: Optimization of BMP2-K3Plk expression in E.coli strain BL21(DE3)pLys
BL21(DE3)pLys cells were transformed with the BMP2-K3Plk construct and the protein expression was induced using different medium, incubation temperature and time. Induced and uninduced clones were lysed, analyzed by SDS-PAGE under reducing conditions and visualized by Coomassie Brilliant Blue staining. Additionally, BMP2-wt was expressed in a clone carrying BMP2-K3Plk plasmid with reversed amber codon mutation using the standard expression conditions.

As there was no BMP2-K3Plk expression observed in the strain BL21(DE3)plysS, another *E.coli* strain BL21(DE3), lacking the gene coding for lysozyme, was co-transformed with both, pET11a-pyrtRNA-BMP2-K3Plk and pRSFduet-pyrtRNAsynth vectors, and additionally a series of propargyl-lysine concentrations was tested for the most efficient induction. Expression was performed overnight at 37°C. As shown in Figure 20B BMP2-K3Plk expression was most successful with propargyl-lysine concentration of 10mM, whereas expression with 1mM of propargyl-lysine could not be observed. Also, no expression was observed in samples induced with IPTG without propargyl-lysine added.
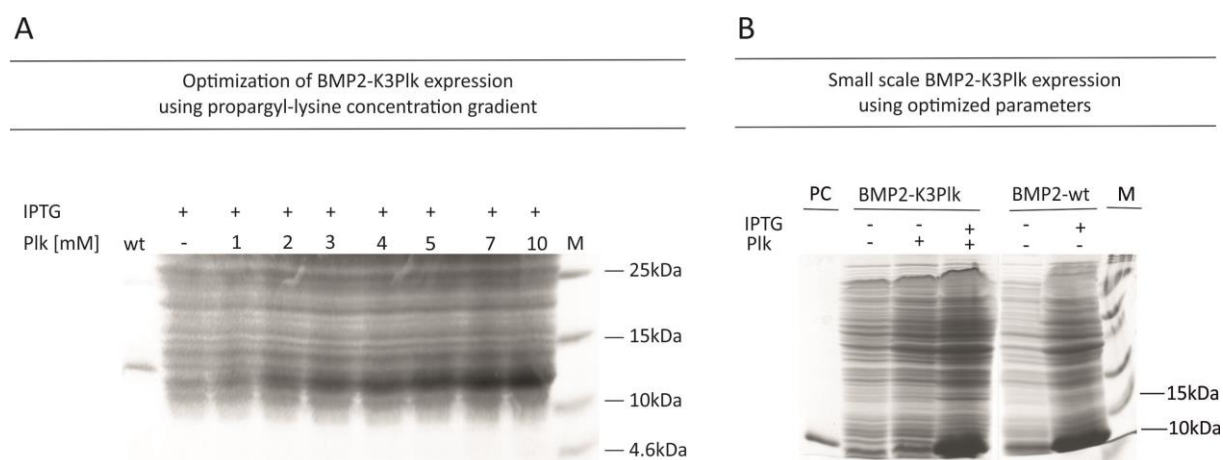
Figure 20: Evaluation of BMP2-K3Plk expression *in E.coli* strain Bl21(DE3)

(A) Evaluation of BMP2-K3Plk expression using a propargyl-lysine (plk) concentration gradient. BMP2-K3Plk expression in BL21(DE3) was performed overnight and was optimized using increasing concentrations of propargyl-lysine. Lanes: wt – BMP2-wt; 1-10 – concentrations of Plk; M – protein marker; (B) Evaluation of 100-ml BMP2-K3Plk expression. Protein expression was performed overnight in presence of 10mM propargyl-lysine. Legend: 1. PC – purified BMP2-wt, M – protein marker.

Because Coomassie Brilliant Blue stains all the proteins present in the bacterial lysate the identity of BMP2-K3Plk was verified by Western blot analysis using BMP2 specific antibody (Figure 21). In all 4 BMP2-K3Plk clones and the clone coding for wildtype BMP2 induced by addition of 1mM IPTG a positive signal was detected in presence of the propargyl-lysine. As positive control the pET11a-pyrtRNA_BMP2-K3Plk vector with reversed amber codon mutation was used.
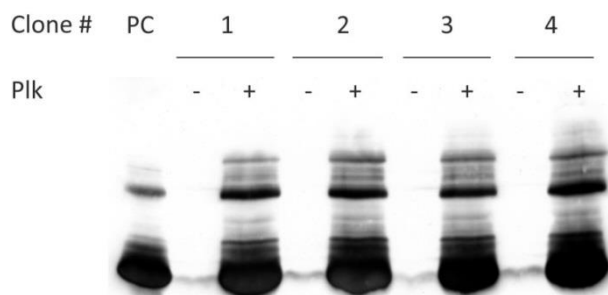
Figure 21: Western blot analysis of monomeric BMP2-K3Plk

Expression of BMP2-K3Plk in *E.coli* strain BL21(DE3) was verified by Western blot analysis using BMP2 antibody. Legend: PC – BMP2-wt.

2.3 Mass spectrometry of BMP2-K3Plk monomers from small scale preparation

After verification of BMP2-K3Plk identity a small scale (100ml) expression of BMP2-K3Plk variant was performed in order to verify whether and how many propargyl-lysine residues were successfully integrated into BMP2 polypeptide chain. 1,8g of the bacterial pellet was obtained from 100ml expression culture. The protein was then isolated from inclusion bodies and analyzed by mass spectrometry. Figure 22C depicts a theoretical isotopic mass distribution of the expected BMP2-K3Plk monomers. It was shown in the past that wildtype BMP2 and its variants expressed in *E.coli* are posttranslationally modified in that their N-terminal methionine is cleaved off. Therefore the deconvoluted MS spectrum of BMP2-K3Plk was compared to the theoretical isotopic distribution of BMP2-K3Plk monomers lacking the N-terminal methionine. The theoretical mass of the reduced monomeric BMP2 with cleaved-off N-terminal methionine and with propargyl-lysine introduced instead of lysine in the position 3 is 13058.408 Da (Figure 22C). The mass of the measured sample was 13058.537 Da (Figure 22A,B) which is in a very good agreement with theoretically calculated mass for BMP2-K3Plk. This experiment also answered the question how many propargyl-lysine residues were introduced in the BMP2-K3Plk polypeptide during translation process. Because of the high concentration of propargyl-lysine in the medium, there was an uncertainty whether this high concentration would not affect the specificity of native tRNA synthetases for their cognate amino acids. Nevertheless, as shown by the MS measurement BMP2-K3Plk was shown to contain only one propargyl-lysine residue within the polypeptide chain.
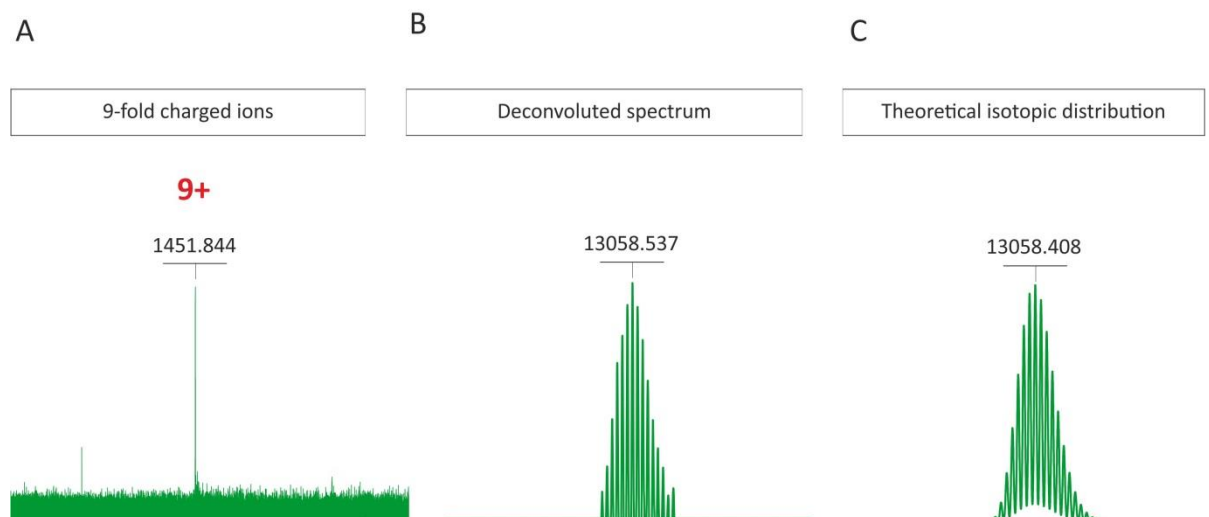
Figure 22: Mass spectrometry of BMP2-K3Plk monomers

BMP2-K3Plk monomers from the small scale preparation were analyzed by mass spectrometry in order to validate the presence and number of propargyl-lysine residues. The measured mass of the BMP2-K3Plk monomer was compared to the theoretical isotopic distribution of monomeric BMP2-K3Plk containing one propargyl-lysine substitution: (A) Measured spectrum of 9-fold charged BMP2-K3Plk monomer ions (X-axis 900-2100). The m/z ratio was equal 1451,844 which corresponds to the mass of 13058.596 Da (1451,844*9-8=13058,596). The measured mass is in agreement with the theoretically calculated mass of BMP2 containing one propargyl-lysine substitution; (B) Deconvoluted spectrum of BMP2-K3Plk monomers (X-axis 13000-13100). The measured mass was equal 13058,537 Da which is in agreement with theoretically calculated mass for BMP2-K3Plk monomers with reduced cysteine residues; (C). Theoretical isotopic distribution modeling of BMP2-K3Plk monomers was based on the formula: C 578, H 894, N 161, O 167, S9 [+1].

2.4 Refolding and purification of BMP2-K3Plk (small scale)

According to the present knowledge the only biological form of BMP2 able to activate Smad signaling cascade upon binding to type I and type II receptors is a dimer. Therefore, in order to obtain functional dimers and to verify whether introduction of propargyl-lysine interfered with the renaturation process, a small scale refolding (3mg of BMP2-K3Plk monomers) was performed (Figure 23A). As shown in the figure below the BMP2-K3Plk band of the same electrophoretic mobility as dimeric wildtype BMP2 could be detected under non-reducing conditions. Additionally, the dimeric band could not be visualized by the Coomassie Brilliant Blue staining when SDS-PAGE was performed under reducing conditions. Instead, a prominent band of monomeric molecular weight could be visualized.
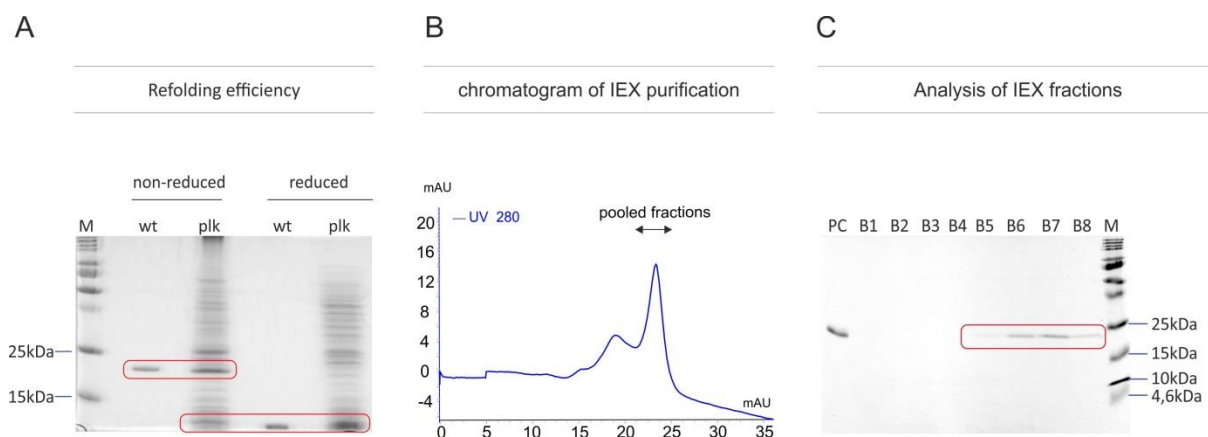
Figure 23: Small scale refolding and purification of BMP2-K3Plk

(A) Evaluation of the BMP2-K3Plk refolding. K3Plk monomers purified from the bacterial inclusion bodies were renatured in order to obtain dimers. The refolding efficiency was analyzed by SDS-PAGE and Coomassie Brilliant Blue staining. Wildtype BMP2 was used as a reference. Dimeric and monomeric BMP2-wt and BMP2-K3Plk are marked red. Legend: M - protein marker, wt – BMP2-wt, plk – BMP2-K3Plk; (B) Chromatogram of BMP2-K3Plk purified by IEX chromatography. After the small refolding process BMP2-K3Plk was purified by IEX chromatography in order to separate refolded dimers from BMP2-K3Plk monomers and impurities extracted from the inclusion bodies. Pooled BMP2-K3Plk fractions containing dimeric protein are marked with an arrow; (C) Analysis of BMP2-K3Plk fractions separated by IEX chromatography. The fractions separated by IEX chromatography were analyzed by SDS-PAGE under reducing and non-reducing conditions and stained with Coomassie Brilliant Blue. Reduced and non-reduced wildtype BMP2 was used as positive control. Fractions representing dimeric BMP2-K3Plk are marked red. Legend: M - protein marker, PC – BMP2-wt.

The products of the refolding process were then separated by cation exchange chromatography (Figure 23B). Approx. 70 µg of the dimeric BMP2-K3Plk could be recovered from the IEX column. The chromatogram of eluted BMP2-K3Plk showed 2 typical peaks for BMP2. The second peak represented the dimeric protein, whereas the first one constituted probably the monomeric BMP2-K3Plk. Eluted fractions were analyzed by SDS-PAGE and Coomassie Brilliant Blue staining (Figure 23C). The peak eluted as first from the chromatography column could not be visualized by the Coomassie Brilliant Blue staining, probably because of too low protein concentration. The fractions eluted within the second peak contained solely dimeric protein. Fractions representing dimeric BMP2-K3Plk were pooled, dialyzed, and analyzed by mass spectrometry.

2.5 Mass spectrometry of refolded BMP2-K3Plk (small scale)

Apart from monomeric BMP2-K3Plk, also the refolded protein was analyzed by mass spectrometry. Here, the expected theoretical mass of 1H+ charged BMP2-K3Plk homodimers

without N-terminal methionines, and including 7 disulfide bridges was 26101.700 Da (Figure 24B).

A

B
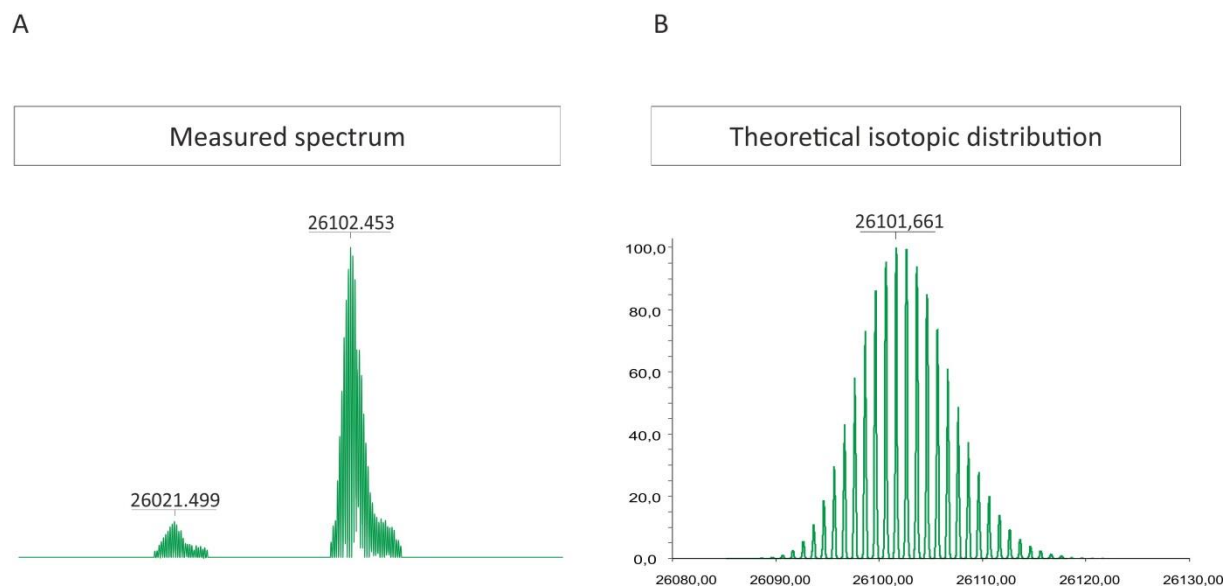
Figure 24: Mass spectrometry of dimeric BMP2-K3Plk (small scale)

(A) Deconvoluted spectrum of refolded BMP2-K3Plk (small scale); (B) Theoretical isotopic distribution of BMP2-K3Plk dimers. The calculated mass of the most frequently represented isotope is 26102,669 Da. The chemical formula used for isotopic distribution modeling was: C 1156, H 1773, N 322, O 334, S18 [+1].

Figure 24A represents the deconvoluted spectrum of dimeric BMP2-K3Plk with the measured mass of 26102.453Da. The difference of approx. 0.75Da between the theoretically calculated value and the measured mass is within the margin of error for MS-ESIT (<1Da), therefore the measured mass corresponds perfectly to the theoretically calculated value for dimeric BMP2-K3Plk. The deconvoluted spectrum shows a homogenous protein population in terms of the amino acid composition and the number of the disulfide bridges. Based on the mass of the molecule it is however not feasible to verify whether the disulfide bridges have been formed between the same residues as in wildtype BMP2. A small protein fraction representing the mass of 26021.5Da (Figure 24A) could be generated by partial N-terminal alanine cleavage from a small percentage of the protein.

2.6 Large scale preparation of BMP2-K3Plk

Based on positive outcome from preliminary small scale experiments a large scale expression was performed in TB medium supplemented with 10mM propargyl-lysine. The induction was performed by addition of IPTG to a final concentration of 1mM. As depicted in Figure 25A a strong expression was visible in the induced sample, and no expression could be detected in the non-induced sample. Per one 1L of culture approx. 12,5g of bacterial pellet was recovered yielding approx. 1,4g of inclusion bodies.
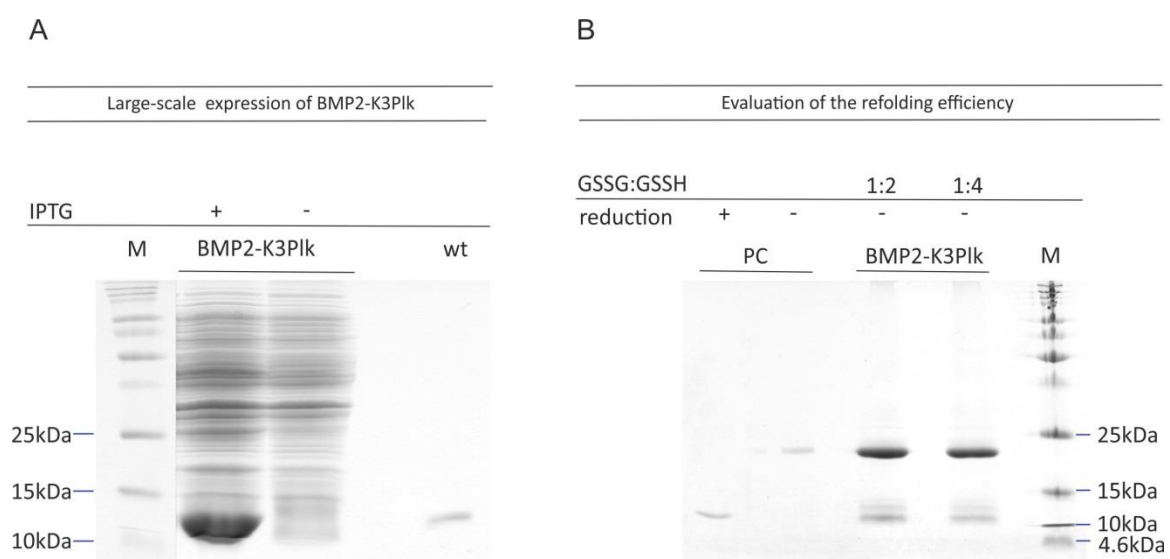
Figure 25: Large scale preparation of BMP2-K3Plk

(A) Large scale expression of BMP2-K3Plk. BMP2-K3Plk was expressed in BL21(DE3), isolated from inclusion bodies and analyzed by SDS-PAGE and Coomassie Brilliant Blue staining. The separation was performed under reducing conditions. Wildtype BMP2 was used as positive control. Legend: M – protein marker, wt – BMP2-wt, 1 - BMP2-K3Plk after o/n induction; 2 - BMP2-K3Plk 1h after Plk addition, -IPTG; (B) Large scale refolding of BMP2-K3Plk. Refolded protein was analyzed by SDS-PAGE and Coomassie Brilliant Blue staining. Wildtype BMP2 was used as positive control. Two different ratios of GSSG to GSH used for the refolding (1:2 and 1:4) were compared. Legend: PC – purified BMP2-wt, M – protein marker.

BMP2-K3Plk monomers purified from the inclusion bodies were renatured and the refolding efficiency was analyzed by SDS-PAGE and Coomassie Brillinat Blue staining. As shown in Figure 25B the majority of monomers transferred to the refolding buffer formed dimers. The efficiency of refolding was comparable between the 2 buffer compositions used: supplemented with GSSG to GSH ratio of 1:2 or 1:4. Refolded protein was then purified by ion-exchange chromatography and eluted fractions were analyzed by SDS-PAGE and Coomassie Brilliant Blue staining.
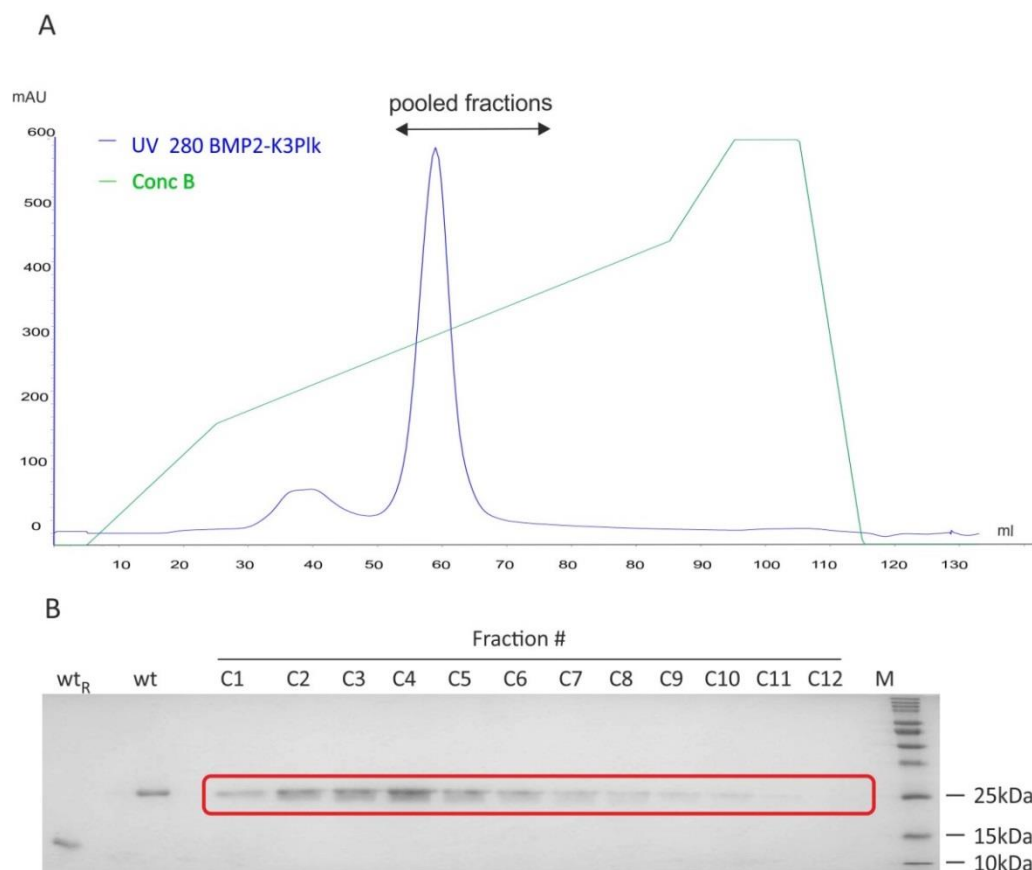
Figure 26: IEX chromatography of large scale BMP2-K3Plk preparation

(A) Chromatogram of cation-exchange purification of BMP2-K3Plk (large scale). Pooled fractions are marked with an arrow; (B) Fraction analysis of purified BMP2-K3Plk dimers purified by IEX chromatograpyhy. Fractions were analyzed by SDS-PAGE and Coomassie Brilliant Blue staining. Pooled fractions containing dimeric BMP2-K3Plk are marked red. Legend: wt_R – reduced BMP2-wt; wt – BMP2-wt non-reduced; C1-C12 – IEX fractions; M – protein marker.

The eluted fractions were analyzed by SDS-PAGE in order to select fractions containing BMP2-K3Plk dimers. All dimeric fractions were pooled, dialyzed, and concentrated. An overall yield of refolded BMP2-K3Plk dimers per 1L of culture was approx. 7mg of biologically active BMP2-K3Plk.

2.7 Western blot analysis of refolded BMP2-K3Plk homodimers (large scale)

As Coomassie Brilliant Blue provides only information about the approximate molecular weight of a protein the identity of the refolded and purified BMP2-K3Plk dimers were analyzed by Western blot under non-reducing and reducing conditions. The staining showed specific bands corresponding to the size of the wildtype BMP2 (Figure 27).
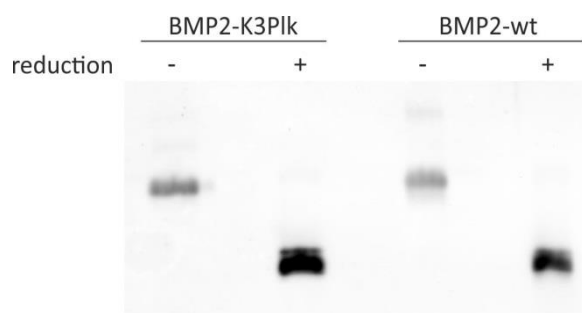
Figure 27: Western blot of refolded BMP2-K3Plk homodimers

Refolded BMP2-K3Plk was analyzed by Western blot under reducing and non-reducing conditions. Reduced BMP2 samples are indicated with '+' and non-reduced with '-'. As positive control wildtype BMP2 was used.

2.8 Analysis of BMP2-K3Plk dimers by mass spectrometry (large scale)

In order to acquire more detailed information about the molecular weight of the BMP2-K3Plk obtained from the large scale expression mass spectrometry analysis was performed. In contrast to the deconvoluted MS spectrum of BMP2-K3Plk from the small-scale preparation showing the mass of 26102.4kDa (Figure 24A), a heterogeneous population of 26105.9 and 26102.1 Da for the large-scale preparation (Figure 28) was detected. Wildtype BMP2 contains 7 cysteines involved in the formation of 3 intramolecular disulfide bridges and 1 intermolecular disulfide bridge forming a dimer. The expected mass of 1H+ charged BMP2-K3Plk homodimers without N-terminal methionine, and including 7 SS-bridges is 26101.7 Da (Figure 24B). The heterogeneous population of the measured sample appears as two overlapping isotopic distribution spectra (Figure 28). The population of 26102.1 Da represents BMP2-K3Plk dimers with the proper pattern of disulfide bridges, whereas the population of 26105.9 BMP2-K3Plk represents dimers missing 2 disulfide bridges, as their mass is 4H+ smaller than the mass of the expected, theoretically calculated BMP2-K3Plk dimer. Therefore, BMP2-K3Plk from the large preparation is a mixture of dimers, originating probably from monomers with either 2, or 3 SS-bridges. The location of the missing disulfide bridges remains unclear, however the intermolecular bonds are intact as visualized in Figure 27. Additionally, the signal of 25835.8 Da present also in the BMP2-wt (data not shown) indicates a partial N-terminal cleavage from a small percentage of the protein missing 2 disulfide bridges, as cleavage of 2 alanine residues and 1 glutamine would result in a mass of

25831.6 Da. The small protein fraction with the mass of 26087.8 Da was generated most probably due to desamination or dehydratization resulting from the ionization procedure. The protein fraction with the mass of 26020.9 Da could be a result of the terminal alanine cleavage of one BMP2-K3Plk subunit. Overall, the MS data show that majority of BMP2-K3Plk dimers are homogenous in terms of their N-terminal composition and propargyl-lysine incorporation.

A

B
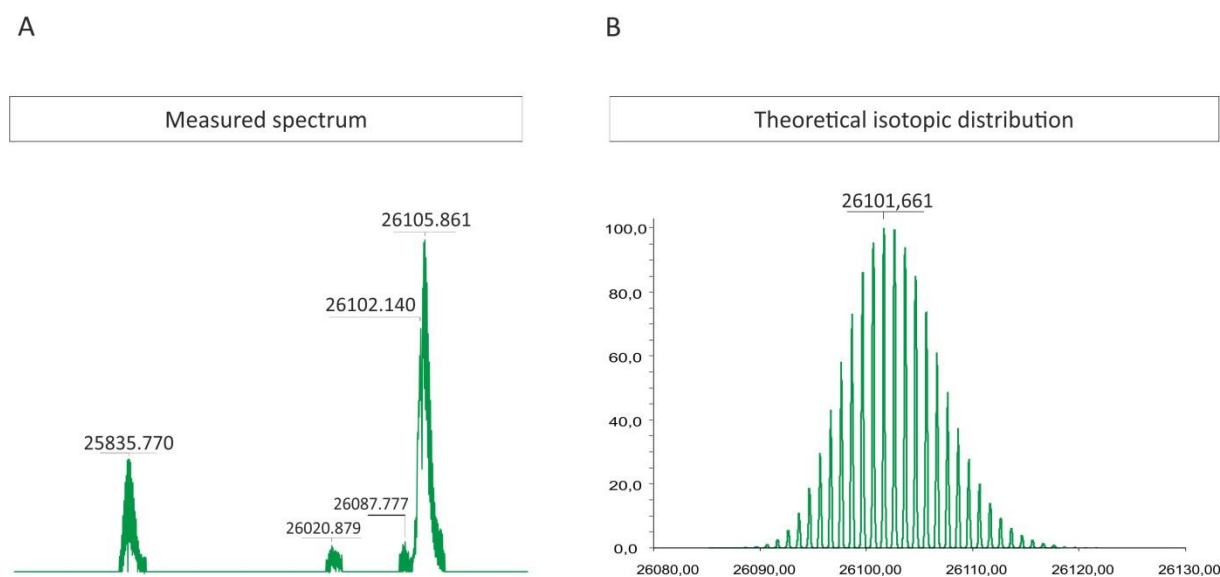
Figure 28: Mass spectrometry of refolded BMP2-K3Plk (large scale).

Refolded BMP2-K3Plk was analyzed by mass spectrometry in order to validate the successful incorporation of propargyl-lysine residue at the N-terminus of each BMP2-K3Plk subunit. The figure presents deconvoluted isotopic distribution of the measured spectrum. The mass of 26102.1Da and 26105.9Da represent refolded dimeric BMP2 containing one propargyl-lysine substitution within each monomer. The measured mass of 26105.9Da differs from the predicted BMP2-K3Plk mass by 4Da, indicating, that a fraction of the protein contained 5 instead of 7 disulfide bridges.

2.9   SPR analysis using BMPRIA and ActRIIB receptor ectodomains

After validation of proper incorporation of propargyl-lysine into the BMP2 polypeptide and successful refolding of BMP2 monomers, the binding of the BMP2-K3Plk variant for the main BMP type I and II receptors was verified. Surface plasmon resonance experiments were performed using 6 different analyte concentrations. BMPRIA and ActRIIB receptor ectodomains were immobilized to the chip surface and BMP2-K3Plk was used as an analyte. Each investigated receptor ectodomain (ligand) was immobilized to the separate sensor surface. The principle of the SPR measurement is the relationship between the mass change

on the chip surface and the intensity change of the light reflected from the surface. While an analyte in a solution binds to a ligand immobilized on a sensor surface the refractive index close to the surface changes, reducing thereby an angle and an intensity of the light reflected from the glass side of the SPR chip. This change of the reflected light angle is proportional to the mass change on the sensor chip. By plotting the time-dependent SPR response on the sensor surface the association rate constant (k_a) and a dissociation rate constant and (k_d) values can be extracted. Based on the ratio between k_d to k_a the equilibrium dissociation constant K_D can be calculated.
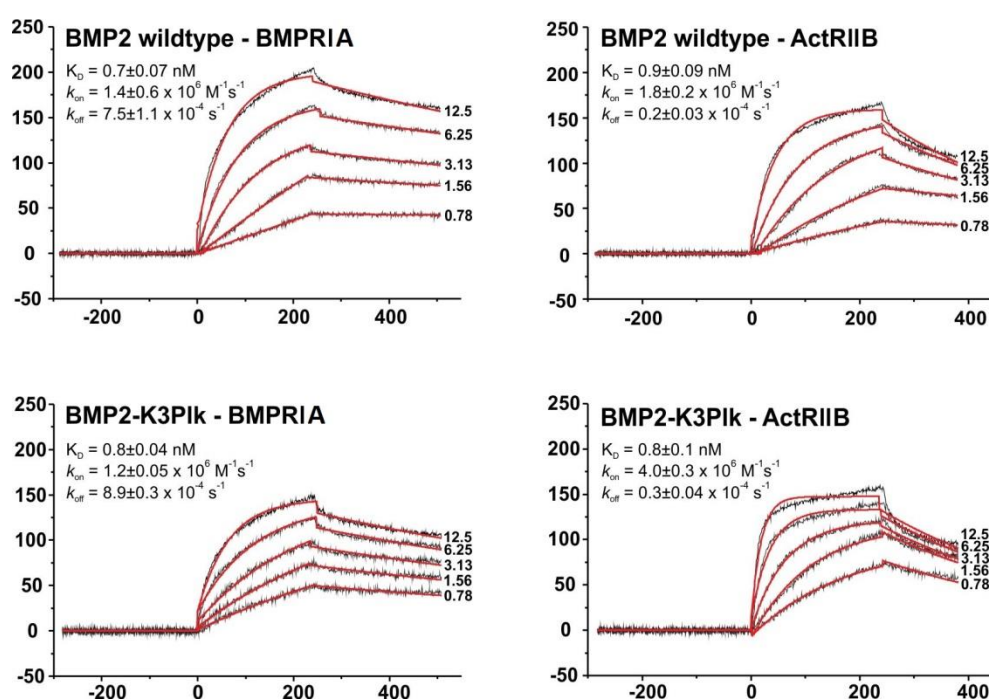
Figure 29: Interaction of BMP2-K3Plk with BMPRIA and ActRIIB receptor ectodomains
In order to examine the interaction of the BMP2-K3Plk variant with type I and type II receptor ectodomain surface plasmon resonance was performed. The measured KD values were in the same range for both measured proteins indicating similar affinity for both receptor ectodomains. The binding constants were determined from two or more independent experiments using at least six different analyte concentrations.

Data from the SPR measurements fitted using the Langmuir binding model showed that the K_D values for both BMP2-wt and BMP2-K3Plk were in the same range, with approx. 0.9nM for the first one and 0.8nM for the latter in case of ActRIIB, and 0.7nM for the BMP2-wt and 0.8nM for BMP2-K3Plk in case of BMPRIA receptor ectodomain (Figure 29). The measured values are in agreement with the values already published for wildtype BMP2 (*83*) and

indicate that the conversion of lysine into propargyl-lysine in the BMP2-K3Plk polypeptide has not changed its affinity to individual BMPRIA and ActRIIB receptor ectodomains.

2.10 Evaluation of biological activity of refolded BMP2-K3Plk

Binding to individual BMP2 receptor ectodomains does not guarantee the biological activity on the cellular level. The main difference between the SPR experiments and cell-based assays is the distribution of the receptors. While the receptor ectodomains are individually immobilized on the chip surface, both types of the receptors are located simultaneously and in close proximity to each other within the cell membrane. Therefore, to verify the biological activity of the BMP2-K3Plk variant a cell-based assay was used. The first 12 basic amino acids at the N-terminus of the BMP2 polypeptide constitute a heparin binding site, which modulates its biological activity. Although it is known that heparin binding site does not participate directly in the receptor assembly, it was shown to contribute to the bioavailability of BMP2 by binding to components of the extracellular matrix. It has been shown, that the BMP2 mutant deprived of the heparin binding site shows increased activity *in vitro* compared to wildtype BMP2. However, exactly the same protein shows decreased bioactivity in vivo (*85*) which could be explained by the fact, that *in vitro* the heparin binding sites bind to heparan sulphates of the ECS, therefore restricting BMP2 binding to its receptors. Moreover, a BMP2 variant containing extended heparin binding site results in increased osteoinductivity *in vivo*, caused by enhanced protein retention within the ECM and thus slower degradation rates (*86*). Because deletion of the heparin binding site significantly affects the activity of BMP2 *in vitro* we investigated whether insertion of propargyl-lysine disrupted the heparin binding capabilities of the N-terminus of BMP2. In such a case the results from *in vitro* bioactivity test would be unreliable. For this purpose, prior to a cell-based experiment, BMP2-K3Plk as well as BMP2-wt was purified using a heparin column. The separation resulted in simultaneous elution of BMP2-K3Plk and BMP2-wt with the maximum elution peaks at a concentration of 790mM NaCl (Figure 30). Simultaneous elution of both proteins shows, that the heparin binding sites of BMP2-K3Plk variant have not been affected.
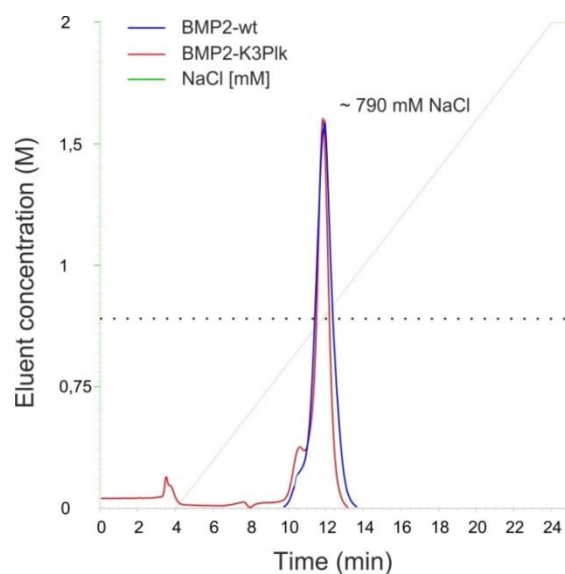
Figure 30: IEX separation of BMP2-K3Plk using a heparin column

BMP2-K3Plk and BMP2-wt were separated using a heparin column. The separation was performed to verify whether the properties of the heparin binding site at the N-terminus of BMP2-K3Plk were affected by the mutation. Both of the proteins were eluted at the same time indicating that the affinity of BMP2-K3Plk to heparin was not decreased by the mutation.

Therefore, in the next step the bioactivity of BMP2-K3Plk was tested in a cell-based assay (Figure 31). The dose response curve of BMP2-K3Plk resembles the curve of BMP2-wt, with EC50 value equal 28,9nM for the wildtype BMP2 and 19,4nM for BMP2-K3Plk. The efficacy of both proteins differed only at the concentration of 200nM, at which the maximum response asymptote was 7.2% lower for the BMP2-K3Plk variant compared to wildtype BMP2. The lower response towards the BMP2-K3Plk variant resulted most probably from a lower solubility of BMP2-K3Plk in the cell culture medium. Moreover, similar potency of BMP2-wt and BMP2-K3Plk also further indicates that the heparin binding site was unaffected in the BMP2-K3Plk variant. If the binding capability of the heparin binding site was decreased in BMP2-K3Plk lower EC50 value and therefore a shift of the dose response curve to the left would be expected.
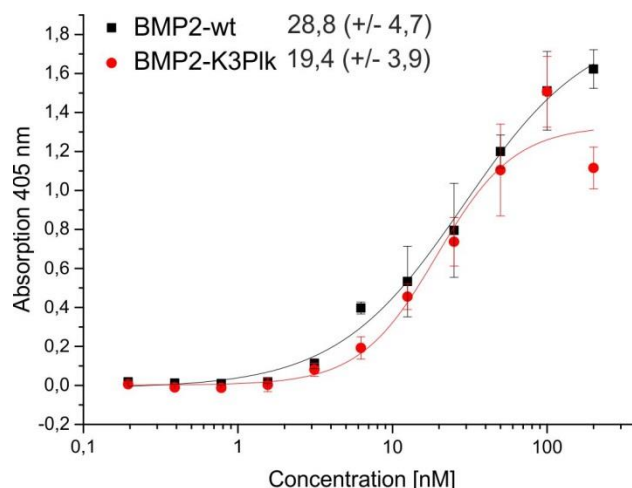
Figure 31: Validation of BMP2-K3Plk biological activity

Biological activity of BMP2-K3Plk was tested using C2C12 cells. Under conditions of serum starvation and exposure to BMP2 C2C12 cells undergo differentiation with expression of alkaline phosphatase. Expression of alkaline phosphatase is proportional to the concentration of BMP2 applied to the cells. As positive control BMP2-wt was used. The EC50 values were generated using using logistic model y = A2 + (A1-A2)/(1 + (x/x0)^p). Each data point represents the mean absorption value from 3 biological replicates ± SD.

2.11 Optimization of coupling conditions

After performing the biochemical and cell-based experiments indicating that the properties of the BMP2-K3Plk variant are similar to wildtype BMP2 the optimal coupling conditions were to be determined in order to couple BMP2-K3Plk in a controlled and site-specific manner to polymeric structures.

2.11.1 Click reaction catalyzed by UV irradiation

Considering the dimeric nature of BMP2-K3Plk, a standard CuAAC click reaction seemed to be a suboptimal choice considering the use of sodium ascorbate as a reducing agent. Therefore, in the first trial a 5kDa pox-cys polymer terminally functionalized with an –SH group, allowing for the site-specific reaction with the propargyl group of the BMP2-K3Plk variant was used. The reaction was triggered by a free radical starter generated by UV irradiation at 365nm in presence of DMPA (2,2-Dimethoxy-2-phenylacetophenone). There is only one functional alkyne group within each BMP2 monomer that could be targeted by the reaction with the thiolated 5kDa pox-cys polymer. The reaction could occur exclusively

between the thiol group of the polymer and the alkyne group of the protein, but as a consequence a second bond could be formed between an SH group of another polymer and remaining unsaturated alkene of the protein. Consequently it was expected that the protein species of 31kDa (1 molecule of the polymer coupled), 36kDa (2 molecules of the polymer coupled), 41kDa (3 molecules of the polymer coupled), and 46kDa (4 molecules of the polymer coupled) could be detected.
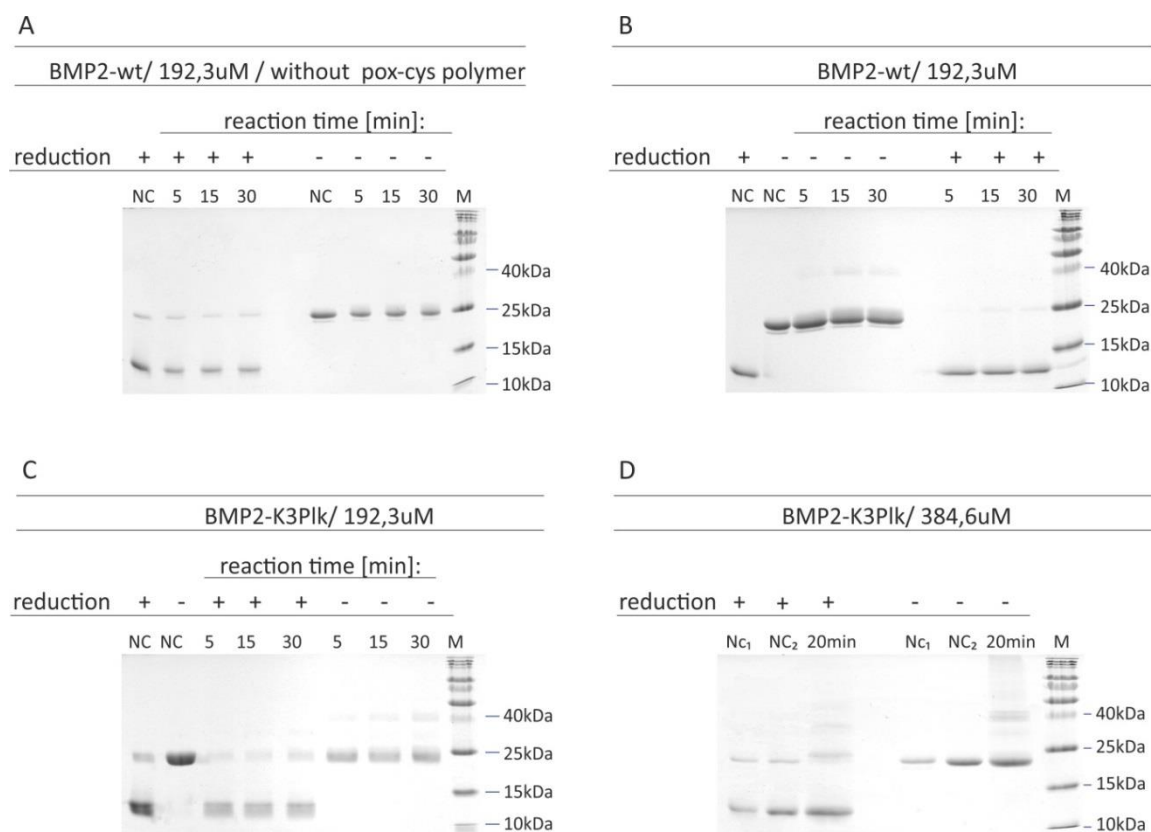
Figure 32: Poxylation of BMP2-K3Plk catalyzed by UV irradiation
In order to establish the optimal coupling conditions BMP2-K3Plk was reacted with 5kDa poly(2-oxazoline) polymer terminally functionalized with a sulfhydryl group (pox-cys). As negative control BMP2-wt was used. All samples were analyzed by SDS-PAGE and Coomassie Brilliant Blue staining under reducing and non-reducing conditions. Reduction step was performed using β-merkaptoethanol: (A) Wildtype BMP2 at the concentration of 193,3μM was incubated in the reaction conditions for 5,15 and 30min without the pox-cys. Legend: NC – untreated BMP2-wt; M – protein marker (B) Wildtype BMP2 at the concentration of 193,3μM was reacted with the pox-cys polymer for 5,15, and 30min. Legend: NC – untreated BMP2-wt; M – protein marker; (C) BMP2-K3Plk at the concentration of 192,3 μM was reacted with the pox-cys polymer for 5,15, and 30min. Legend: NC – untreated BMP2-K3Plk; M – protein marker; (D) BMP2-K3Plk at the concentration of 384,6μM was reacted with the pox-cys polymer for 20min. Legend: NC$_1$ – BMP2-wt untreated; NC$_2$ – BMP2-K3Plk untreated; M – protein marker.

Unfortunately, none of the tested reaction conditions: 5, 15 and 30 min. reaction with final BMP2-K3Plk concentration of 192,3µM (Figure 32C) or 20min. reaction with final BMP2-K3Plk concentration of 384,6µM (Figure 32D) resulted in satisfactory reaction efficiency. Bands corresponding to a molecular weight of 40kDa (Figure 32C,D) have been visualized in the Coomassie Brilliant Blue staining, however they appeared faint and occurred also in a negative control, where the wildtype BMP2 was used (Figure 32B). When wildtype BMP2 was incubated without the pox-polymer in the reaction conditions no additional bands could be visualized in the coomassie staining. Therefore appearance of the 40kDa bands in the negative control of BMP2-wt incubated with the pox-polymer (Figure 32B) might indicate that the reaction conditions were not 100% specific for terminal alkynes and alkenes. To additionally analyze an influence of the UV treatment on the BMP2-wt activity, products of the BMP2-wt reaction with and without the pox-polymer were subsequently tested in the cell-based bioactivity assay. It was shown in the alkaline phosphatase assay, that the efficacy of the treated BMP2-wt (in both BMP2-wt samples: with and without the pox-cys polymer) was decreased proportionally to the duration of the reaction (Figure 33A,B). Considering the fact that no additional bands could be detected in the coomassie staining for wildtype BMP2 incubated without the pox-cys polymer (Figure 32A) the decrease of the efficacy seems to depend on the free radicals generated by UV irradiation and not by the presence of the higher molecular weight structures.
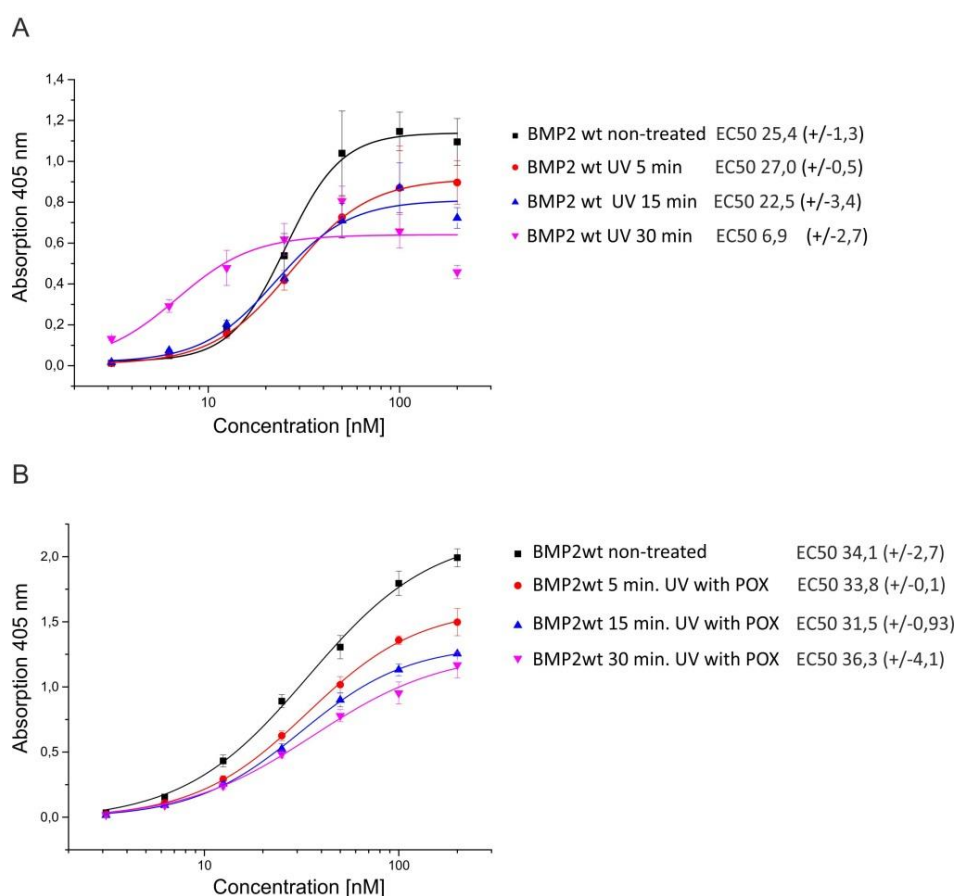
Figure 33: Bioactivity of BMP2-wt upon treatment by UV click reaction conditions

Bioactivity of BMP2-wt exposed to UV click reaction conditions was evaluated in C2C12 cells. Expression of alkaline phosphatase by C2C12 cells is dependent on the activity of BMP2-wt applied to the cells. Log 2 dilutions of BMP2-wt were performed. The EC50 values were generated using using logistic model $y = A2 + (A1-A2)/(1 + (x/x0)^p)$. Each point represents mean values of 3 biological replicates ± SD (A) Activity of BMP2-wt exposed to UV click reaction conditions without the pox-cys polymer; (B) Activity of BMP2-wt reacted with pox-cys polymer using UV click reaction conditions.

2.11.2 Copper catalyzed azide-alkyne cycloaddition

As the UV/radical-triggered click reaction did not result in a satisfactory efficiency and specificity, copper(I)-catalyzed alkyne-azide cycloaddition was performed between BMP2-K3Plk dimers and a 2,5kDa pox polymer terminally functionalized with an azide group. CuAAC reaction is known for its extreme specificity and good efficiency rates, which benefits however from higher reaction temperatures, neutral pH and high concentrations of the reactants. The bioconjugation using CuAAC reaction is challenging because of the sensitivity of proteins to redox reactions (e.g. reducing agents), and limited working protein

concentrations. In the following reaction 76.9μM concentration of the protein was used. Because the solubility limit of BMP2-wt in salt-containing buffers oscillates within the limit of 1μM, Millipore water was used as a diluent. As one BMP2-K3Plk monomer was able to react with only one pox-azide molecule two additional bands should be expected on the gel: 28,5kDa (one molecule of azide-pox attached) and 31kDa (two molecules of azide-pox attached).
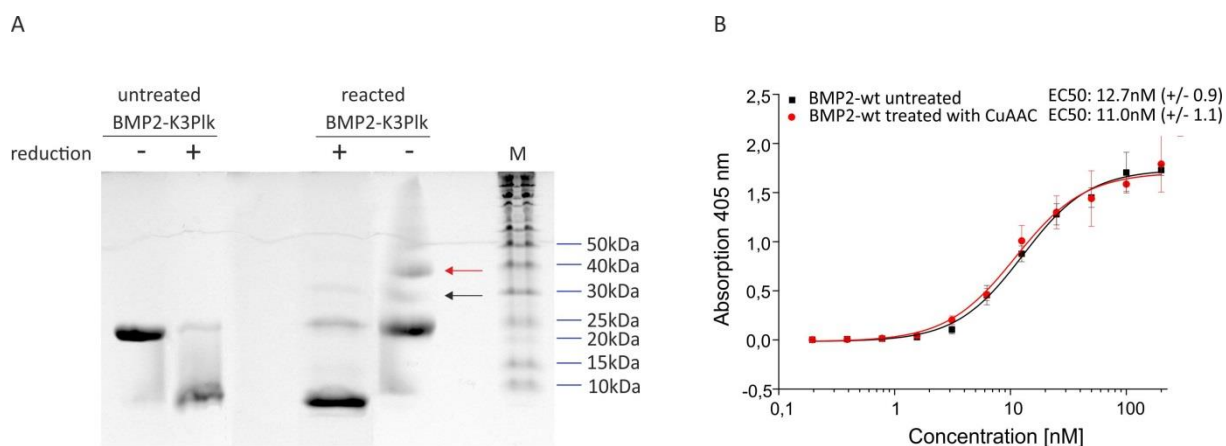
Figure 34: Poxylation of BMP2-K3Plk using copper catalyzed azide-alkyne cycloaddition
BMP2-K3Plk was reacted with a 2,5kDa poly(2-oxazoline) polymer functionalized with a terminal azide group (pox-azide) using standard click reaction conditions with sodium ascorbate. (A) SDS-PAGE and Coomassie Brilliant Blue staining of BMP2-K3Plk reacted with pox-azide; (B) Evaluation of BMP2-K3Plk bioactivity upon coupling with the pox-azide polymer. The bioactivity was measured in C2C12 cells using alkaline phosphatase assay. Cells were incubated with log-2 dilutions of BMP2-K3Plk. The EC50 values were generated using using logistic model $y = A2 + (A1-A2)/(1 + (x/x0)^p)$. Each point represents the mean value from at lesast 2 biological replicates ± SD.

Despite the reaction conditions had no influence on the bioactivity of wildtype BMP2 (Figure 34B) the reaction between azide-functionalized pox-polymer and the BMP2-K3Plk variant led to formation of non-specific higher molecular bands corresponding to the mass of approx. 40kDa visible in the coomassie staining, indicated with a green arrow (Figure 34A). The modified BMP2-K3Plk of approx. 40kDa could not be detected under reducing conditions indicating that the non-specific band represented BMP2-K3Plk multimers coupled by disulfide bridges. A band of poxylated BMP2-K3Plk corresponding to the expected molecular weight of 30kDa, indicated with a red arrow, was also observed upon coomassie staining. This band however was very faint, and still present in the reducing conditions with the same

electrophoretic motility as the non-reduced sample. If the band of 30kDa was the expected product, a band of approx. 15kDa should be visible in the coomassie staining under reducing conditions. Indeed a band of 15kDa was observed in the coomassie staining, it was however very faint. The band of approx. 30kDa was still visible under reducing conditions which could result from the incomplete reduction of higher molecular bands. Nevertheless, the presence of higher molecular weight structures might indicate that reduction of copper (II) sulfate by sodium ascorbate or the CuAAC reaction between the azide-functionalized pox-polymer and BMP2-K3Plk changed the redox potential of the solution leading to reduction, successive formation of cysteine bridges, and formation of higher molecular weight structures. The presence of the faint band of expected molecular weight of approx. 30kDa led to an assumption that the classical click reaction using Copper (II) sulfate and sodium ascorbate was to some extent successful but needed further optimization and better tools for the detection of the coupled protein. Redox reactions between $CuSO_4$ and sodium ascorbate generate reactive oxygen species that might affect the structural integrity and thus bioactivity of BMP2-K3Plk. In order to verify how free radicals and reducing agent present in the reaction influence BMP2 structural integrity an overnight incubation of BMP2-wt was performed at RT in water with different molar ratios of sodium ascorbate to copper (II) sulfate (Figure 35). Upon incubation only with sodium ascorbate and $CuSO_4$ BMP2-wt was degraded in a concentration-dependent manner, as no protein was visible in the coomassie staining at higher ratios of sodium ascorbate to copper (II) sulfate. Large excess of sodium ascorbate over copper sulphate (II) resulted in distinctive protein degradation (Figure 35A) as well as formation of multimers/aggregates mostly of approx. 40kDa but also higher, which were too large to enter the SDS-PAGE gel (Figure 35B). Under reducing conditions bands with slower electrophoretic mobility than the BMP2-wt monomers appeared (Figure 35A, indicated with red arrows), which may indicate partial fragmentation of BMP2-wt.
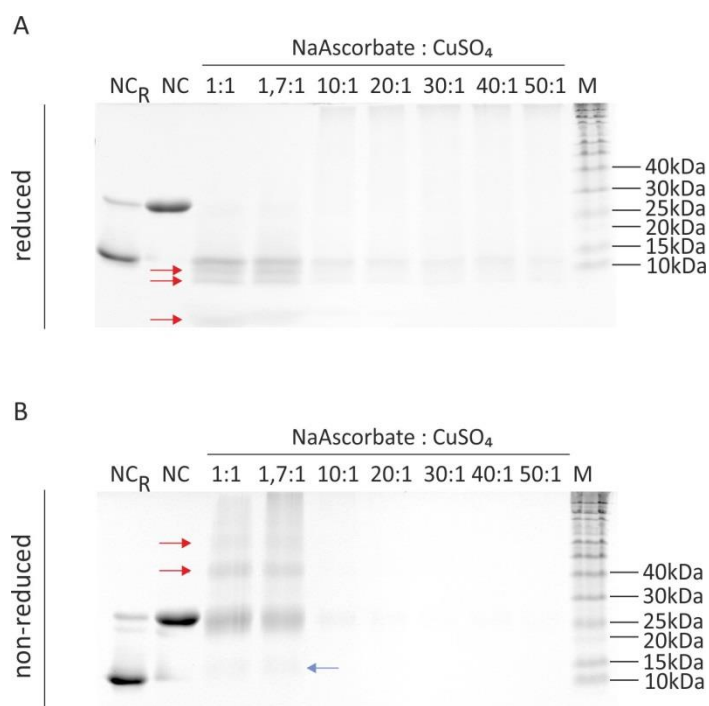
Figure 35: Effect of sodium ascorbate and CuSO₄ on BMP2-wt

BMP2-wt was exposed to different molar ratios of sodium ascorbate to $CuSO_4$. The samples were analyzed by SDS-PAGE, and Coomassie Brilliant Blue staining under reducing and non-reducing conditions. A) reducing conditions. The bands representing cleaved BMP2-wt is indicated with arrows; B) non-reducing conditions. The bands representing multimeric BMP2-wt are marked with red arrows. The bands representing cleaved BMP2-wt is indicated with a blue arrow. Legend: NC_R – reduced BMP2-wt untreated; NC - BMP2-wt untreated; 1:1 – 50:1 – increasing molar ratios of sodium ascorbate to $CuSO_4$; M – protein marker.

Due to the unsatisfactory results obtained using classical copper(I)-catalyzed alkyne-azide cycloaddition (CuAAC) further optimization of the reaction conditions was performed in the next steps. For further optimization small functionalized molecules were used instead of the functionalized polymers.

Because incubation of BMP2-wt in the solution containing sodium ascorbate and copper (II) sulfate resulted in excessive protein degradation and fragmentation Tris(3-hydroxypropyltriazolyl-methyl)amine was used in the next step as a protective agent. THTPA exerts a protective function in the click reaction, by intercepting free radicals resulting from $CuSO_4$: NaAsc redox reactions. Reactive oxygen species can oxidize side chains of amino acids, such as histidine. THPTA was also shown to prevent protein hydrolysis by Cu(II)

byproducts. 5-times molar excess of THPTA over the copper (II) sulfate has been recommended in other studies (*87*). In the following experiment it was verified whether increasing concentrations of THPTA improve the reaction efficiency and reduce the number of BMP2-K3Plk multimers formed during CuAAC reactions. BMP2-K3Plk was coupled to 3-azido-7-hydroxycoumarin in presence of varying ratios of THPTA to $CuSO_4$ to for 24h. 100µM CuSO4 and 5mM NaAsc was used in all samples. 3-azido-7-hydroxycoumarin is a non-fluorescent molecule, which becomes fluorescent upon coupling with an azide group. It was expected that coupling to a small molecule instead of a polymer would facilitate the reaction efficiency because of the possibility of using much higher concentrations.
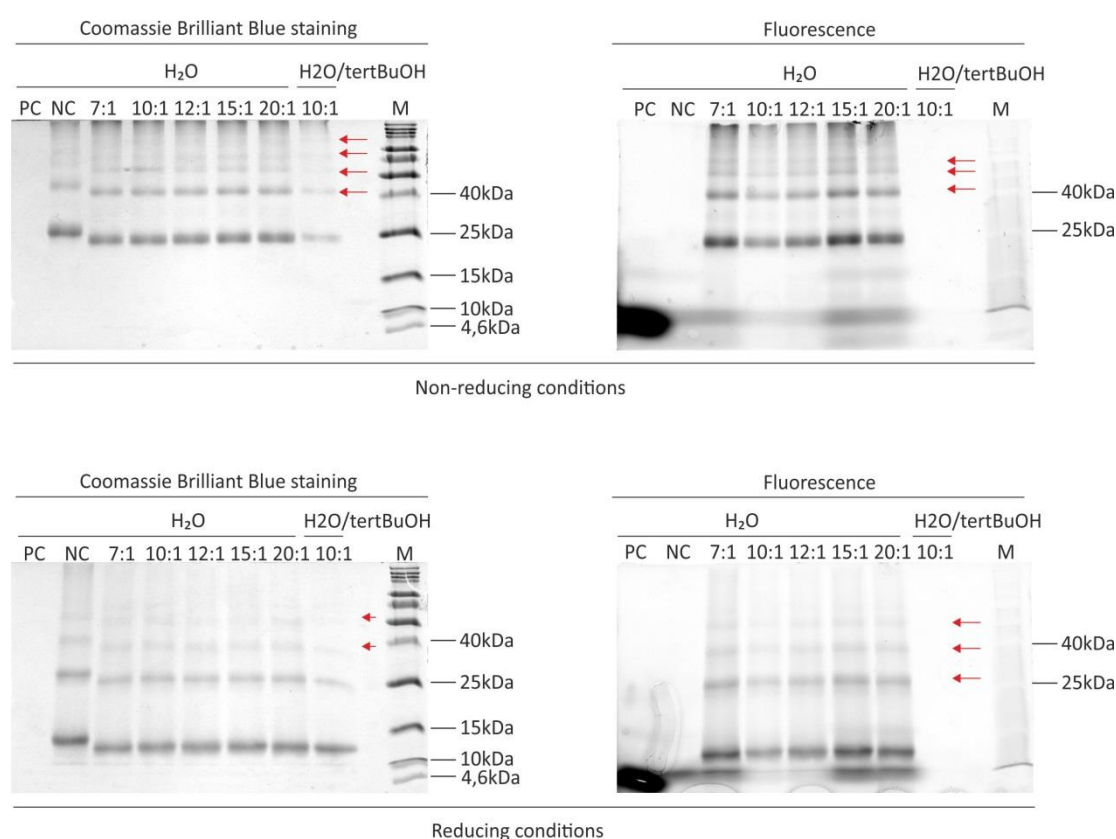
Figure 36: Effect of THPTA on CuCAAC efficiency and BMP2 integrity

BMP2-K3Plk was coupled to 3-Azido-7-hydroxycoumarin using CuAAC reaction conditions supplemented with THPTA. Increasing molar ratios of THPTA to $CuSO_4$ were tested in order to evaluate the protective role of THPTA for BMP2 integrity. Upon coupling 3-Azido-7-hydroxycoumarin becomes a fluorescent dye. The samples were analyzed by SDS-PAGE, Coomassie Brilliant Blue and fluorescent staining. Reactions were performed in water. The reaction with 10:1 molar ratio of THPTA to $CuSO_4$ was performed in H2O/tertBuOH (2eq:1eq). Legend: PC - propargyl alcohol coupled to 3-Azido-7-hydroxycoumarin; NC – BMP2-wt reacted with 3-Azido-7-hydroxycoumarin; 7:1 – 20:1 - BMP2-K3Plk reacted with 3-Azido-7-hydroxycoumarin in presence of increasing molar ratios of THPTA to $CuSO_4$. Multimers are indicated with arrows.

The successful coupling was observed in all the experimental samples, except for the negative control and BMP2-K3Plk reacted in the presence of tert-butanol. No difference in terms of multimers formation and reaction efficiency was detected upon incubation with different concentrations of THPTA (Figure 36). However, no protein species smaller than mw=13kDa (visible in the Figure 35A) were any longer present in SDS-PAGE indicating, that addition of THPTA could prevent BMP2-K3Plk fragmentation. Appearance of the higher molecular weight structures of approx. 40kDa (indicated with red arrows) can be observed in the coomassie staining under non-reducing conditions (observed also in previous experiments: Figure 35, Figure 34, and Figure 32B,C,D). However, these structures disappear partially in the reducing conditions which may indicate that the protein multimers were generated by formation of intermolecular disulfide bridges.

Because for the future coupling experiments BMP2-K3Plk needed to be site-specifically biotinylated, instead of 3-azido-7-hydroxycoumarin, a short PEG4-carboxamide-6-Azidohexanyl-Biotin linker was used for further reaction optimization. To reach optimal reaction efficiency the coupling was performed at two different temperatures and with several different reaction times (Figure 37 and Figure 38A). All reactions were performed in 3.7M urea and 0.1M HEPES buffer pH 7.2.

Figure 37: Site-specific biotinylation of BMP2-K3Plk at 37°C

BMP2-K3Plk was coupled to PEG4-carboxamide-6-Azidohexanyl-Biotin using CuAAC coupling conditions at 37°C in urea buffer. The samples were analyzed by SDS-PAGE, coomassie staining and Western blot. Western blot was developed using Streptavidin-Alexa Fluor® 488 Conjugate. The reactions were performed over the time course of 1h. BMP2-K3Plk and BMP2-wt multimers are indicated with arrows. Two negative controls were used : BMP2-wt reacted with PEG4-carboxamide-6-Azidohexanyl-Biotin and BMP2-K3Plk reacted with PEG4-carboxamide-6-Azidohexanyl-Biotin without CuSO$_4$ in the reaction buffer. As positive control wildtype BMP2 biotinylated using the standard NHS chemistry was used. Legend: M – protein marker; wt – BMP2-wt reacted with PEG4-carboxamide-6-Azidohexanyl-Biotin; NC - BMP2-K3Plk reacted with PEG4-carboxamide-6-Azidohexanyl-Biotin without CuSO$_4$ in the reaction buffer; PC – BMP2-wt wildtype BMP2 biotinylated using the standard NHS chemistry.

As shown in the picture above the click reaction occurred rapidly at 37°C but again led to formation of multimers larger than 40kDa (Figure 37). These multimers could not be observed in the negative control where $CuSO_4$ was not added (Figure 37 lane NC). In the negative control a faint band of the coupled protein was present in in the fluorescent staining. This may suggest that the presence of sodium ascorbate alone in the reaction mixture neither influences the formation of the multimers nor leads to the reduction of disulfide bridges. Formation of multimers was also observed for the wildtype BMP2 which was biotinylated using conventional NHS coupling (Figure 37 lane PC). Direct quantification of the coupled relative to uncoupled protein is not feasible by comparing Western blot and Coomassie Brilliant Blue staining. However, some bands present in the fluorescent staining (representing the coupled protein) marked with a red arrow are barely visible in the coomassie staining. Also the proportion between the bands of approx. 40kDa to the bands of approx. 25kDa is different comparing the fluorescent and Coomassie Brilliant Blue staining which might indicate high sensitivity of the fluorescent staining and lower than expected reaction efficiency.

In order to reduce the rate of multimers formation the reaction was performed as well at RT. Already after 1 min. of incubation the biotinylated product was detectable in the Western blot (Figure 38 lane 1). The reaction was performed for 1, 2, 5 and 15 min. The maximal biotinylation was observed after 15 min. (Figure 38 lane 15). Reaction conditions at room temperature were chosen due to low multimers formation in comparison to the reaction at 37°C. In order to evaluate the reaction efficiency biotinylated and non-biotinylated BMP2-K3Plk was purified by RP-HPLC (Figure 38B). However, the elution peak of both proteins appeared simultaneously, revealing the same hydrophobicity of the biotinylated and non-biotinylated protein and thus the separation could not be achieved. Therefore, to quantify the efficiency of the reaction, BMP2-K3Plk was coupled to azide-functionalized AlexaFluor® dye and the percentage of the coupled protein in the total protein sample was calculated. The results showed that after 15min. reaction at RT approx. 11% of total BMP2-K3Plk was fluorescently labelled. The time of the reaction could be prolonged to improve the coupling efficiency, however in order to prevent formation of a higher number of multimers these conditions were used for further experiments.
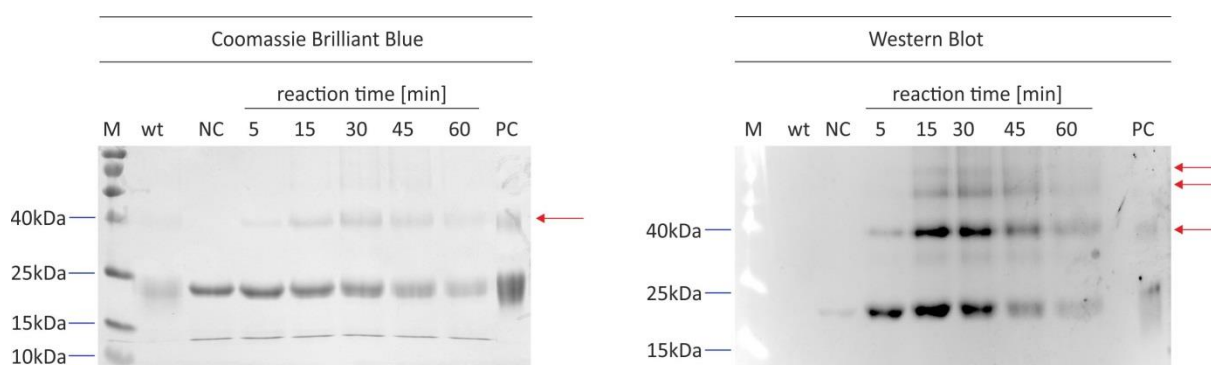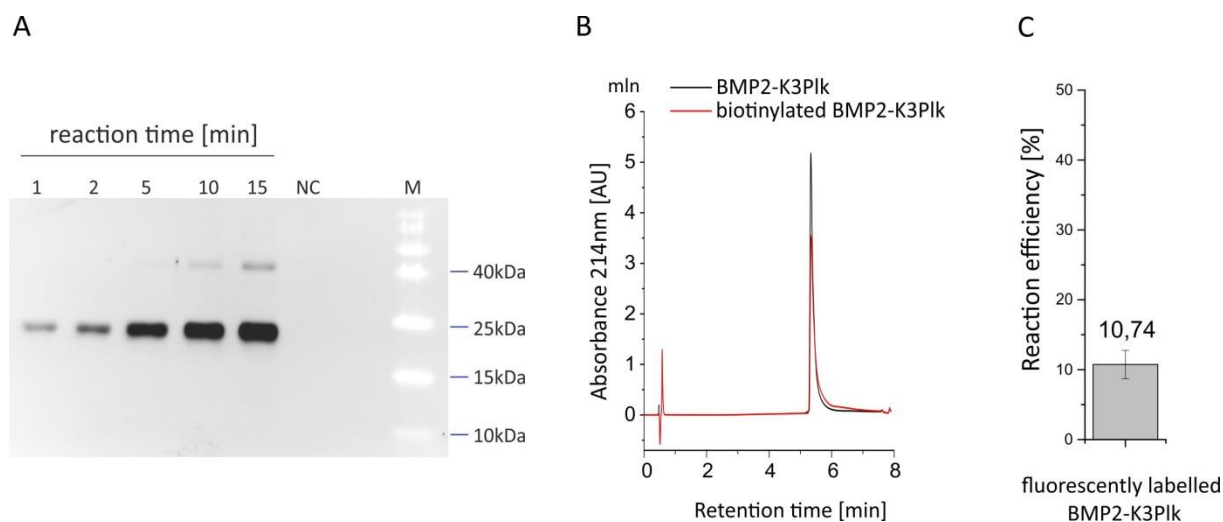
Figure 38: Copper catalyzed site-specific biotinylation of BMP2-K3Plk at RT

BMP2-K3Plk was coupled to PEG4-carboxamide-6-Azidohexanyl-Biotin using CuAAC coupling conditions at RT in urea buffer. (A) Western blot. The samples were analyzed by SDS-PAGE and Western blot.. Western blot was developed using Streptavidin-Alexa Fluor® 488 Conjugate. The reactions were performed over the time course of 15min.. As negative control the reaction was performed in absence of $CuSO_4$. Legend: NC – BMP2-K3Plk reacted with PEG4-carboxamide-6-Azidohexanyl-Biotin for 15min. in absence of $CuSO_4$; M – protein marker; (B) Reversed phase chromatography of biotinylated BMP2-K3Plk. In order to evaluate the efficiency of biotinylation BMP2-K3Plk reacted for 15min. at RT with PEG4-carboxamide-6-Azidohexanyl-Biotin was subjected to reversed phase chromatography. As reference non-treated BMP2-K3Plk was used. The evaluation of reaction efficiency was not feasible with this method as reacted and non-reacted BMP2-K3Plk were eluted with the same retention time. (C) Evaluation of the coupling efficiency. BMP2-K3Plk was coupled to Alexa Fluor® 488 Azide using CuAAC reaction conditions for 15min. at RT. The percentage of the labelled protein in the total protein sample was evaluated by fluorescent measurement. The diagram represents the mean value of 3 replicates ± SD.

2.12 Site-specific biotinylation of BMP2-K3Plk

In order to immobilize BMP2-K3Plk in a site-specific manner to a surface two parallel strategies were followed: direct covalent coupling to azide-functionalized agarose beads and coupling via a short biotinylated PEG linker functionalized with an azide group. Coupling using a short linker could increase the flexibility of the ligand immobilized to a surface. In case of immobilization via a linker BMP2-K3Plk was first coupled to PEG4-carboxamide-6-azidohexanyl-biotin in a site-specific manner using the CuAAC click chemistry. In the second step the biotinylated protein was incubated with neutravidin-functionalized agarose beads. In order to evaluate the influence of biotinylation on the BMP2-K3Plk activity a bioactivity assay was performed (Figure 39). It was expected that the site-specific biotinylation of BMP2-K3Plk would not influence its activity since the propargyl-lysine residues of the protein are situated outside of the receptor binding sites. The results showed that EC50 value

for the untreated BMP2-K3Plk was 23.5nM (+/- 3.3) and 39.2nM (+/- 4.5) for the biotinylated BMP2-K3Plk. Although the EC50 value for the biotinylated BMP2-K3Plk was lower in comparison to the untreated sample, 39.2nM is still in the activity range reported for the BMP2-wt in the literature (*88*).
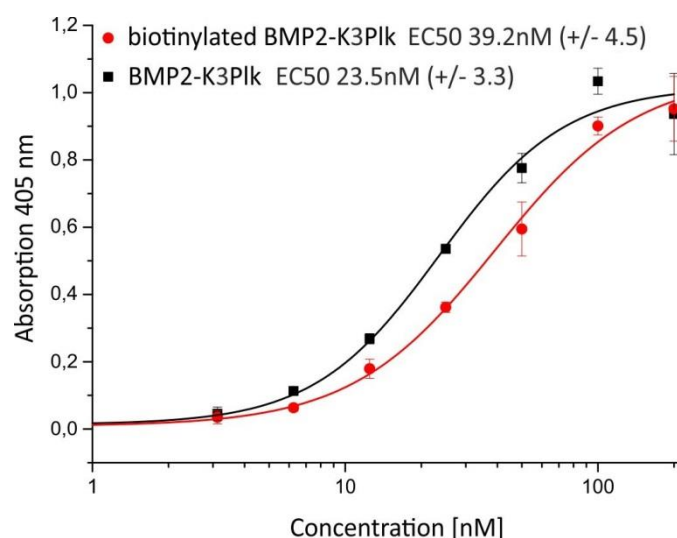
Figure 39: Bioactivity validation of site-specifically biotinylated BMP2-K3Plk

The bioactivity was measured in C2C12 cells using alkaline phosphatase assay. Cells were incubated with log-2 dilutions of non-treated and site-specifically biotinylated BMP2-K3Plk. The EC50 values were generated using using logistic model y = A2 + (A1-A2)/(1 + (x/x0)^p). Each point represents the mean value from at lesast 2 biological replicates ± SD.

2.13 Immobilization of BMP2-K3Plk to neutravidin-agarose beads

BMP2-K3Plk variant was further coupled to neutravidin agarose beads. As a negative control BMP2-wt was used with the same reaction conditions. The majority of the uncoupled protein remained in the supernatant (Appendix, Fig. 2). The rest of the uncoupled protein was extensively washed with the HBS_{500} buffer, 4M $MgCl_2$, and PBS. For the BMP2-K3Plk the non-coupled protein was already completely washed with the first HBS_{500} washing step (Appendix, Fig. 2). Wildtype BMP2 was observed in the supernatant however no bands were visible in the subsequent washing steps. Possibly, a part of the uncoupled wildtype BMP2 remained adsorbed to the surface of the beads. Multiple bands are visible in the supernatant of coupled BMP2-K3Plk in SDS-PAGE. These bands were not visible previously in WB

developed using fluorescent neutravidin (Figure 38). This difference might be caused by the sensitivity difference between silver and fluorescent staining. The silver staining can already detect 1ng of the protein whereas the staining using a neutravidin Alexa fluor 488® depends strongly on the WB efficiency and the stringency of the washing steps. Formation of the multimers could also be affected by a higher reaction volume, more intensive mixing of the reaction and therefore higher exposure to oxygen from the air.

As first analysis of BMP2 immobilized to the beads a fluorescent staining was performed. The staining was performed in order to validate the coupling and to elucidate whether a part of wildtype BMP2 remained non-covalently bound to the surface of the beads. The coupling was verified by fluorescent staining with a BMP2-antibody.
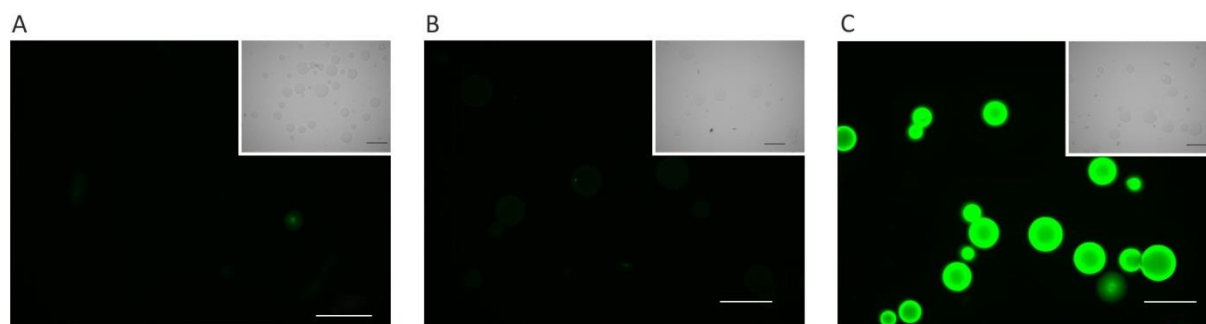
Figure 40: Detection of BMP2-K3Plk coupled to neutravidin agarose beads
BMP2-K3Plk was site-specifically and covalently coupled to PEG4-carboxamide-6-Azidohexanyl-Biotin. The biotinylated product was then coupled to neutravidin agarose beads by bioaffinity interaction. BMP2-wt and uncoupled beads were used as negative controls. The presence of BMP2 on the beads was verified by incubation with the primary BMP2 antibody and secondary fluorescent antibody. The scale bars represent 200nm. (A) uncoupled neutravidin agarose beads; (B) neutravidin agarose beads reacted with BMP2-wt; (C) neutravidin agarose beads coupled to BMP2-K3Plk.

Results obtained from the fluorescent microscopy showed no detectable staining for uncoupled neutravidin-agarose beads (Figure 40A). The same beads reacted with wildtype BMP2 also showed no fluorescent signal (Figure 40B) indicating that wildtype BMP2 could not be immobilized under these conditions. Only neutravidin-agarose beads which were coupled with the BMP2-K3Plk variant showed an intensive fluorescent signal (Figure 40C) indicating specific covalent coupling of BMP2-K3Plk onto neutravidin-agarose beads.

2.13.1 Quantification of BMP2-K3Plk immobilized to neutravidin beads

Since fluorescent visualization does not allow a quantitative analysis of BMP2 coupled to the beads, a colorometric BCA (bicinchoinic acid) protein assay was performed. Determination of the BMP2-K3Plk amount immobilized per bead is crucial for perspective *in vivo* studies. For *in vivo* experiments a precise dose of the protein should be applied at the implantation site in order to be able to relate the effect of the treatment to the applied dose. Gaining the knowledge of the protein quantity immobilized per bead (or per cm^2 of an implant) is essential for the personalization of any implant. Saturation of the scaffold that is optimal for the bone healing process needs to be determined during initial *in vivo* studies also taking into account different sites of the body. Thereby a personalized scaffold dependent on the position of the defect might be constructed. Such modification can be achieved by the adaptation of the reaction time (e.g. concentration of BMP2-K3Plk applied to the reaction) or adaptation of the number of functional groups present within the scaffold.
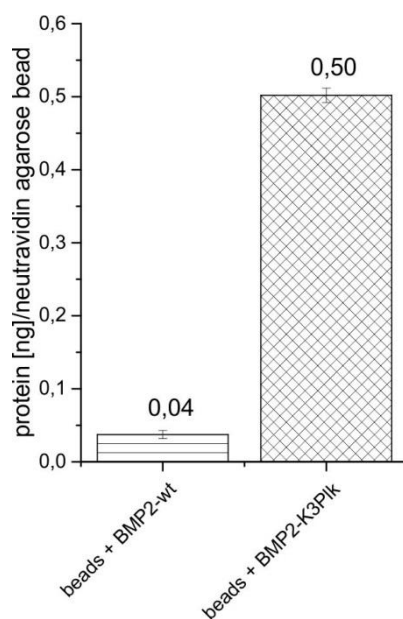
Figure 41: Quantification of BMP2-K3Plk coupled to neutravidin-agarose beads
The quantity of BMP2-K3Plk in nanograms was quantified using BCA protein assay. Beads reacted with BMP2-wt were used as negative control. The mean absorption value for the uncoupled beads was subtracted from the experimental samples. Bars represent the mean values ± SD of 3 replicates.

As depicted in the figure above (Figure 41) approx. 0.50 ng of BMP2-K3Plk was immobilized per one neutravidin-agarose bead, whereas only a background amount of approx. 0.04ng of BMP2-wt per one bead has been detected. The limiting factor determining the saturation of

the biotinylated BMP2-K3Plk on neutravidin-agarose beads was probably the number of neutravidin molecules present on the beads. According to the information provided by the manufacturer 1ml of the settled resin can bind 8mg of biotinylated BSA. However, BSA molecules (BSAmw=66,5) are approx. 2,5 times larger than BMP2-K3Plk dimers, therefore one could estimate that approx. 307nmoles of the BMP2-K3Plk variant could maximally bind to 1ml of the resin. As only 50µl of the neutravidin beads were added to the coupling reaction 7,7nmoles of BMP2-K3Plk could in theory maximally bind to the beads. The amount of the dimeric BMP2 used for the reaction was 10nmoles which means that the BMP2 molecules were used at excess.

2.13.2 Interaction of bead-immobilized BMP2-K3Plk with the BMPRIA receptor ectodomain

To verify whether BMP2-K3Plk immobilized on neutravidin-agarose beads preserved a bioactive structure towards main BMP2 receptor, the coupled protein was incubated with fluorescently-labelled BMPRIA receptor ectodomain.
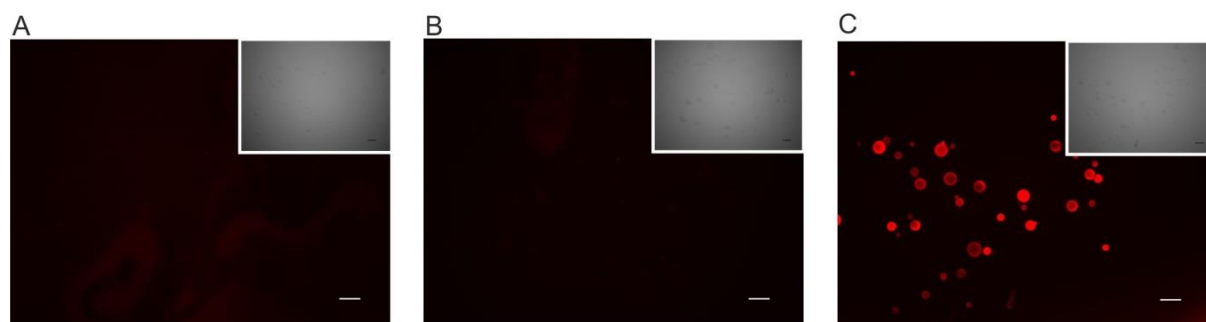
Figure 42: Interaction of BMP2-K3Plk immobilized to neutravidin beads with BMPRIA receptor ectodomain
The neutravidin-agarose beads coupled to BMP2-K3Plk were incubated with fluorescently-labelled BMPRIA ectodomain. The beads were washed and visualized by the fluorescent microscopy. As control uncoupled beads and beads reacted with BMP2-wt were used. The scale bars represent 200nm. (A) uncoupled beads; (B) neutravidin agarose beads reacted with BMP2-wt; (C) neutravidin beads coupled to BMP2-K3Plk.

According to expectations the results showed no staining for uncoupled neutravidin beads (Figure 42A), as well as for the beads reacted with BMP2-wt which indicates that BMPRIA receptor ectodomain did neither interact with uncoupled beads, nor with the beads that had been previously reacted with BMP2-wt (Figure 42B). The beads showed no detectable

autofluorescent signal. On the contrary, an intensive fluorescent signal was detected for beads coupled to BMP2-K3Plk variant (Figure 42C). These results indicate that only the beads coupled to the BMP2-K3Plk variant were able to bind molecules of fluorescently-labelled BMPRIA ectodomain. As showed in the previous experiments (Figure 40B and Figure 41) only a background amount of the protein could be detected on the beads reacted with BMP2-wt, therefore it was expected that the beads should also not bind to the BMPRIA ectodomain. It has been shown in the previous SPR experiment (Figure 29) that uncoupled BMP2-K3Plk binds to the immobilized BMPRIA ectodomain with similar K_D value as wildtype BMP2. In this experiment it was investigated whether BMP2-K3Plk immobilized to the solid phase is still able to bind to BMPRIA ectodomain, which is a key mechanism for the signal transduction in a cell based assay. The results prove that upon coupling BMP2-K3Plk is indeed able to bind to the main BMP type I receptor ectodomain. Nevertheless, the quantitative efficiency of binding cannot be determined solely by fluorescent visualization.

2.13.3 Osteogenic potential of BMP2-K3Plk coupled to neutravidin-agarose beads

As final test a cell based assay was performed in order to investigate whether the beads coupled to BMP2-K3Plk show bioactive function towards BMP2-responsive cells. Therefore, neutravidin-agarose beads covalently coupled to BMP2-K3Plk were directly applied onto undifferentiated C2C12 cells monolayer and the assay was incubated for 3 days in a serum starvation conditions – enabling differentiation into osteoblastic lineage. Even though the previous experiments showed that BMP2-K3Plk was successfully immobilized on neutravidin-agarose beads and it was able to interact with the main BMP2 receptor ectodomains in a free as well as immobilized state it was still not known whether the cells exposed to BMP2-K3Plk- functionalized beads would be able to initiate the differentiation events. The difference between the SPR experiments and the cell-based assay using the beads covalently coupled to BMP2-K3Plk is that in the cellular assay both reactants: the BMP2 receptors and BMP2-K3Plk are immobilized: BMP2-K3Plk covalently coupled to the beads and BMP2 receptors as a part of the cellular membrane. Therefore the interaction between both reactants is strongly dependent on the number of the receptors present on the cell surface that are able to interact with BMP2-K3Plk immobilized on the beads. A question to answer should also be what percentage of a cell surface is covered by the functionalized beads and how many receptors on the cell surface need to be simultaneously activated in order to trigger the differentiation events. Another difference, compared to the SPR measurement, is that in

the cell-based experiment both kinds of BMP2 receptors (type I and type II) being a part of the signaling complex are located in a close proximity on the cellular surface. Therefore, it was unknown whether the rigid conformation of immobilized BMP2-K3Plk will hinder the binding with type II BMP2 receptors. Therefore, the aim of the following experiment was elucidate whether the beads coupled to BMP2-K3Plk were and potent enough to trigger osteogenic differentiation of BMP2-responsive C2C12 cells.
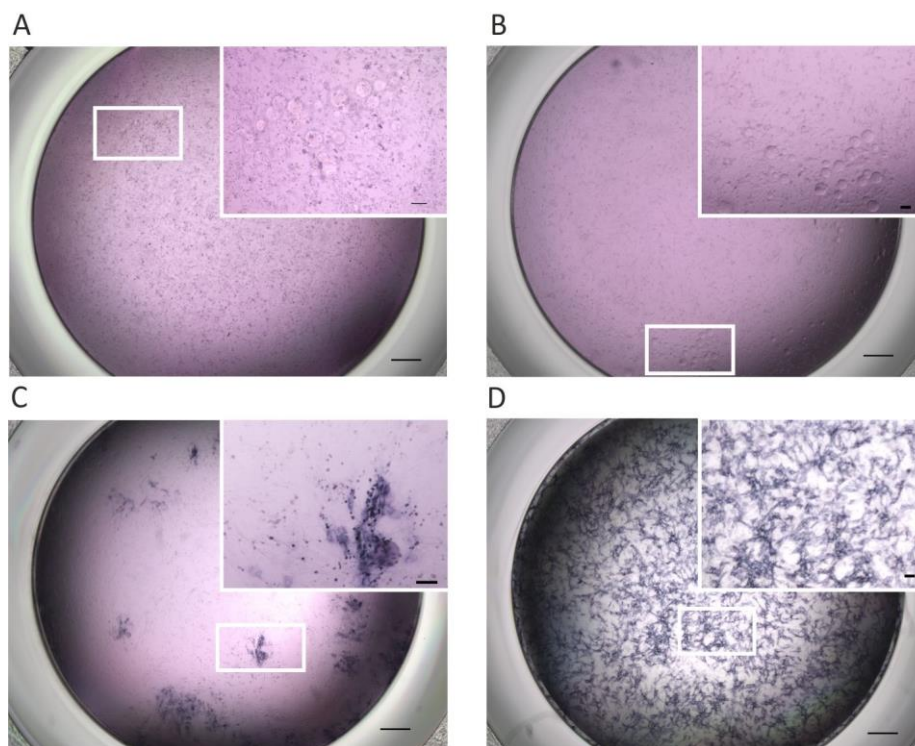
Figure 43: Expression of alkaline phosphatase by C2C12 cells upon exposure to neutravidin-beads coupled to BMP2-K3Plk

Neutravidin agarose beads covalently coupled to BMP2-K3Plk were applied to C2C12 monolayer culture and overlaid with low-melting agarose. Differentiation of C2C12 cell was visualized by dark blue staining of alkaline phosphatase. As negative control uncoupled beads and beads reacted with BMP2-wt were used. As positive control 25nM of soluble BMP2-wt was used. The scale bars represent 500nm in the main pictures and 100nm in the enlargement.. (A) uncoupled neutravidin-agarose beads; (B) neutravidin-agarose beads reacted with BMP2-wt; (C) neutravidin-agarose beads coupled to BMP2-K3Plk; (D) 25nM soluble BMP2-wt

As shown in the figure above, the ALP staining was detected in the well where BMP2-K3Plk-functionalized beads were transferred (Figure 43C) and the staining was highly restricted to the area where the beads were applied. On the contrary, no staining was detected in the area surrounding the beads that were reacted with BMP2-wt (Figure 43B). Similarly, no staining could be detected in wells supplemented with uncoupled beads (Figure 43A). As positive

control 25nM of soluble BMP2-wt was used (Figure 43D) which showed, as expected, uniform staining across the whole well. The above experiment reveals that despite multiple unknown variables that need to be taken into account in the cellular and *in vivo* experiments, BMP2-K3Plk-functionalized beads (carrying 0.5ng of immobilized protein per bead) show biological activity towards C2C12 cells. Nevertheless, for prospective *in vivo* experiments, further analysis should be performed to verify the lowest possible amount of immobilized BMP2-K3Plk per bead that is still able to trigger cell differentiation cascade.

2.14 Direct immobilization of BMP2-K3Plk to azide-functionalized agarose beads

Parallel to linker-mediated coupling, BMP2-K3Plk variant was directly covalently coupled to azide-functionalized agarose beads. Also here BMP2-wt served as negative control in the same reaction conditions. Direct coupling has certain advantages over a linker-mediated immobilization, therefore it was a step forward towards optimization of the BMP2-K3Plk-functionalized beads. Direct coupling reduces the number of immobilization steps, minimizes the cost and does not involve intermediary products, such as streptavidin and biotin. When considered as a future implant material, the beads should optimally not introduce any additional biologically active substances that could have an influence on the regeneration and metabolic processes at the implantation site, such as neutravidin. The beads were thoroughly washed after the coupling procedure (Appendix, Fig.3) and the majority of uncoupled protein remained in the supernatant. Also here, similarly to the immobilization using a biotinylated linker the multimers of BMP2-K3Plk and BMP2-wt were visible in the coomassie staining. The rest of the uncoupled protein was extensively washed with the HBS_{500} buffer, 4M $MgCl_2$, and PBS. Similarly to the coupling via a biotinylated linker no BMP2-wt was detectable in the washing steps. Therefore, a part of BMP2-wt could be non-specifically adsorbed to the surface of the beads, which was verified in the following steps. Similarly to the BMP2-K3Plk immobilization via a bifunctional linker, also here the coupling was validated by fluorescent microscopy. As previously, azide-functionalized agarose beads were incubated with anti-BMP2 antibody and subsequently with a secondary fluorescent antibody. The results of the experiment are depicted below.
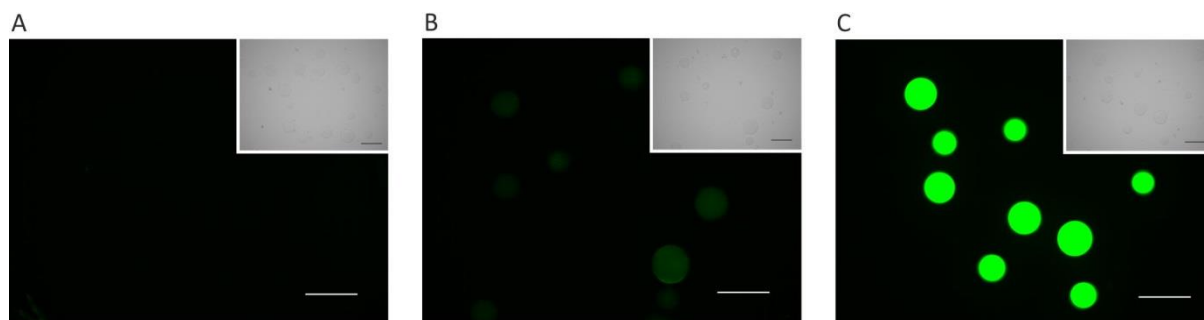
Figure 44: Detection of BMP2-K3Plk immobilized to azide-functionalized agarose beads

BMP2-K3Plk was covalently and site-specifically coupled to azide-functionalized agarose beads. Upon extensive washing steps the presence of BMP2 on the beads was verified by incubation with primary BMP2 antibody followed by a fluorescent secondary antibody. Beads reacted with BMP2-wt and uncoupled beads were used as negative controls. The scale bars represent 200nm. (A) uncoupled azide-functionalized agarose beads; (B) azide-functionalized agarose beads reacted with BMP2-wt; (C) azide-functionalized agarose beads coupled to BMP2-K3Plk.

As visualized in the figure above no fluorescence was detected for uncoupled beads (Figure 44A). In the beads, which had been previously reacted with BMP2-wt, a faint fluorescent signal was observed (Figure 44B). This confirms the assumptions from the SDS-PAGE of the washing steps, that a fraction of BMP2-wt could be immobilized on the beads. It was shown that BMP2-wt is unable to react with azide groups (Figure 37), therefore the weak coating occurred most probably by physical adsorbtion to the surface of the beads. In contrast, beads coupled to the BMP2-K3Plk variant showed a prominent fluorescent signal (Figure 44C). In order to evaluate the coupling efficiency the protein quantification was performed in the further step.

2.15 Quantification of BMP2-K3Plk immobilized to azide-functionalized agarose beads

To determine the quantity of BMP2-wt and BMP2-K3Plk immobilized on azide-functionalized agarose beads, a colorimetric BCA protein assay was used. As shown in the figure below (Figure 45) approx. 0,38ng of BMP2-K3Plk has been successfully immobilized per agarose bead, whereas only a background amount of approx. 0,04ng of BMP2-wt has been detected per azide-agarose bead.
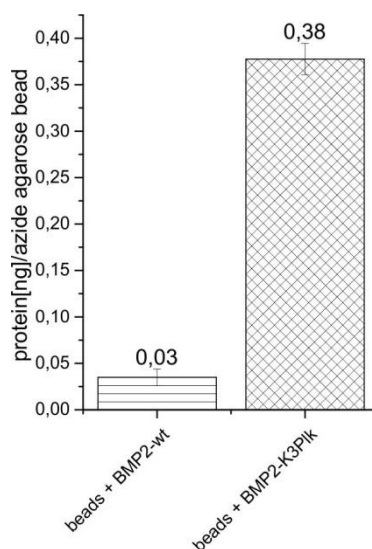
Figure 45: Quantification of BMP2-K3Plk immobilized to azide-agarose beads.

The quantity of BMP2-K3Plk coupled to azide-agarose beads was quantified in nanograms using BCA protein assay. Beads reacted with BMP2-wt were used as negative control. The mean absorption value for the uncoupled beads was subtracted from the experimental samples. Bars represent the mean values ± SD of 3 replicates.

The amount of immobilized BMP2-K3Plk and BMP2-wt is in the same range as for the linker-mediated immobilization (Figure 41). In both scenarios azide groups were present in excess in the coupling reaction. In case of the linker-mediated immobilization PEG4-carboxamide-6-azidohexanyl-biotin was used at 10x molar excess compared to BMP2-K3Plk dimers. However, here the limiting factor was probably the amount of neutravidin molecules present on the surface of the beads. In case of the direct coupling to azide-functionalized agarose beads approx. 20 times molar excess of azide groups compared to dimeric BMP2-K3Plk was used. Therefore the saturation of the active groups on the beads should not be the limiting factor. The distribution of the active groups on the bead surface and the dimensions of BMP2 molecules could play a critical role in this case. No information on the maximal protein binding capacity was provided by the manufacturer, but it can be assumed that the saturation of the functional azide groups was not a limiting factor of the reaction.

2.16 Interaction of agarose bead-immobilized BMP2-K3Plk with BMPRIA receptor ectodomain

Similarly as for linker-mediated coupling of BMP2-K3Plk to neutravidin-agarose beads, also azide-functionalized agarose beads coupled to wildtype BMP2, BMP2-K3Plk as well as non-coupled beads were incubated with fluorescently-labelled BMPRIA receptor ectodomain. The incubation with fluorescent BMPRIA ectodomain was performed in order to validate the affinity of immobilized proteins towards the main BMP2 type I receptor.
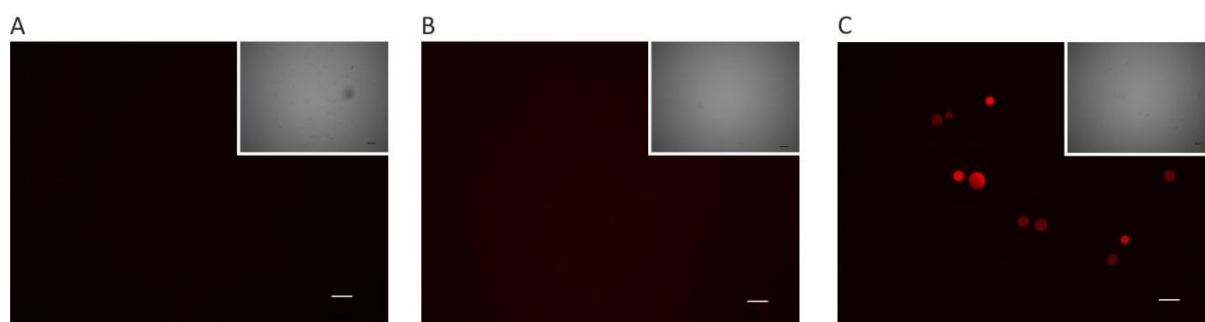
Figure 46: Interaction of BMP2-K3Plk immobilized to azide-functionalized agarose beads with BMPRIA receptor ectodomain

The azide-functionalized agarose beads coupled to BMP2-K3Plk were incubated with fluorescently-labelled BMPRIA ectodomain. The beads were washed and visualized by the fluorescent microscopy. As controls uncoupled beads and beads reacted with BMP2-wt were used. The scale bars represent 200nm. (A) non-coupled azide-functionalized agarose beads; (B) azide-functionalized agarose beads reacted with BMP2-wt; (C) azide-functionalized agarose beads coupled to BMP2-K3Plk.

As shown above, there was no fluorescent signal detected for the uncoupled beads (Figure 46A), nor for the beads reacted with wildtype BMP2 (Figure 46B). This indicates that BMPRIA receptor ectodomain did neither interact with non-coupled beads, nor with the beads reacted with BMP2-wt. It was unknown whether BMP2-K3Plk directly immobilized on the azide-functionalized beads will retain enough flexibility to come in contact with BMP2-binding residues of the receptor ectodomain. However, similarily to BMP2-K3Plk immobilized via a linker, BMP2-K3Plk directly coupled to azide-functionalized beads showed a fluorescent signal on the surface of the beads, indicating an interaction between immobilized BMP2-K3Plk and BMPRIA receptor ectodomain (Figure 46C).

2.17 Osteogenic potential of BMP2-K3Plk-coupled to azide-functionalized beads

To finally verify the osteogenic potential of BMP2-K3Plk covalently and site-specifically coupled to azide-functionalized polymeric structures, non-coupled beads, beads reacted with wildtype BMP2, and beads covalently coupled to the BMP2-K3Plk variant were applied onto monolayer of C2C12 myoblast progenitor cells. The cells and beads were subsequently overlaid with agarose to assure their immobilization. After 3 days in serum starvation conditions cells were examined for osteogenic differentiation. In the first approach BMP2-K3Plk was covalently coupled to azide-functionalized silica particles, followed by harsh washing steps. The physical characteristics of azide-functionalized silica particles provide certain benefits in cell-based experiments and microscopical visualization. The silica beads are well visible using the light microscopy and sink to the bottom of the agarose gel when applied to C2C12 cells enabling direct contact between the particles and the cell surface. However, despite harsh washing conditions applied to beads directly after coupling procedure, wildtype BMP2 still remained non-covalently adsorbed to the surface of the beads. This might be observed in Figure 47C,D. Optimally, no staining should be observed in these wells, as CuAAC reaction does not result in coupling between wildtype BMP2 and functional azide groups on the surface of the beads. Therefore, no BMP2-wt should remain on the beads. Apart from the alkaline phospatase staining detected in the proximity of azide-functionalized silica beads coupled to BMP2-K3Plk (Figure 47E,F), the release of physically adsorbed BMP2-wt also triggered differentiation of C2C12 cells visualized by the dark blue staining (Figure 47C,D). Physical adsorbtion of BMP2-wt led to a conclusion that despite their indisputable visual advantages, silica particles are not an appropriate material to study covalent BMP2 immobilization. As the reaction for both: BMP2-K3Plk and BMP2-wt was performed for 15min and 2h a decreased bioactivity of the both proteins coupled for 2h compared to 15min. was observed (Figure 47C,E). In the wells supplemented with the beads treated for 2h a weak, and random staining for alkaline phosphatase was detected, which was not co-localized with the beads (Figure 47C,E). On the contrary in the wells supplemented with the beads reacted with BMP2-K3Plk and BMP2-wt only for 15min. a strong ALP staining close to the beads could be detected (Figure 47D,F).
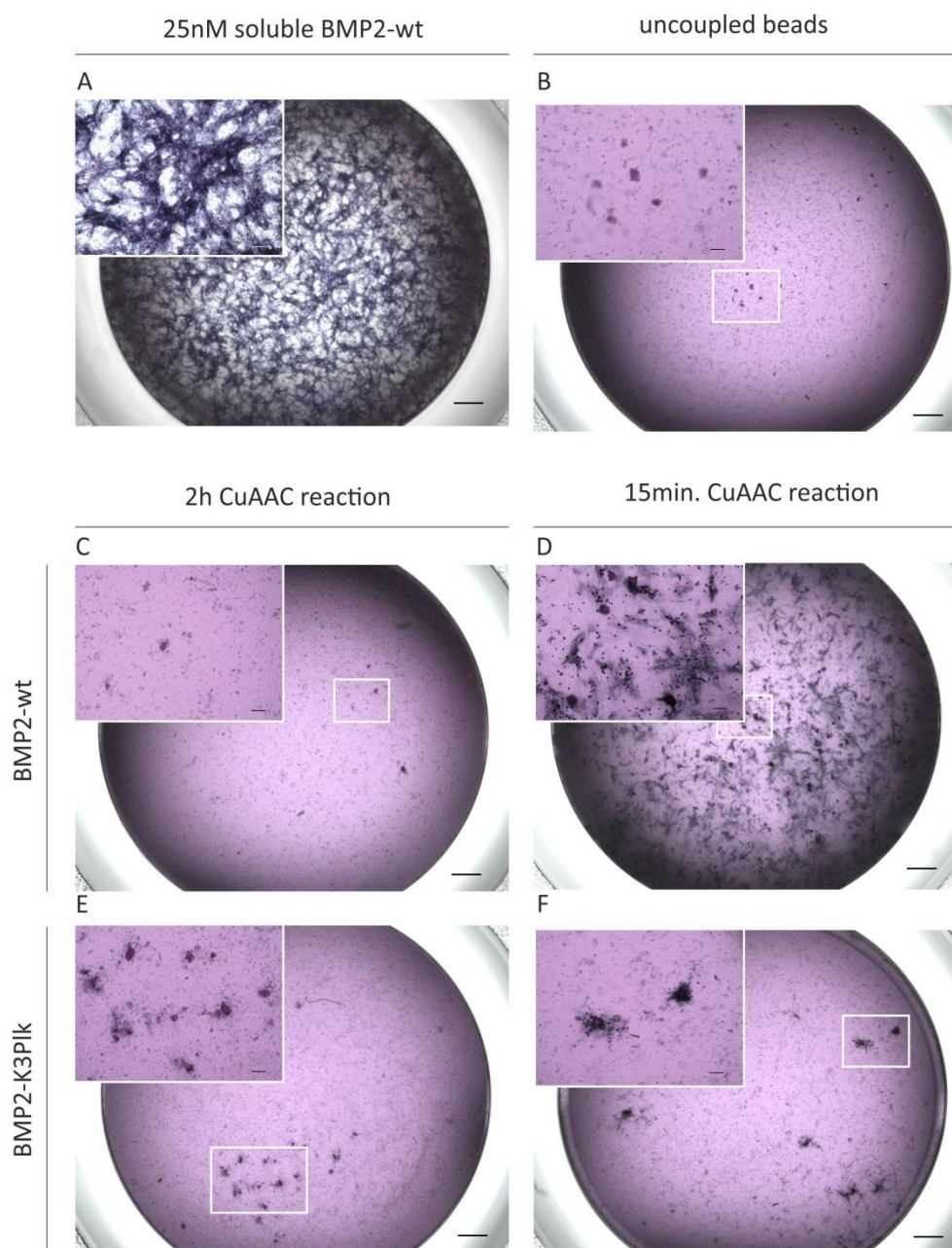
Figure 47: Expression of alkaline phosphatase by C2C12 cells upon exposure to azide-functionalized silica particles covalently coupled to BMP2-K3Plk

Silica particles were coupled to BMP2-K3Plk for 15min. or 2h using CuCAAC reaction. The aim of the experiment was to improve the attachment of the beads to the cell surface compared to agarose beads and to compare the bioactivity of BMP2-K3Plk reacted with the silica particles for 15min. to particles reacted with BMP2-K3Plk for 2h. As negative controls uncoupled azide-functionalized silica particles and azide-functionalized silica particles reacted with BMP2-wt were used. As positive control 25nM soluble BMP2-wt was used. (A) 25nM soluble BMP2-wt; (B) uncoupled azide-functionalized silica particles; (C) azide-functionalized silica particles reacted with BMP2-wt for 2h; (D) azide-functionalized silica particles reacted with BMP2-wt for 15min.; (E) azide-functionalized silica particles coupled to BMP2-K3Plk for 2h; (F) azide-functionalized silica particles coupled to BMP2-K3Plk for 15min.

Considering the results from the above experiment showing adsorbtive properties of the silica particles BMP2-K3Plk was covalently coupled to azide-functionalized agarose beads using CuAAC reaction scheme of 15min. and 2h. The beads were applied onto C2C12 cells as described previously.
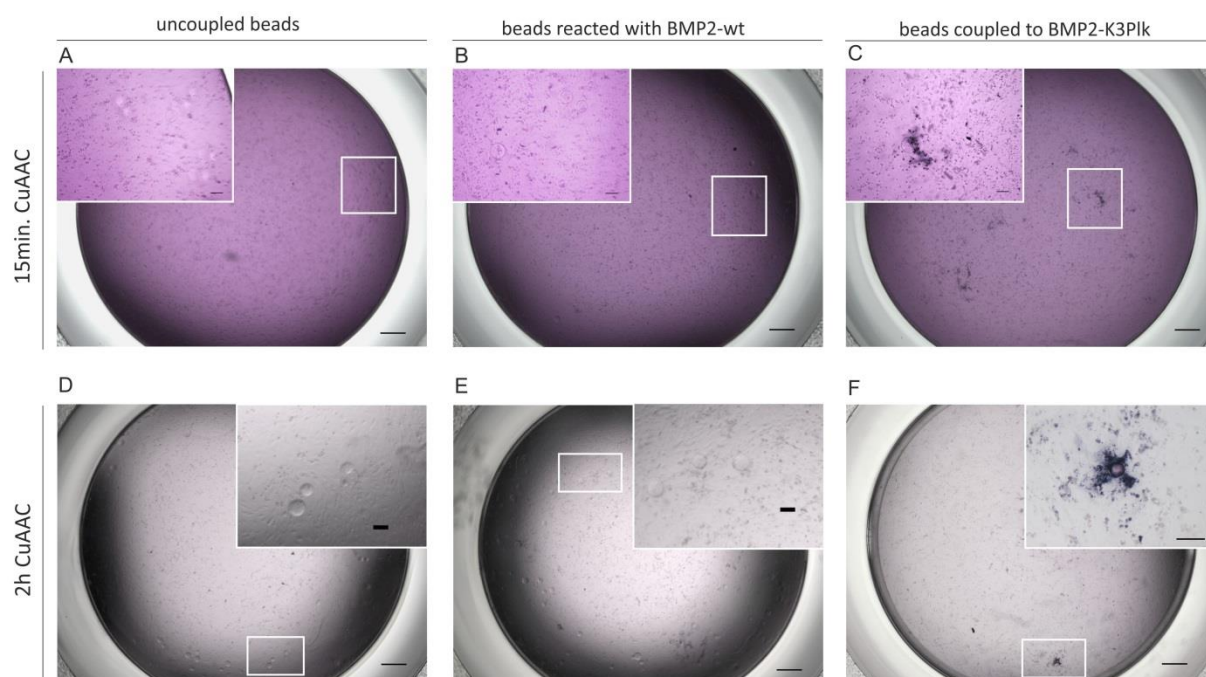
Figure 48: Expression of alkaline phosphatase by C2C12 cells upon exposure to azide-functionalized agarose beads covalently coupled to BMP2-K3Plk

Azide-functionalized agarose beads covalently coupled to BMP2-K3Plk for 15min. and 2h were applied to C2C12 monolayer culture and overlaid with low melting agarose. Differentiation of C2C12 cell was visualized by dark blue staining of alkaline phosphatase. As negative controls uncoupled beads and beads reacted with BMP2-wt were used. The scale bars represent 500nm in the main pictures and 100nm in the enlargement.

As shown in the Figure 48A,B and Figure 48D,E in wells supplemented with uncoupled azide-functionalized beads, as well as with beads reacted with wildtype BMP2 no ALP staining could be detected indicating that the background amount of BMP2-wt adsorbed to the surface of the beads (Figure 44B) was too low to induce BMP2-dependent ALP expression. In contrast to these results, localized osteogenic differentiation was observed in the wells supplemented with beads covalently coupled to BMP2-K3Plk, with the staining strictly restricted to the position of the well where the beads were applied (Figure 48C,F). The difficulty of applying azide-functionalized beads to the cell-based assay was that the beads embedded in the agarose layer were partially fixed above the cell surface. This caused a situation where a part of the beads was not in the direct contact with the surface of the cells.

The beads fixed on the top of the agarose layer could also not be observed while the cells were visualized using microscopy. Moreover, the agarose beads were not clearly distinctive during microscopical visualization because of their transparent characteristics. Whereas all silica beads transferred to the wells could be captured during microscopical visualization of the ALP staining, the visualization of agarose beads imposed some difficulties. In light of the results from the cell based assay involving azide-functionalized silica particles (Figure 47C,E vs D,F) it could also be noticed here that more azide-functionalized agarose beads coupled to BMP2-K3Plk were able to induce ALP expression in the cell culture well when the coupling reaction had been performed for 15min. (Figure 48C) compared to 2h (Figure 48F). Therefore, it may be assumed, that an extended duration of the CuAAC reaction is not desirable when BMP2-K3Plk is coupled to macroscopic structures, such as agarose beads. Even when shorter reaction time may correspond to lower coupling efficiency, the bioactivity of the coupled beads seems clearly higher for the shorter reaction time.

IV.   Discussion

Despite intensive research in the field of tissue engineering and tremendous achievements in material sciences leading to development of biocompatible and bio-mimicking synthetic scaffolds, treatment of skeletal injuries, especially non-healing bone defects still remains a challenge of nowadays medicine. Even though some treatment strategies seem to be promising based on positive outcomes from in vitro experiments, many of them show unsatisfactory results in animal studies, and the majority fails upon facing randomized clinical trials. Various approaches have been tested so far in terms of skeletal defect repair, from implanting plain biocompatible scaffolds, which provide mechanical stability and the growth surface for osteoblasts (*89–92*), through delivery of genes coding for specific bone-inducing growth factors (*93, 94*), up to transplantation of pluripotent mesenchymal stem cells (*95, 96*). The cocktail of growth factors in the extracellular space strongly determines differentiation and repair events within the tissue, therefore one of the strategies to induce bone regeneration would be implementation of biomimetic scaffolds functionalized with osteogenic factors, which might be then either freely released into the extracellular space or remain covalently attached to trigger differentiation through juxtacrine signaling. Various scaffolds enriched in growth factors, responsible for cellular differentiation or tissue vascularization have been developed in the past (*97, 98*). One of them (i.e. INFUSE® Bone Graft), containing recombinant BMP2 as an active agent, has been approved by the Food and Drug Administration (FDA) already in 2002. BMP2 is one of the most potent osteogenic growth factors, which introduces superior bone forming characteristics to the scaffold. However, the bottleneck of the INFUSE bone graft is its narrow application range, which entails unapproved medical practices, leading to severe health consequences. It has been reported that as much as 85% of procedures using BMP2-containing INFUSE® bone grafts were performed off-label (*99*), which means that the implantation manner or place of implantation was either not tested or it has not been positively evaluated in clinical trials. The consequences of such treatments are the severe side effects that have not been investigated in detail. According to FDA the response mechanism is not known, and no common typical markers have been identified so far (*100*). However, it has been estimated, that the amount of recombinant BMP2 adsorbed to the single INFUSE® graft is higher than it could be detected in 1000 human bone defects (*64*). Therefore, the superphysiological amount of BMP2

immobilized within such implants allows one to speculate that the quantity, characteristics, and mode of signal transmission of BMP2 immobilized therein are directly associated with the side effects mentioned before.

BMPs belong to a large TGF-β family whose members transmit intercellular signals by binding to two types of receptors – 4 different type I and 4 different type II receptors. Upon receptor binding the type I receptor gets activated by the constitutively active type II receptor, which initiates the phosphorylation cascade of SMAD molecules, which further transmit the signal into the cell nucleus. Of these two types of receptors the type I BMPRIA receptor is the one which shows the highest affinity towards the BMP2 ligand, with a KD value of 0.8nM. The type II receptor whose recruitment is also obligatory for signal transduction binds BMP2 with much lower affinity. Among three type II receptors the one which binds BMP2 with the strongest affinity is ActR-IIB with a KD value of 6.3nM, which means 10 times lower affinity than to the BMPRIA receptor (*83*). Because of the dimeric nature of the BMP2 ligand different ligand-receptor assemblies are possible. As a dimer, BMP2 contains receptor binding domains for the type I and the type II receptor chains within each monomer, which allows simultaneous binding of 2 type I and 2 type II receptors, thereby enabling formation of a heterohexameric ligand-receptor complex. The heterohexameric complexes are characterized by a very high sensitivity to BMP2, and a BMP2 concentration as low as 100-300pM is able to trigger SMAD activity in C2C12 cells. However, the signal declines already after approx. 1-2h (*83*). An alternative receptor arrangement may involve only one type I receptor and two type II receptors. Such an assembly represents the majority of the BMP2 receptor complexes present on the surface of C2C12 cells (*83*), which was the cell line used for testing of BMP2 biological activity. In this case half maximal receptor activation can be achieved at ligand concentrations of approx. 10-50nM, which is 100 to 500 fold higher than suggested for the heterotetrameric receptor assembly. Sustained receptor activation can be achieved upon supplementation with 10nM BMP2, which is also the concentration which triggers upregulation of alkaline phosphatese gene expression - an early marker for osteogenic differentiation (*83*). This sustained receptor activation seem also required in vivo. Therefore in case of regeneration of bone defects, a sufficient BMP2 dose supported by its continuous exposure needs to be provided. This might be achieved by different strategies, such as implantation of osteomimetic scaffolds decorated with immobilized BMP2. Immobilization to the scaffold circumvents the limitations imposed by physicochemical characteristics of BMP-2. For bone regeneration purposes BMP-2 cannot be just injected into the body at the defected site, because its half-life in body fluids is too short. Upon intravenous injection BMP proteins

are rapidly cleared from the circulation. Their half-life upon injection differs depending on the model organism used and it has been estimated to be 16min. in the rat and 6,7min. in nonhuman primates (*101, 102*). Because of this fast clearance BMP2 needs to be delivered directly into the defect site in tandem with some kind of a carrier. Such a structure needs to fulfill a wide range of conditions with the most important ones being biocompatibility, mechanical resistance, osteoconductivity and osteoinductivity. This means that the implant material would optimally be biodegradable with the degradation rate close to the rate of new bone formationand and not trigger any unwanted immunological reactions. An optimal implant should also provide a good environment for pluripotent stem cells migrating from the blood stream or surrounding tissues to the wound site in order to enable repopulation of the defected bone area. Therefore, a well-balanced porosity and surface modification need to be considered for medical applications. Size and shape of the scaffold are of a high relevance when it comes to cell-cell contacts. When synthetic or natural beads are to be used as a scaffold, the particles need to be large enough to provide a growth surface for incoming cells and simultaneously enable interaction between cells residing on neighbouring beads. Stability of the bone defects, especially those qualified as critical-size defects is of the highest importance. While critical-size bone defects occurring in the scull area do not require strong stabilization, defects in the weight-bearing bones have to be carefully secured. Therefore, apart from all the aforementioned implant criteria a mechanical stability is a basic prerequisite for a successful outcome of any orthopedic intervention. Yet, in combination with BMP2, an implant fulfilling all the above criteria additionally needs to assure stable release of the protein over the period of several months. This cannot be achieved by physical adsorption of BMP2 to the scaffold, as the protein tends to diffuse over prolonged period of time. Physical adsorption is considered as suboptimal choice as it is inevitably associated with occurrence of burst releases. This is characterized by a sudden and burst release of the majority of bound BMP2 from the implanted scaffold material over the period of several days. Such phenomena are undesired because of 2 main reasons. Firstly, the majority of the protein is removed from the environment and therefore the implant cannot fulfill its primary role. Second disadvantage is that the high local concentration of BMP2 might lead to rapid immunological reactions, which has been repeatedly observed in case of the INFUSE® bone graft. It is not known so far what happens on the cellular level when high doses of BMP2 are released into the extracellular environment. BMP2 is a growth factor that is weakly soluble under physiological conditions. It is best soluble under conditions of low salt concentrations and acidic pH, which are different in physiological fluids. Therefore, one could assume that a bulky release of

BMP2 causes its rapid precipitation and clear-up. In general conclusion, application of high doses of BMP2 by physical adsorption is ineffective and generates high production costs which are not translated into an optimal clinical outcome. There are other methods of physical BMP2 immobilization, which have been investigated in the past, such as encapsulation within hydrogel matrices (*103–105*). Other groups focused on coupling BMP2 to the scaffold via affinity tags. Introduction of any affinity tag within BMP2 sequence is however strictly limited to its N-terminal end, because its C-terminus is buried in the hydrophobic protein core (*106*). Placing the tag in any other position would most likely affect the structure of the protein and its activity. Long tags introduced at the N-terminus of BMP2 are also likely to affect its refolding efficiency, as they might significantly change protein parameters and ionic charge localized at the modified end. A great advantage of genetic codon expansion is that an artificial amino acid could theoretically be introduced at any position within BMP2 sequence without changing significantly its biological and physicochemical characteristics. In this work fully functional dimers of BMP2-K3Plk were generated, with biological activity comparable to the wildtype protein and, as verified by purification using a heparin column, substitution of lysine into propargyl-lysine has not changed the local ionic charge at the N-terminus. Moreover, one great disadvantage of all currently used BMP2 immobilization strategies is an uncontrollable local concentration of BMP2 at the implantation site. Depending on the size of the defect different scaffold dimensions might be used, which entails varying amounts of BMP2 released thereof. Therefore, considering the individual differences in the defect size and thus different sizes of the used implant clinical trials cannot be fully standardized. Several clinical studies have been performed with BMP2 used for treatment of critical-size bone defects. In order to achieve satisfactory bone healing varying quantities of encapsulated BMP2 were recommended depending on the size of the defect, degree of vascularization and implantation site. Pilot clinical trials with BMP2 delivered in granules composed in 60% of hydroxyapatite and in 40% of tricalcium phosphate showed that the optimal dose of BMP2 for inter-transverse arthrodesis and for anterior inter-body fusion is 20mg and 4.2-12mg respectively (*107*). In the randomized clinical study involving 279 patients with degenerative lumbar disc disease varying amounts of BMP2 adsorbed to collagen sponges were applied – from 4.2 to 8.4 mg -depending on the implant size used for each patient. Other publications reported BMP2 doses between 6 and 12 mg per carrier, which was reviewed in detail in Smoljanović et al (*108*). Apart from differences resulting from various defect sizes one needs to consider species-related disparities when interpreting results from animal experiments. When the collagen sponge soaked with BMP2 was used in the bone defect of the rhesus

monkey the most optimal BMP2 dose was estimated to be 1.5mg per collagen carrier (*109*), while only 0.4mg was used in the sheep bone defect (*110*). We hypothesized, that the most controllable way of delivering BMP2 within an implant, providing its maximal exposure, is its covalent immobilization, as already 0.2 ng/cm^2 of immobilized BMP2 were reported to trigger Smad-dependent signaling in BMP2-responsive cells in vitro (*111*). In general, all observations indicate the importance of sustained exposure of BMP2 ligands towards its cognate receptors and minimal doses of applied BMP2 still facilitating bone healing. In the scenario involving covalent immobilization the biological activity of BMP2 would be determined by the half-life time of the scaffold and possibly, by the proteolytic degradation of the protein. However, covalent immobilization of BMP2 has been so far achieved solely by targeting the primary amines of lysine residues. This strategy leads to random positioning of the protein, compromised biological activity, and suboptimal availability towards BMP2 receptors (*112*).

Generally recognized as an undesired side effect, a moderate burst release has yet been proven to be beneficial in some cases. By studying two kinds of hydrogel polymers, one with a low and steady release and the second one showing an initial burst release and further sustained release of BMP2, Bhakta et al showed that the greater bone formation was observed in the latter case in a rat ectopic bone model (*113*). This phenomenon was thought to be triggered by the delayed recruitment of progenitor cells in case of the steady-release hydrogel. Therefore, it has been proposed that an ideal system for BMP2 delivery would involve an initial burst release initiating recruitment of progenitor cells, followed by the sustained exposure of BMP2 towards osteoprogenitor cells, thereby triggering their osteoblastic differentiation. In line with this concept is a theory that using BMP2 in a suboptimal manner does not fully exploit its osteogenic capabilities and therefore such extreme doses of BMP2 are currently used in clinics (*114*). Following this idea our beads functionalized with covalently coupled BMP2-K3Plk might be modified by potentially soaking with low amounts of free wildtype BMP2. In this way a low burst release could be initially achieved followed by sustained juxtacrine exposure towards osteoprogenitor cells, which had migrated into the bone-defect area.

In our work, we investigated two different ways to couple BMP2 to macroscopic structures in a site-specific and covalent manner. For this purpose we used two BMP2 variants, one of which contained an additional cysteine residue thus allowing a coupling by e.g. thiol-iodoacetyl chemistry. Seven cysteines of the wildtype BMP2 are precisely buried within its structure forming intra- and inter-molecular disulfide bridges. Therefore an additional, free

cysteine residue is a promising target for site-specific immobilization. However, this approach carries also some disadvantages. In order to activate the sulfhydryl group of extra cysteine residues, the protein needs so be mildly reduced, which might lead to reduction of other cystine residues and consequently to disruption of internal disulfide bridges. In such situations 100% site-directed immobilization would not possible and the biological activity of the product would likely be affected. The second mutant, BMP2-K3Plk, contained the unnatural amino acid propargyl-lysine which was introduced by genetic codon expansion directly during bacterial protein expression (*115*). A number of pyrrolysine analogs has been synthetized so far and tested for compatibility with *M.barkeri* tRNA^{pyl}/PylRS pair (*116*). For the purpose of this work we chose propargyl-lysine based on a previous publication which showed that this pyrrolysine-derivative most effectively matches the intracellular tRNA^{pyl}/PylRS pair and is efficiently introduced via the amber stop codon at the desired position (*117*). Two different expression hosts were examined for efficient translation of BMP2-K3Plk. Expression induction in BL21(DE3)pLysS strain has not resulted in any significant protein expression, despite different media and temperatures were used. The reason for that might be the T7 lysozyme produced by BL21(DE3)pLysS in order to stabilize potentially toxic genes at low expression level, by inhibiting the activity of T7 polymerase. Inhibited polymerase blocks in turn the transcription of genes downstream of the T7 promoter. Because expression of genes in which an amber codon has been introduced is characterized by slow expression rates, additional suppression mechanisms resulted probably in a complete inhibition of translation. Furthermore, in order to maintain the plasmid encoding T7 lysozyme the bacterial culture was additionally supplemented with high doses of chloramphenicol. In the situation where translation beyond an in-frame amber-codon requires already 2 plasmids maintained by ampicillin and kanamycin supplementation, additional production of chloramphenicol acetyltransferase may greatly inhibit synthesis of the desired gene, as bacterial resources are used for expression of antibiotics-resistance coding genes. Taking into account that both kanamycin and chloramphenicol interfere with the bacterial translation machinery, 2 components of the BMP2-K3Plk translation: the BMP2-K3Plk gene and the pyrrolysyl-tRNA synthetase gene might have been expressed at too low yields , leading to an unsuccessful expression of the modified BMP2 gene. On the contrary, prominent BMP2-K3Plk production was observed when expressed in the *E.coli* strain BL21(DE3). In our experiment, where a range of propargyl-lysine concentrations was used, 10mM propargyl-lysine was found to be the most effective in terms of protein expression, while addition of 1mM of propargyl-lysine has not resulted in any significant expression

yield, which stands in opposition to other proteins which were produced using similar expression systems, such as FGF-2 (*117–120*), which according to our knowledge is the only growth factor which has been expressed with a site-specifically incorporated artificial amino acid. The measured internal concentration of lysine in bacterial cells (*Streptococcus faecalis)* is in the range of 0.035-0.05M, which is up to 5 times higher than that of propargyl-lysine used in our experiment. It is known that the amino acid concentration is greatly increased within the cell cytosol relative to the concentration in the medium. It is possible that the transport of propargyl-lysine across the membrane of E.coli is slower and less efficient than that of the native amino acids, therefore demanding higher initial concentrations (*121*).

Upon successful expression and refolding of BMP2-K3Plk, its biological activity was verified using pre-myoblastic C2C12 cells, which is a well characterized cell line for validating BMPs biological activity (*122*). The assays showed comparable EC50 values for both wildtype BMP2 and the BMP2-K3Plk variant with a difference of the response level observed only at high BMP2 concentrations being probably the consequence of lower solubility of the BMP2-K3Plk variant in medium compared to wildtype BMP2. Similarly, the bioactivity of the second mutant, BMP2-A2C, was examined. The EC50 value of BMP2-A2C was shown to be higher and the maximal ALP response markedly reduced compared to the wildtype BMP2. This result might be explained by the presence of multimeric population of BMP2-A2C variant. It was not feasible to separate BMP2-A2C dimers from multimeric structures neither by ion-exchange chromatography nor by reverse phase HPLC. Hypothesizing that only the dimeric fraction of BMP2 shows full biological activity, the BMP2-A2C multimers most probably affected the result of the ALP assay. One hypothesis explaining the higher EC50 value of BMP2-A2C is that the multimers would still be able to bind to the high affinity BMPR-IA receptor with similar affinity as the wildtype BMP-2 but the recruitment of the type IIreceptor could be restricted because of steric hindrance. That would cause decreased number of activated BMP2 receptors on the cell surface leading in turn to lower cellular responses and hence lower efficacy of BMP2-A2C. The multimeric population of the BMP2-A2C variant might therefore act antagonistically towards the activity of dimeric BMP2. After validating the bioactivity of both BMP2 variants, BMP2-K3Plk was site-specifically biotinylated using a short bivalent PEG linker. To achieve optimal coupling conditions different parameters have been tested, including reaction time and temperature. At higher coupling temperature BMP2 bands of higher molecular weight were generated, therefore RT conditions were chosen for further experiments. Despite some multimers formed during the coupling reaction biotinylated BMP2-K3Plk still showed the activity values being in

106

agreement with the values already published for the wildype BMP2 (*123*). The Copper-Catalyzed Azide–Alkyne Cycloaddition (CuAAC) is an attractive reaction for site-specific protein immobilization as, in contrary to an uncatalyzed reaction it generates only one regioisomer. It transforms terminal alkynes and organic azides exclusively into 1,4-disubstituted 1,2,3-triazoles, thereby providing a uniform protein population (*124*). However, despite its undiscussable advantages, CuAAC reactions should be carefully adapted for particular applications. When used for protein conjugation one needs to consider a changed redox potential and harmful reactive oxygen species generated upon reduction of $CuSO_4$ by sodium ascorbate. Therefore, an addition of a protective ligand is desirable when working with sensitive proteins. THPTA plays a protective role in CuAAC reactions by reducing protein hydrolysis caused by Cu(II) byproducts and capturing radicals and reactive oxygen species arising from redox reactions, which could potentially oxidize amino acid residues, such as histidine (*87*). However, addition of THPTA does not solve the problem of BMP2 multimerization. After long incubation time multimeric species of BMP2 were observed in SDS-PAGE, indicating protein crosslinking. In order to eliminate the side effects caused by the redox reactions CuAAC reaction might be performed without the use of sodium ascorbate and $CuSO_4$. Instead, Cu ions on the first oxidation state can be successfully used. Nevertheless, such reaction involves the use of extremely unstable chemical compounds, such as CuBr, CuI or CuCl, which makes the reaction less efficient. Use of copper and azide compounds in living systems, which are the key components of the CuAAC click reaction, is controversial as azide compounds are considered toxic agents. Sodium azide, frequently used as a preservative in biological samples or laboratory reagents, prevents bacterial growth at very low concentrations and the azide anion is a strong cytotoxin towards which no antidote exists so far and therefore NaN_3 ingestion or inhalation is very dangerous for humans (*125*). Thus use of azide compounds for production of human implants seems suboptimal. Nevertheless, it has been documented that, in contrary to inorganic azide anion and aryl azides, organic alkyl azide compounds are safe for humans. They are not prone to photodecomposition and they are stable at physiological temperatures. Whereas the fear of using azides is still present in biomedical applications, organic azides, such as Zidovudine, also known as azidothymidine (AZT), are already used in clinically approved drugs, such as antiretroviral agent (*126*). Likewise for azide reagents, the concentration of copper compounds in biological samples has to be tightly controlled because of their cytotoxic effect. The recommended upper threshold of copper concentration in biological materials should not exceed 15ppm (parts per million, 1mg/l = 1ppm) (*127*) whereas the concentration of $CuSO_4$

in the coupling reaction between BMP2-K3Plk and the beads was approx. 8ppm. Taking into account that the beads were thoroughly washed upon coupling with several solvents, the copper concentration in the final sample is unlikely to exceed the acceptable standards but it should be precisely analyzed.

After selecting the right parameters for click chemistry reactions BMP2-K3Plk was coupled to polymeric beads following two different strategies. In the first approach the site-specifically biotinylated BMP2-K3Plk was coupled to neutravidin agarose beads. The binding affinity of biotin-neutravidin complex is extremely high, comparable even to a covalent bond ($KD = 10^{-15M}$) (*128*). Binding via a short biotinylated PEG linker facilitated the coupling reaction and provided higher spatial flexibility of the ligand. However, for large scale applications the use of a linker would potentially generate higher production costs. Therefore, in the second strategy BMP2-K3Plk was covalently bound directly to azide-activated agarose beads using orthogonal click chemistry. After excessive washing BMP2-K3Plk coupled to both kinds of spherical beads could be detected by immunochemistry using a BMP2 specific antibody. The disadvantage of non-site-directed covalent coupling using e.g. standard NHS/EDC chemistry may be decreased bioactivity resulting from random targeting of primary amines present in receptor binding domains. This may lead to shielding of the receptor binding site and thus to lower binding affinities to the BMP2 receptors. To prove that the immobilized BMP2-K3Plk ligand remained active and preserved its high affinity towards the BMPRIA receptor the coupled beads along with the controls were incubated with the fluorescently-labelled BMPRIA receptor ectodomain. All the beads coupled to the BMP2-K3Plk mutant either using linker-mediated or direct covalent coupling showed positive fluorescent signal. Analysis of BMP2-A2C-coupled beads was performed accordingly. Also this BMP2 variant was successfully coupled to iodoacetyl-functionalized beads in a covalent manner. However, the main difference between the BMP2-A2C variant compared to BMP2-K3Plk is the lack of reaction specificity. When wildtype BMP2 was reacted with the iodoacetyl-functionalized beads using the same reaction conditions as for BMP2-A2C it was also successfully coupled to similar extent. The reason for the aforementioned observations may be derived from the course of the reaction. In order to activate the free sulfhydryl groups of the N-terminal cysteine a mild reduction was performed in the first step. However, the unspecific reduction reaction could generate reduction of cysteine residues present at different positions of the polypeptide chain. That occurrence would lead to an opening of disulfide bridges and unspecific coupling reactions. Therefore, results from fluorescent microscopy led

us to conclusion that in BMP2-A2C other than the N-terminally introduced cysteines could also be involved in the coupling reaction resulting, at least to some extent, in a non-site-directed immobilization. When BMP2-A2C-coupled beads were incubated with the fluorescently labelled BMPRIA receptor ectodomain a prominent staining was observed. However, in spite of the comparable amounts of BMP2-wt present on the beads, very weak fluorescent signals were observed in this case, which was most probably caused by disrupted cysteine bridges and thus weaker affinities towards the BMP2 type I receptor. In order to quantitatively compare the results for the both mutants and two different immobilization strategies for the BMP2-K3Plk the particle size, material, as well as saturation and distribution of functional groups within the beads should be uniform. However, in this work we used commercially available beads, whose physicochemical properties including size, porosity or number of functional groups were not uniform. Quantitative comparison may therefore be possible only between the proteins immobilized on the same kinds of beads. Consequently, a comparison between different mutants and the different immobilization schemes is possible in a qualitative, but not quantitative manner. The nature of the beads influenced also efficiency of the cellular experiment, as the difference in particle mass was clearly noticeable. While acrylamide and silica particles fixed in agarose gel easily established direct contact with attached cells, some agarose beads were too lightweight to establish contact with the cells. Therefore for the ease of future experiments optimal beads to study covalent immobilization of BMP2 should be in range of at least 100µm in order to cover the majority of the exposed cell surface and firmly settle at the bottom of the well, even when overlaid with a polymeric gel. Small beads are difficult to be microscopically visualized and distinguished from the rounded cells detached from the flask surface. When a bead covers a large cell surface area it is feasible to address a number of BMP2 receptors present on the cells surface simultaneously. Addressing only a few membrane receptors may not be sufficient to generate osteogenic differentiation cascade. Alongside, when the beads are too small higher number of beads per cell is required in order to achieve the same effect. However, the distribution of the seeded beads is non-controllable, therefore the particles may not cover all addressed cells homogenously. Consequently, some of the cells could be differentiated upon contact with the particles, and some not – depending on the saturation of the particles on the cell surface. Therefore, we propose that the bead size for the cellular experiment in the range between 100 and 150µm would be optimal.

We previously verified that both of our mutants: BMP2-K3Plk and BMP2-A2C were biologically active as soluble proteins and that upon immobilization they retained their affinity towards the main BMP type I receptor. We further wanted to confirm that the immobilized mutants were indeed biologically active therefore we performed differentiation experiments using the cell-based assays. The amount of immobilized BMP2-K3Plk was determined to be 0.4-0.5ng/bead for azide- and neutravidin-functionalized agarose beads respectively and 2.5ng/bead of BMP2-A2C for iodoacetyl-acrylamide beads. The average bead surface area used in this work was approx. $31415.93\mu m^2$. It was measured that approx.0.38ng, which is $8,8x10^9$ molecules of BMP2-K3Plk were immobilized to one azide-functionalized agarose bead. Estimating that only 10% of a bead surface coupled to BMP2-K3Plk would come in contact with the surface of the cell, approx. $8,8x10^8$ of immobilized BMP2-K3Plk molecules would be able to interact with the BMP2 receptors. It has been measured that there are approx. 50-200,000 BMP receptor complexes distributed within the membrane of C2C12 cells (*83*). Assuming that also only 10% of the cell surface comes in contact with the surface of the bead, $8,8x10^8$ BMP2-K3Plk molecules would be able to activate 5000 BMP2 receptor complexes, which is approx. 176000 times more than required for equimolar interaction. Therefore, theoretically the saturation of BMP2 on the beads used in this work could be markedly reduced still maintaining the osteogenic potential of the beads. Following the hypothesis that already subnanograms of immobilized BMP2 are able to initiate osteogenic differentiation (*111*) we exposed BMP2-responsive C2C12 cells to close contact with beads coupled to BMP2-K3Plk and BMP2-A2C mutants. Such setup would also provide a clue whether BMP2 has to be transported into the intracellular space in order to achieve full activity. It has been previously reported that upon binding BMP2 is internalized together with its receptors in a process of clathrin- and caveolin-mediated endocytosis (*129*). Despite the BMP2-K3Plk variant was generated for prospective medical applications its potential application range is very broad. Site-specifically labelled BMP2-K3Plk molecules could be used for protein tracking in vivo in order to further elucidate the internalization mechanisms. Tracking of BMP2 is also important in animal experiments to identify the degradation rate of the scaffold and to define what happens with BMP2 molecules upon scaffold degradation. Another application field for the BMP2-K3Plk might be its site-specific coupling to microarray matrices for screening of BMP2 ligands and co-receptors or to chromatography medium giving a possibility for more efficient purification of BMP2 specific antibodies or BMP2 receptors.

There has been an uncertainty in the BMP field whether formation of the complex between the ligand and type I and II receptors on the cell surface is sufficient for the signal transmission. It is not known so far what exactly happens with the complex upon internalization and whether there are any differences in the signaling pathway depending on whether the ligand gets internalized inside the cell or not. However, in vitro studies demonstrated already that covalently immobilized BMP2 is still potent to trigger osteoblastic differentiation by juxtacrine signaling in a SMAD-dependent manner (*111, 130–132*), which implicates that internalization of BMP2 is rather an additional regulatory step (*129*). Similar observations have been published for other growth factors, such as VEGF-mimetic peptides (*133, 134*), and chemically tethered EGF. It has been shown, that covalently immobilized EGF showed better biological responses than its physically adsorbed counterpart. This has been explained by the accumulation of a high local protein concentration at the surface of the scaffold as well as by decreased down-regulation of EGF-receptor-complex endocytosis. Internalization of ligand-receptor complexes depletes both – growth factors and its receptors from the available signaling pool of the extracellular environment (*135*). In another study it was shown that the saturation of immobilized BMP2 as low as $0.2 ng/cm^2$ was already able to induce SMAD-dependent signaling in C2C12 cells, whereas in our work approx. $1,6 ng/cm^2$ BMP2-K3Plk was immobilized on azide-functionalized agarose beads. In that study a remarkable observation was that whereas receptor-mediated SMAD-phosphorylation was declined already after 180 min. upon treatment with free BMP2, the signal was still stable when exposed to the immobilized ligand. The signal quenching upon treatment with free BMP2 might have been caused by proteolytic degradation or internalization of the ligand-receptor complexes, thereby depleting the ligand from the extracellular space (*111*). For the purpose of our experiment C2C12 cells were seeded onto 96-well plate and the beads were applied on top of them and overlaid with 0.4% low melting agarose in order to keep them stationary. The staining for the alkaline phosphatase, which is an early osteoblastic marker revealed areas of differentiated cells exactly in the positions were the beads had been applied. Therefore, it indicates that the differentiation of cells was triggered selectively by BMP2-K3Plk which was immobilized in a site-specific and covalent manner on the beads. This conclusion arises because no staining was observed in the areas where beads previously reacted with wildtype BMP2 were applied. On the contrary, beads that were conjugated to BMP2-A2C also showed patches of staining in their proximity but the same beads incubated with wildtype BMP2 also induced localized differentiation of C2C12 cells. This may indicate, that the coupling reaction was not completely site-specific, targeting rather random cysteines.

Considering the fact that BMP2-K3Plk dimers contain 2 propargyl groups (1 within each monomer) formation of heterodimers between wildtype BMP2 and BMP2-K3Plk would generate the dimers containing only one reactive propargyl group. Pure population of BMP2-wt/BMP2-K3Plk heterodimers would then provide even greater special flexibility of the ligand compared to BMP2-K3Plk homodimers while covalently coupled to the scaffold. Therefore optimization of heterodimers refolding and its further purification would be a step forward towards generation of bone implants with fully flexible and site-specifically immobilized BMP2.

V. Conclusions

In conclusion, we demonstrated generation and site-specific immobilization of two BMP2 variants: BMP2-K3Plk and BMP2-A2C. We have shown that the BMP2-A2C variant immobilized on the beads was able to interact with the BMPRIA receptor ectodomain and induced differentiation of C2C12 cells in a cell-based assay, despite showing decreased efficacy as an uncoupled protein. However, it was also shown that the BMP2-A2C variant could be, at least to some extent, immobilized on the beads in a non-site-specific manner by possible reduction of the internal disulfide bridges under the used reaction conditions. Therefore, the reducing conditions for coupling of the BMP2-A2C variant should be refined and precisely defined. By adjusting the concentration of a reducing agent it may be feasible to modulate which of the disulfide bridges of the BMP2-A2C variant are targeted in the first place. Optimally, only the additional terminal cysteine coupled to a glutathione molecule should be reduced. By using such mild conditions the efficiency of the reducing step and consequently coupling efficiency might be however decreased.

BMP2-K3Plk variant generated by genetic codon expansion and further immobilized on the surface preserved the activity and characteristics of the wildtype protein. Both coupling strategies, direct as well as mediated by a short PEG-biotin linker, led to successful site-specific immobilization of the BMP2-K3Plk variant on the beads, which retained high affinity towards the main BMP type I receptor ectodomain. However, the coupling conditions led to formation of BMP2-K3Plk multimers which could be in the future eliminated by applying a copper-free reaction conditions. Full functionality of the BMP2-K3Plk variant has been finally confirmed in the cell-based assay, where the coupled beads demonstrated osteogenic potential by specific and locally restricted induction of alkaline phosphatase, which is an osteogenic marker, in myoblastic progenitor cells. Therefore we propose that the BMP2-K3Plk variant may be potentially used for biochemical applications as well as for bone graft procedures, while site-specifically and covalently linked to a biocompatible scaffold, especially at the sites of the body where state of the art medical techniques fail to yield a satisfactory therapeutic effect.

VI.   Outlook

The applicability of the system described in this work needs to be further proven in the critical-size defect animal model using a biocompatible scaffold material, such as e.g. collagen matrices. Further optimization is also needed considering the coupling conditions, such as elimination of the sodium ascorbate, which generates reactive oxygen species in contact with $CuSO_4$. One of the possibilities would be usage of copper element with an oxidation state +1, such as CuBr or introduction of a pyrrolysine analog containing a terminal azide group instead of the propargyl group. Such modification would open a broad range of possible reaction schemes, including copper-free click reactions, such as strain-promoted azide -alkyne click chemistry or the phosphine-mediated Staudinger ligation. In order to use this system in a clinical environment further optimization considering the quantity of BMP2-K3Plk immobilized on the scaffold should be implemented. It is of a high importance to determine the lowest effective BMP2-K3Plk saturation on the scaffold. This optimization would reduce the production cost of an implant and maintain the most physiological surrounding for the bone tissue. In this work we hypothesized that the activity of the immobilized ligand will be restricted mainly by the scaffold degradation rate. However, further in vivo experiments need to be performed in order to verify this hypothesis.

VII. Appendix

DNA sequences of BMP2 variants

BMP2-K3Plk

ATGGCTCAAGCC**TAG**CACAAACAGCGGAAACGCCTTAAGTCCAGCTGTAAGAGACACCCTTTGTA
CGTGGACTTCAGTGACGTGGGGTGGAATGACTGGATTGTGGCTCCCCCGGGGTATCACGCCTTTTA
CTGCCACGGAGAATGCCCTTTTCCTCTGGCTGATCATCTGAACTCCACTAATCATGCCATTGTTCAG
ACGTTGGTCAACTCTGTTAACTCTAAGATTCCTAAGGCATGCTGTGTCCCGACAGAACTCAGTGCTA
TCTCGATGCTGTACCTTGACGAGAATGAAAAGGTTGTATTAAAGAACTATCAGGACATGGTTGTGG
AGGGTTGTGGGTGTCGCTAA

BMP2-A2C

ATGGCTCAA**TGC**AAACACAAACAGCGGAAACGCCTTAAGTCCAGCTGTAAGAGACACCCTTTGTA
CGTGGACTTCAGTGACGTGGGGTGGAATGACTGGATTGTGGCTCCCCCGGGGTATCACGCCTTTTA
CTGCCACGGAGAATGCCCTTTTCCTCTGGCTGATCATCTGAACTCCACTAATCATGCCATTGTTCAG
ACGTTGGTCAACTCTGTTAACTCTAAGATTCCTAAGGCATGCTGTGTCCCGACAGAACTCAGTGCTA
TCTCGATGCTGTACCTTGACGAGAATGAAAAGGTTGTATTAAAGAACTATCAGGACATGGTTGTGG
AGGGTTGTGGGTGTCGCTAG
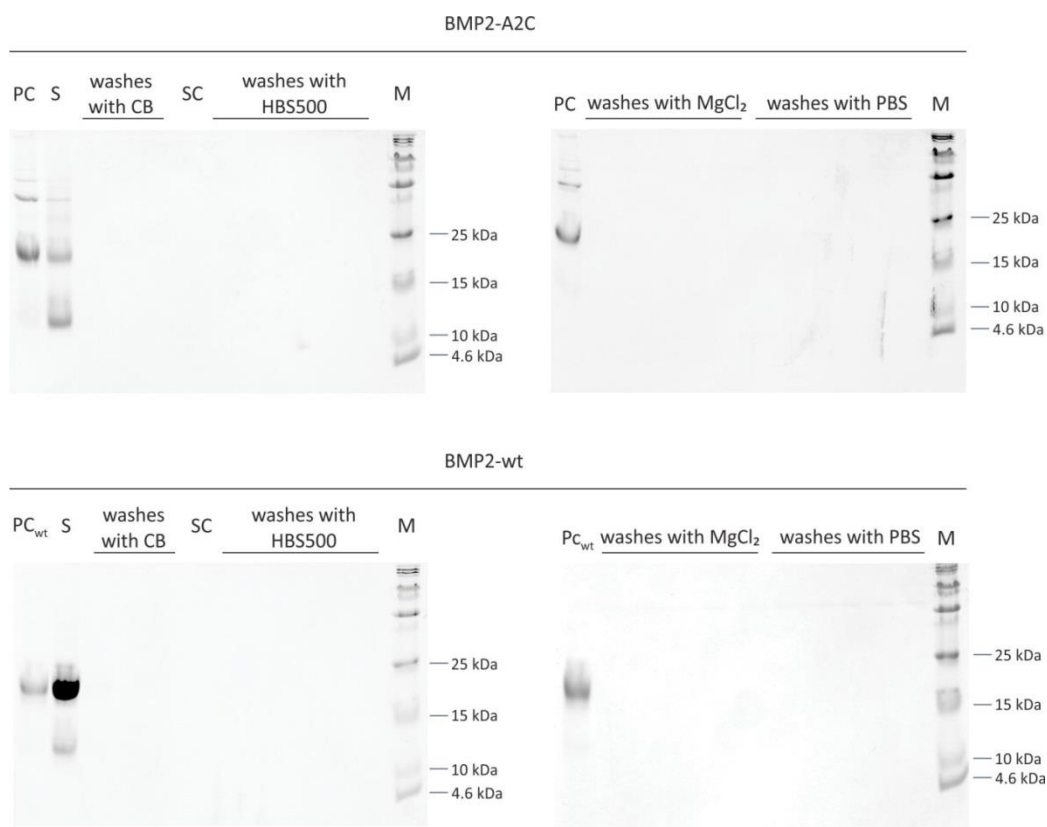
Appendix Figure 1: Washing steps after immobilization of BMP2-A2C on iodoacetyl-functionalized beads
Legend: PC_{wt} – untreated BMP2-wt; CB – coupling buffer; S – supernatant; SC – supernatant after incubation with cysteine; M – protein marker.
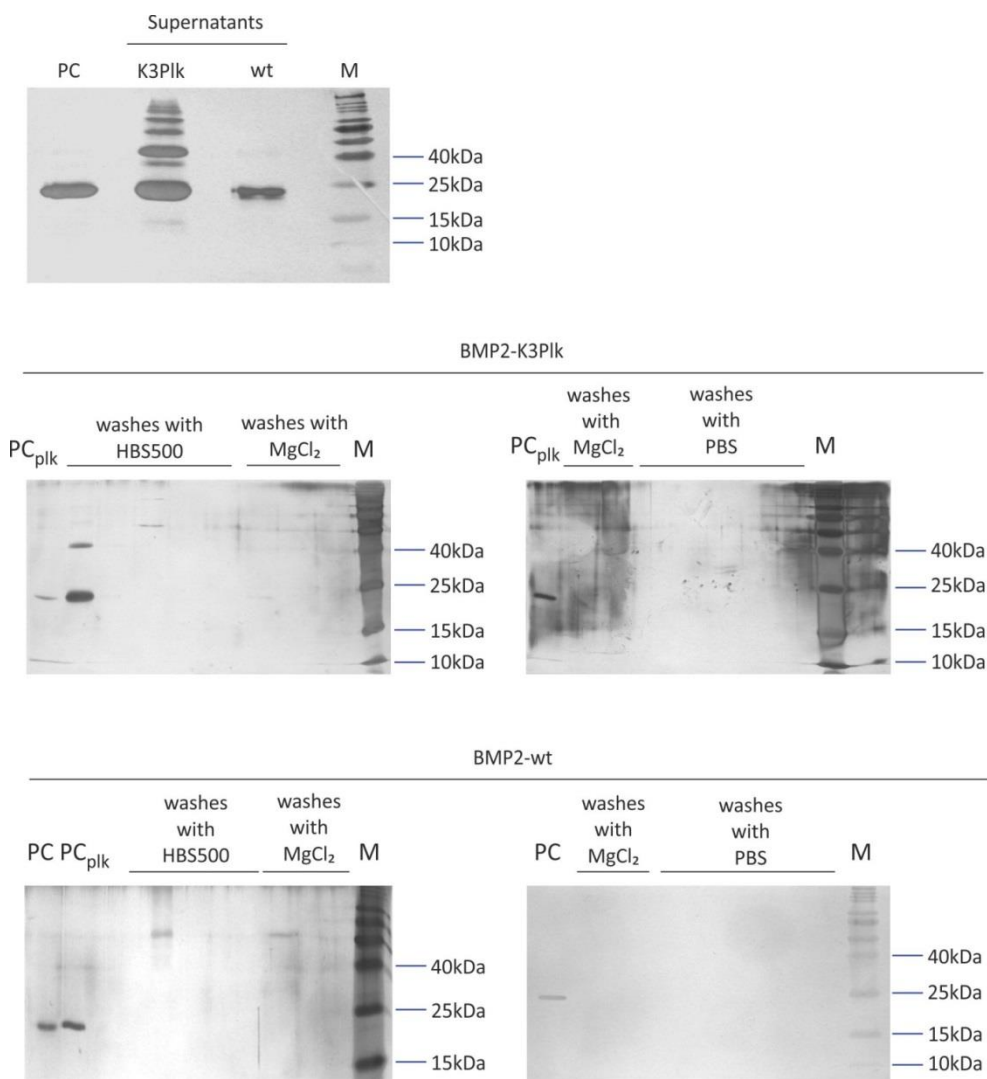
Appendix Figure 2: Washing steps after immobilization of BMP2-K3Plk on neutravidin-agarose beads

Legend: PC – untreated BMP2-wt; PC$_{plk}$ – untreated BMP2-K3Plk; M –protein marker.
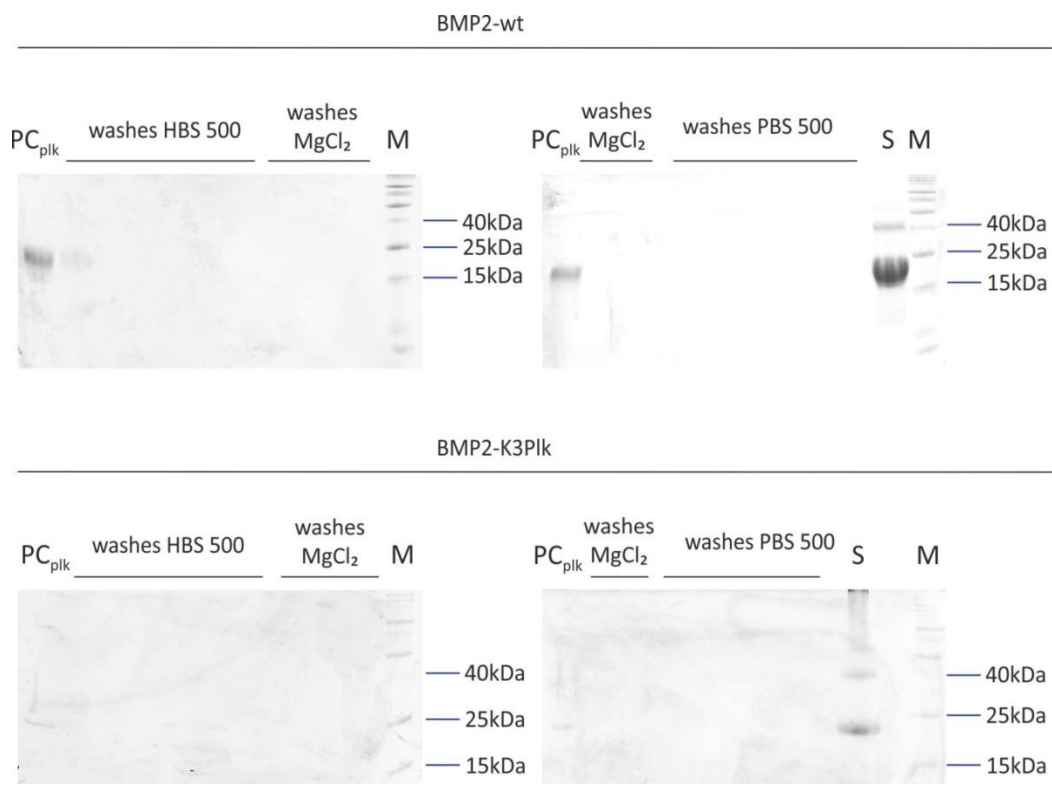
Appendix Figure 3: Washing steps after immobilization of BMP2-K3Plk on azide-functionalized agarose beads

Legend: PC – untreated BMP2-wt; PC$_{plk}$ – untreated BMP2-K3Plk; S – supernatant; M –protein marker.

Buffers and solutions:

Ampicillin 1mg/mL	1g Ampicillin 10mL Millipore water
APS 40% (w/v)	400mg ammonium persulfate Dissolve in 1ml of deionized water
Benzonase buffer	100mM tris pH 7,1 1mM EDTA 3mM MgCL$_2$ 80u/mL Benzonase (final Concentration)
Blocking buffer	5% (w/v) milk powder in TBST
Chloramphenicol 50mg/mL	0,5g chloramphenicol Ad 10ml ethanol absolut
Coomassie destainer	10% isopropanol 10% acetic acid 80% dH$_2$O
Coupling buffer for iodoacetyl chemistry	50mM tris pH 8.5 5mM EDTA 6M urea
CuAAC buffer	Stock solutions 20mM CuSO4 in Millipore water 100mM NaAscorbate in Millipore water 50mM THPTA in Millipore water 1x buffer: 0,1M HEPES; 3,7M Urea; 50μM CuSO4; 5mM NaAscorbate; 250μM
Extraction buffer	50mM NaAc pH 5,0 1mM EDTA 6M GuCL 1mM DTT (fresh)
HBS-150 buffer	10mM HEPES pH 7,4 150mM NaCl 3,5mM EDTA
HBS-500 buffer	10mM HEPES pH 7,4 500mM NaCl 3,5mM EDTA
HPLC buffer A	0,1% TFA in dH$_2$O
HPLC buffer B	Acetonitril 100%
IEX buffer A	20mM NaAcetate pH 4,5 30% isopropanol
IEX buffer B	20mM NaAcetate pH 4,5 30% isopropanol 2M NaCl
IEX urea buffer A	100mM tris pH 5.5 300mM NaCl 5mM EDTA

	6M Urea
IEX urea buffer B	100mM tris pH 5.5 2M NaCl 5mM EDTA 6M Urea
Kanamycin 50mg/mL	0,5g kanamycin 10mL Millipore water
LB	50g trypton 25g yeast extract 50g NaCl Ad 5L pH 7,5
LB-agar	5g trypton 2,5g yeast extract 5g NaCl 7,5g agar Ad 0,5L pH 7,5
Lysis buffer 1	0,1 M Glycin pH 8,5 1% Triton-x-100 1 mM $MgCl_2$ 1 mM $ZnCl_2$
Lysis buffer 2	0,1 M Glycin pH 8,5 1 mM $MgCl_2$ 1 mM $ZnCl_2$
Paranitrophenyl-phosphate solution	Per 1plate: 1,5ml of 20 mg/ml paranitrophenyl-phosphate solution in H_2O diluted 1:10 with lysis buffer 2.
PBS 1x	137 mM NaCl 2.7 mM KCl 10 mM Na_2HPO_4 1.8 mM KH_2PO_4
PI-buffer	23,1g KH_2PO_4 125,4 K_2HPO_4 ad 1L Millipore water
Refolding buffer (BMP2-A2C)	50mM Tris-HCl pH 8,5 50mM Tris-HCl pH 8,5 1 M NaCl 5 mM EDTA 0,5 M GuHCl 0,75 M CHES 2 mM Glutathion reduced 1 mM Glutathion oxidized
Refolding buffer (BMP2-K3Plk)	50mM Tris pH 8.0-8.2 2M LiCl 5mM EDTA 25mM CHAPS 2mM GSH

	1mM GSSG
Running Buffer 10x	30.3g tris base 144.0g glycine 10.0g SDS ad 1L with dH$_2$O
SDS-PAGE sample buffer	3.55ml dH$_2$O 1.25 0.5M tris-HCl, pH 6.8 2.5 ml glycerol 2.0 ml 10% (w/v) SDS 0.2ml 0.5% (w/v) bromophenol blue ad 9.5ml For reducing SDS-PAGE add 50µl β-mercaptoethanol to 950 µl buffer prior to use
STE buffer	10mM tris pH 8,0 150mM NaCL 1mM EDTA 375mM saccharose 1/1000 β-mercaptoethanol (fresh)
TAE buffer 1x	40 mM tris acetate 1 mM EDTA pH 8.2 - 8.4
TB medium	60g bacto trypton 120g yeast 20ml glycerol Ad 4,5L Millipore water 500ml PI-buffer
TBS buffer	10mM tris pH 8,0 150mM NaCL
TBS buffer 10x	25mM tris base pH=7,6 150mM NaCl
TBSE buffer	10mM Tris pH 8,0 150mM NaCL 1mM EDTA 1/1000 β-mercaptoethanol (fresh)
TBST buffer 1x	100ml of 10x TBS buffer 1ml tween Fill up to 1L
TE buffer	100mM tris pH 7,0 20mM EDTA
Transfer buffer 10x	1.92M glycine 0.25M trizma base
Transfer buffer 1x	10ml of 10x transfer buffer 20% Methanol 0.03 % SDS Ad 100ml with Millipore water
Triton buffer	60mM EDTA pH 7,0 6% (v/v) triton X-100

	1,5M NaCL
TSS buffer	2,5ml 1M MgCl$_2$ (95,21g/mol) 5g PEG3000 (2700-3300g/mol) 2,5ml DMSO (78,13 g/mol) Ad 50ml with LB medium pH 6,5 sterilized and stored at -20°C
Acrylamide/Bis (30% T, 2.67% C)	87.6g acrylamide 2.4g N'N'-bismethylene-acrylamide ad 300ml with dH$_2$O
Tris-HCl 0.5M, pH 6.8	6g tris base 60ml deionized water adjust pH to 6.8 ad 100ml with dH$_2$O
Tris-HCl 1.5M; pH 8.8	27.23g tris base 80ml deionized water pH to 8.8 ad 150ml with dH$_2$O

SDS-PAGE Gel formulation (10ml)					
	Gel percentage [%]	DDI H$_2$O	30% degassed acrylamide/bis [ml]	Gel buffer [ml]	10% (w/v) SDS [ml]
Upper tris	4	6.1	1.3	2.5	0.1
Lower tris	12	3.4	4.0	2.5	0.1
12.5µl of 40% APS and 5 µl TEMED for the resolving gel and 12.5µl of 40% APS and 10 µl TEMED for the stacking gel.					

Solutions for the silver staining
Stock solutions: 50% (v/v) aceton in dH$_2$O 50% (w/v) TCA in dH$_2$O 20% (w/v) silver nitrate in dH$_2$O (stored in dark at 4°C) 10% (w/v) Sodium thiosulfate pentahydrate (Na$_2$S$_2$O$_3$) in dH$_2$O (stored in dark at 4°C) 1% (v/v) glacial acetic acid 37% (w/w) formaldehyde
Working solutions: Solution 1) 60ml acetone stock; 1,5ml TCA stock; 25µl formaldehyde Solution 2) 60ml acetone stock Solution 3) 100µl Na$_2$S$_2$O$_3$ stock in 60ml dH$_2$O Solution 4) 800µl silver nitrate stock; 600µl formaldehyde; 60ml dH$_2$O Solution5) 1,2g Na$_2$CO$_3$; 25µl formaldehyde, 25µl Na$_2$S$_2$O$_3$ stock in 60ml dH$_2$O

List of equipment

Equipment	Model	Supplier/Producer
Agarose electrophoresis system	PerfectBlue™ Horizontal mini Gel System	Peqlab
Amicon concentrating cell 400ml	UFSC40001	Merck KGaA
Amicon concentrating cell 50ml	UFSC05001	Merck KGaA
Autoklav Tecnoclav Giessen Tischautoklav Varioklav	Biomedis Systec H+P	
Bacterial shaking incubator	Multitron Standard	Infors HT
Bacterial incubator 37°C		Memmert
Bench centrifuge	Heraeus Multifuge X1R Centrifuge	ThermoScientific
Cell culture incubator	Heraeus Incubator	ThermoScientific
Centrifuge	Avanti J-26 XP	Beckman Coulter
Chromatography system	ÄKTA avant FPLC	GE Healthcare
	BioLogic Duo-Flow Protein Purification System	Bio-Rad
	LaCHromUltraTM HPLC	Hitachi
Fluorescent microscope	BZ-9000 (BIOREVO)	Keyence
Fume hood		Prutscher
Microcentrifuge	Centrifuge 5417R	Eppendorf
Microscope	Axiovert 40C	Zeiss
pH-meter		Mettler Toledo
Plate reader	Infinite M200	Tecan Deutschland GmbH
QuickStand Benchtop System (Hollow Fiber Cartridge, 5000 NMWC, surface 650cm^2	UFP-5-C-4MA	GE Healthcare
Rotor	Rotor JA-10	Beckman Coulter
Rotor	Rotor JLA 8.1	Beckman Coulter
Rotor	Rotor JA-25.50	Beckman Coulter
scale		Satorius
scale	ABJ 220-4M	Kern&Sohn GmbH
scale	EG 2200-2NM	Kern&Sohn GmbH
SDS-PAGE chamber system	PerfectBlue™ Doppel-Gelsystem Twin M	Peqlab
SDS-PAGE gel imaging	FluorChemQ	Biozym Scientific GmbH/Cell

system		Biosciences
Semi-dry blotting chamber	PerfectBlue™'Semi-Dry' Electro Blotter Sedec™M	Peqlab
Sterile hood	Safe 2020 class II safety cabinet EN 12469:2000	ThermoScientific
Surface Plasmon Resonance System	ProteOn XPR36 biosensor system	Bio-Rad
Thermocycler	Labcycler Gradient	SensoQuest GmbH
Ultrasonic	Digital Sonifier 250	Branson
UV- Photometer	Evolution 60S	ThermoScientific

Laboratory material	Supplier	Headquarters	Order number
Amicon Ultra-15 Centrifugal Filter Unit with Ultracel-10 membrane	Merck KGaA	Darmstadt (GER)	UFC901024
HiTrap^{TM} Heparin HP	GE Healthcare	Little Chalfont (UK)	17-0406-01
HiTrap^{TM} SP FF	GE Healthcare	Little Chalfont (UK)	17-5157-01
MobiSpin Column 'F'	Mobitech	Goettingen (GER)	M105010S
Poly-prep® Chromatography columns	BioRad	Hercules, California 94547 (USA)	731-1550
RP C4 column	Machery-Nagel	Düren (GER)	760194.40
Ultrafiltration regenerated cellulose Discs 3kDa, 5kDa, 10kDa NMWL	Merck KGaA	Darmstadt (GER)	PLBC04310 PLCC04310 PLGC07610 PLCC07610
XK26 GE Healthcare column	GE Healthcare	Little Chalfont (UK)	28-9889-51

List of chemicals

Chemical	Supplier	Headquarters	Order number
(+) - Sodium L-ascorbate	Sigma-Aldrich GmbH	München (GER)	A7631-100G
1,4-Dithiothreitol (DTT)	Carl Roth GmbH	Karlsruhe (GER)	6908.4
1-Step™ NBT/BCIP substrate solution	ThermoFisher Scientific	Waltham, Massachusetts (USA)	34042
Acetic acid (100%)	Carl Roth GmbH	Karlsruhe (GER)	6755.2
Acetone (99,5%)	Carl Roth GmbH	Karlsruhe (GER)	5025.5
Acrylamide 30 %	Carl Roth GmbH	Karlsruhe (GER)	A124.2
Agarose	Biozym	Hessisch Oldendorf	840006
Ampicillin sodium salt	Carl Roth GmbH	Karlsruhe (GER)	K029.2
Antarctic phosphatase	New England Biolabs GmbH	Frankfurt am Main (GER)	#M0289L
Anti-BMP2 antibody - Differentiation marker	Abcam		ab 17885
azide agarose beads	Jena biosciences	Jena (GER)	CLK-1038-2
BamHI (Fast Digest enzyme)	ThermoFisher Scientific	Waltham, Massachusetts (USA)	FD0054
Benzonase	Merck		71205-3
Bromphenol blue Na-salt	Carl Roth GmbH	Karlsruhe (GER)	A512
CHAPS	Merck		220201-1KG
CHES			
Chloramphenicol	Carl Roth GmbH	Karlsruhe (GER)	3886.2
Chloroform	Sigma-Aldrich GmbH	München (GER)	372978-1L
Copper(II) sulfate, anhydrous	Alfa Aesar		A13986
D(+) Saccharose	Carl Roth GmbH	Karlsruhe (GER)	9097.1
Disodium phosphate (Na2HPO4)	Hartenstein		CN35
DMEM (1X) + GlutaMAX™	Gibco		61965-026
DMSO	Sigma-Aldrich GmbH	München (GER)	D8418-50ML /D4540-500ML
Donkey Anti-Rabbit IgG H&L (Alexa Fluor® 488) preadsorbed antibody	Abcam		ab150061
EDTA	Sigma-Aldrich GmbH	München (GER)	E5134-1kg
Ethanol, absolute	Sigma-Aldrich GmbH	München (GER)	32205-2.5L
Ethidium bromide	Hartenstein		CE80
FCS	Bio&Sell	Feucht	Lot BS210601.5

FCS	Lonza	Cologne	Lot 8SBO16
Glycerin	Carl Roth GmbH	Karlsruhe (GER)	3783.2
Glycine	Carl Roth GmbH	Karlsruhe (GER)	3908.2
Guanidin- hydrochlorid	Carl Roth GmbH	Karlsruhe (GER)	0037.7
HEPES	Sigma-Aldrich GmbH	München (GER)	H4034-100G/ H3375-1KG
Hydrochloric acid (37%, 1M)	Carl Roth GmbH	Karlsruhe (GER)	4625.2
Hydrochloric acid 1N	Carl Roth GmbH	Karlsruhe (GER)	K025.1
Hydrochloric acid 6N	Carl Roth GmbH	Karlsruhe (GER)	0281.1
IPTG (Isopropyl β-D-1-thiogalactopyranoside)	Carl Roth GmbH	Karlsruhe (GER)	2316.5
Isopropanol	Sigma-Aldrich GmbH	München (GER)	33539-2.5-GL-R
Kanamycin Sulfate	Carl Roth GmbH	Karlsruhe (GER)	T832.3
KAPAHiFi PCR Kit	peqLab		07-KK2100-02
L- Arginin	Carl Roth GmbH	Karlsruhe (GER)	3144.2
Lamda DNA/Pstl Marker	ThermoScientific	Waltham, Massachusetts (USA)	SM0361
L-Cysteine hydrochloride	Roth		3468.1
L-Glutathione oxidized (GSSG)	Sigma-Aldrich GmbH	München (GER)	G4376-10G
L-Glutathione reduced (GSH)	Sigma-Aldrich GmbH	München (GER)	G4251-50G
Lithium chloride (LiCl)	Carl Roth GmbH	Karlsruhe (GER)	P007.2
Magnesium chloride hexahydrate	Carl Roth GmbH	Karlsruhe (GER)	HN03.1
Methanol	Sigma-Aldrich GmbH	München (GER)	32213-2.5L
Milk powder	Carl Roth GmbH	Karlsruhe (GER)	T145.1/ T145.3
Monosodium phosphate (NaH2PO4)	Carl Roth GmbH	Karlsruhe (GER)	T879.2
NdeI	ThermoFisher Scientific	Waltham, Massachusetts (USA)	ER0581
NeutrAvidin Agarose beads	Thermoscientific	Waltham, Massachusetts (USA)	29201
NHS-activated Texas Red	Lifetechnologies		T6134
NovaBlue cells	Novagen		
P- Nitrophenyl phosphate Disodium HexaHyd	Sigma-Aldrich GmbH	München (GER)	N4645-1G
PEG4-carboxamide-6-Azidohexanyl-Biotin	Lifetechnologies		B10184
Penicillin/Streptomycin 100x	PAA	Cölbe (GER)	P11-010
Pierce™ BCA Protein Assay Kit	ThermoFisher Scientific	Waltham, Massachusetts	23227

		(USA)	
p-nitro-phenyl-phosphate	Sigma-Aldrich GmbH	München (GER)	N4645-5G
Potassium chloride (KCl)	Sigma-Aldrich GmbH	München (GER)	P9333-1KG
Potassium dihydrogen phosphate ($H_2 KO_4 P$)	Sigma-Aldrich GmbH	München (GER)	04248-5KG
potassium phosphate dibasic (K2HPO4)	Sigma-Aldrich GmbH	München (GER)	60230-5KG
Propargyl Alkohol	Sigma-Aldrich GmbH	München (GER)	P50803-100ml
ProSieve QuadColor Protein Marker	Biozym		830537
Protein marker	Lonza		00193837
QIAGEN Plasmid MAXI Kit	QIAGEN	Hilden (GER)	12163
Qiagen Plasmid Maxi Kit	Qiagen	Hilden (GER)	12163
Qiaquick Gel Extraction Kit	Qiagen	Hilden (GER)	28704
QIAquick PCR Purification Kit	Qiagen	Hilden (GER)	28104
Silver nitrate	Merck		1.015.120.025
Sodium acetate	Sigma-Aldrich GmbH	München (GER)	S2889-1KG
Sodium carbonate (Na_2CO_3)	Carl Roth GmbH	Karlsruhe (GER)	A135.1
Sodium chloride	Sigma-Aldrich GmbH	München (GER)	S7653-5KG
Sodium Dodecyl sulfat (SDS)	Carl Roth GmbH	Karlsruhe (GER)	CN30.3
Sodium hydroxide solution (NaOH)	Carl Roth GmbH	Karlsruhe (GER)	KK71.1
Sodium hydroxide solution (NaOH)	Merck		1.09137.1000
Sodium thiosulfate pentahydrate ($Na_2S_2O_3$)	Merck		1.06516.0500
Streptavidin- Alexa Fluor® 488 Conjugate	lifetechnologies	Darmstadt (GER)	S-32354
T4 DNA Ligase	ThermoScientific	Waltham, Massachusetts (USA)	EL0011
T4- Polynucleotide Kinase 10U/µl	ThermoScientific	Waltham, Massachusetts (USA)	EK0031
TCEP	Sigma-Aldrich GmbH	München (GER)	C4706-2G
TEMED	Carl Roth GmbH	Karlsruhe (GER)	2367.2
tert.-Butanol	Carl Roth GmbH	Karlsruhe (GER)	AE16.2
THPTA	Baseclick	München (GER)	BCMI-006-100
Trichloroacetic acid (TCA)	AppliChem		A1431.0250
Triton-X 100	Sigma-Aldrich GmbH	München (GER)	X100-1L

Trizma Base (Tris(hydroxymethyl)-aminomethan)	Sigma-Aldrich GmbH	München (GER)	T6066-5KG
Trypan blue	Sigma-Aldrich GmbH	München (GER)	T8154-100ML
Trypsin (10x)	Invitrogen GmbH	Darmstadt (GER)	15400-054
Trypton/ Pepton aus Casein	Carl Roth GmbH	Karlsruhe (GER)	8952.2
Tween® 20	Sigma-Aldrich GmbH	München (GER)	P7949-500ml
UltraLink ioodoacetyl resin beads	ThermoScientific	Waltham, Massachusetts (USA)	53155
Urea	Sigma-Aldrich GmbH	München (GER)	U0631-5KG
Wizard ® Plus SV Minipreps	Promega	Mannheim (GER)	A1460
Wizard® SV Gel and PCR Clean-Up System	Promega	Mannheim (GER)	A9282
Yeast extract	Roth/ Applichem		A1552.1000/ 2363.5/ 2363.2
Zinc chloride	Sigma-Aldrich GmbH	München (GER)	208086-100G
β-mercaptoethanol	Carl Roth GmbH	Karlsruhe (GER)	4227.1

References

1. M. Doblaré, J. M. García, M. J. Gómez, Modelling bone tissue fracture and healing: a review, *Engineering Fracture Mechanics*. **71**, 1809–1840 (2004), doi:10.1016/j.engfracmech.2003.08.003.

2. T. C. Lee, A. Staines, D. Taylor, Bone adaptation to load: microdamage as a stimulus for bone remodelling, *Journal of anatomy*. **201**, 437–446 (2002).

3. N. A. Sims, J. H. Gooi, Bone remodeling: Multiple cellular interactions required for coupling of bone formation and resorption, *Seminars in cell & developmental biology*. **19**, 444–451 (2008), doi:10.1016/j.semcdb.2008.07.016.

4. K. Matsuo, N. Irie, Osteoclast-osteoblast communication, *Archives of biochemistry and biophysics*. **473**, 201–209 (2008), doi:10.1016/j.abb.2008.03.027.

5. P. P. Spicer *et al.,* Evaluation of bone regeneration using the rat critical size calvarial defect, *Nature protocols*. **7**, 1918–1929 (2012), doi:10.1038/nprot.2012.113.

6. D. W. Sanders *et al.,* Critical-sized defect in the tibia: is it critical? Results from the SPRINT trial, *Journal of orthopaedic trauma*. **28**, 632–635 (2014), doi:10.1097/BOT.0000000000000194.

7. Y. H. An, R. J. Friedman, *Animal models in orthopaedic research* (CRC Press, Boca Raton, 1999).

8. J. S. Harris, T. B. Bemenderfer, A. R. Wessel, M. A. Kacena, A review of mouse critical size defect models in weight bearing bones, *Bone*. **55**, 241–247 (2013), doi:10.1016/j.bone.2013.02.002.

9. J. P. Schmitz, J. O. Hollinger, The critical size defect as an experimental model for craniomandibulofacial nonunions, *Clinical orthopaedics and related research*, 299–308 (1986).

10. A. S. Brydone, D. Meek, S. Maclaine, Bone grafting, orthopaedic biomaterials, and the clinical need for bone engineering, *Proceedings of the Institution of Mechanical Engineers, Part H: Journal of Engineering in Medicine*. **224**, 1329–1343 (2010), doi:10.1243/09544119JEIM770.

11. G. M. Calori, E. Mazza, M. Colombo, C. Ripamonti, The use of bone-graft substitutes in large bone defects: Any specific needs?, *Injury*. **42**, S56-S63 (2011), doi:10.1016/j.injury.2011.06.011.

12. H. C. Pape, A. Evans, P. Kobbe, Autologous Bone Graft: Properties and Techniques, *Journal of orthopaedic trauma*. **24**, S36-S40 (2010), doi:10.1097/BOT.0b013e3181cec4a1.

13. T. Blair, *Biomedical textiles for orthopaedic and surgical applications*, *Fundamentals, applications and tissue engineering* .

14. *Allograft vs.Xenograft*, *Practical Considerations for Biologic Scaffolds* (A CME home-study activity, 2008-2011).

15. M. R. Urist, Bone: formation by autoinduction, *Science (New York, N.Y.)*. **150**, 893–899 (1965).

16. W.-C. Liu *et al.,* The effects of 3D bioactive glass scaffolds and BMP-2 on bone formation in rat femoral critical size defects and adjacent bones, *Biomedical materials (Bristol, England).* **9**, 45013 (2014), doi:10.1088/1748-6041/9/4/045013.

17. B. H. Woo *et al.,* Enhancement of bone growth by sustained delivery of recombinant human bone morphogenetic protein-2 in a polymeric matrix, *Pharmaceutical research*. **18**, 1747–1753 (2001).

18. T. Mao *et al.,* An experimental study on rhBMP-2 composite bone substitute for repairing craniomaxillary bone defects, *The Chinese journal of dental research : the official journal of the Scientific Section of the Chinese Stomatological Association (CSA)*. **1**, 21–25 (1998).

19. K. Miyazono, S. Maeda, T. Imamura, BMP receptor signaling: transcriptional targets, regulation of signals, and signaling cross-talk, *Cytokine & growth factor reviews*. **16**, 251–263 (2005), doi:10.1016/j.cytogfr.2005.01.009.

20. H. Cheng *et al.,* Osteogenic activity of the fourteen types of human bone morphogenetic proteins (BMPs), *The Journal of bone and joint surgery. American volume*. **85-A**, 1544–1552 (2003).

21. K. Tsuji *et al.,* BMP2 activity, although dispensable for bone formation, is required for the initiation of fracture healing, *Nature genetics*. **38**, 1424–1429 (2006), doi:10.1038/ng1916.

22. A. Hayrapetyan, J. A. Jansen, van den Beucken, Jeroen J J P, Signaling pathways involved in osteogenesis and their application for bone regenerative medicine, *Tissue engineering. Part B, Reviews*. **21**, 75–87 (2015), doi:10.1089/ten.teb.2014.0119.

23. S. L. Cheng *et al.,* In vitro and in vivo induction of bone formation using a recombinant adenoviral vector carrying the human BMP-2 gene, *Calcified tissue international*. **68**, 87–94 (2001).

24. M. S. Rahman, N. Akhtar, H. M. Jamil, R. S. Banik, S. M. Asaduzzaman, TGF-β/BMP signaling and other molecular events: regulation of osteoblastogenesis and bone formation, *Bone research*. **3**, 15005 (2015), doi:10.1038/boneres.2015.5.

25. G. P. Allendorph, W. W. Vale, S. Choe, Structure of the ternary signaling complex of a TGF-beta superfamily member, *Proceedings of the National Academy of Sciences of the United States of America*. **103**, 7643–7648 (2006), doi:10.1073/pnas.0602558103.

26. C. Sieber, J. Kopf, C. Hiepen, P. Knaus, Recent advances in BMP receptor signaling, *Cytokine & growth factor reviews*. **20**, 343–355 (2009), doi:10.1016/j.cytogfr.2009.10.007.

27. L. Gilboa *et al.,* Bone morphogenetic protein receptor complexes on the surface of live cells: a new oligomerization mode for serine/threonine kinase receptors, *Molecular biology of the cell*. **11**, 1023–1035 (2000).

28. A. Nohe *et al.,* The mode of bone morphogenetic protein (BMP) receptor oligomerization determines different BMP-2 signaling pathways, *The Journal of biological chemistry*. **277**, 5330–5338 (2002), doi:10.1074/jbc.M102750200.

29. T. D. Mueller, J. Nickel, Promiscuity and specificity in BMP receptor activation, *FEBS letters*. **586**, 1846–1859 (2012), doi:10.1016/j.febslet.2012.02.043.

30. A. W. Yasko *et al.,* The healing of segmental bone defects, induced by recombinant human bone morphogenetic protein (rhBMP-2). A radiographic, histological, and biomechanical study in rats, *The Journal of bone and joint surgery. American volume*. **74**, 659–670 (1992).

31. M. Bostrom *et al.,* Use of bone morphogenetic protein-2 in the rabbit ulnar nonunion model, *Clinical orthopaedics and related research*, 272–282 (1996).

32. J. O. Hollinger *et al.,* Recombinant human bone morphogenetic protein-2 and collagen for bone regeneration, *Journal of biomedical materials research*. **43**, 356–364 (1998).

33. S. S. Lee *et al.,* Bone regeneration with low dose BMP-2 amplified by biomimetic supramolecular nanofibers within collagen scaffolds, *Biomaterials*. **34**, 452–459 (2013), doi:10.1016/j.biomaterials.2012.10.005.

34. A. G. Zabka *et al.,* Histomorphometric description of allograft bone remodeling and union in a canine segmental femoral defect model: a comparison of rhBMP-2, cancellous bone graft, and absorbable collagen sponge, *Journal of orthopaedic research : official publication of the Orthopaedic Research Society*. **19**, 318–327 (2001), doi:10.1016/S0736-0266(00)90003-2.

35. I. Hirata, Y. Nomura, M. Ito, A. Shimazu, M. Okazaki, Acceleration of bone formation with BMP2 in frame-reinforced carbonate apatite-collagen sponge scaffolds, *Journal of artificial organs : the official journal of the Japanese Society for Artificial Organs*. **10**, 212–217 (2007), doi:10.1007/s10047-007-0391-2.

36. M. F. Sciadini, K. D. Johnson, Evaluation of recombinant human bone morphogenetic protein-2 as a bone-graft substitute in a canine segmental defect model, *Journal of orthopaedic research : official publication of the Orthopaedic Research Society*. **18**, 289–302 (2000), doi:10.1002/jor.1100180218.

37. C. Ferretti, U. Ripamonti, Human segmental mandibular defects treated with naturally derived bone morphogenetic proteins, *The Journal of craniofacial surgery*. **13**, 434–444 (2002).

38. European Medicines Agency, *Inductos* (21/10/2005).

39. *Medtronic Infuse Bone Graft Reimbursement Guide* .

40. M. M. Shah, M. D. Smyth, A. S. Woo, Adverse facial edema associated with off-label use of recombinant human bone morphogenetic protein-2 in cranial reconstruction for craniosynostosis. Case report, *Journal of neurosurgery. Pediatrics*. **1**, 255–257 (2008), doi:10.3171/PED/2008/1/3/255.

41. B. Perri, M. Cooper, C. Lauryssen, N. Anand, Adverse swelling associated with use of rh-BMP-2 in anterior cervical discectomy and fusion: a case study, *The spine journal : official journal of the North American Spine Society*. **7**, 235–239 (2007), doi:10.1016/j.spinee.2006.04.010.

42. J. D. Smucker, J. M. Rhee, K. Singh, S. T. Yoon, J. G. Heller, Increased swelling complications associated with off-label usage of rhBMP-2 in the anterior cervical spine, *Spine*. **31**, 2813–2819 (2006), doi:10.1097/01.brs.0000245863.52371.c2.

43. U.S. Department of Health and Human Services, *FDA Public Health Notification: Life-threatening Complications Associated with Recombinant Human Bone Morphogenetic Protein in Cervical Spine Fusion* (July 1, 2008).

44. T. G. Carter, P. S. Brar, A. Tolas, O. R. Beirne, Off-label use of recombinant human bone morphogenetic protein-2 (rhBMP-2) for reconstruction of mandibular bone defects in humans, *Journal of oral and maxillofacial surgery : official journal of the American Association of Oral and Maxillofacial Surgeons*. **66**, 1417–1425 (2008), doi:10.1016/j.joms.2008.01.058.

45. R. Xu *et al.,* Safety and efficacy of rhBMP2 in posterior cervical spinal fusion for subaxial degenerative spine disease: Analysis of outcomes in 204 patients, *Surgical neurology international*. **2**, 109 (2011), doi:10.4103/2152-7806.83726.

46. V. Joseph, Y. R. Rampersaud, Heterotopic bone formation with the use of rhBMP2 in posterior minimal access interbody fusion: a CT analysis, *Spine*. **32**, 2885–2890 (2007), doi:10.1097/BRS.0b013e31815b7596.

47. K. W.-H. Lo, B. D. Ulery, K. M. Ashe, C. T. Laurencin, Studies of bone morphogenetic protein-based surgical repair, *Advanced drug delivery reviews*. **64**, 1277–1291 (2012), doi:10.1016/j.addr.2012.03.014.

48. A. Sharma *et al.,* Osteoinduction by combining bone morphogenetic protein (BMP)-2 with a bioactive novel nanocomposite, *Bone & joint research*. **1**, 145–151 (2012), doi:10.1302/2046-3758.17.2000082.

49. Y. Zhao *et al.,* The osteogenic effect of bone morphogenetic protein-2 on the collagen scaffold conjugated with antibodies, *Journal of controlled release : official journal of the Controlled Release Society*. **141**, 30–37 (2010), doi:10.1016/j.jconrel.2009.06.032.

50. W. Kang, D.-S. Lee, J.-H. Jang, Evaluation of Sustained BMP-2 Release Profiles Using a Novel Fluorescence-Based Retention Assay, *PloS one*. **10**, e0123402 (2015), doi:10.1371/journal.pone.0123402.

51. N. Z. Mostafa *et al.,* Cleft palate reconstruction using collagen and nanofiber scaffold incorporating bone morphogenetic protein in rats, *Tissue engineering. Part A*. **21**, 85–95 (2015), doi:10.1089/ten.tea.2014.0075.

52. H. Autefage *et al.,* Adsorption and release of BMP-2 on nanocrystalline apatite-coated and uncoated hydroxyapatite/beta-tricalcium phosphate porous ceramics, *Journal of biomedical materials research. Part B, Applied biomaterials*. **91**, 706–715 (2009), doi:10.1002/jbm.b.31447.

53. R. Bansal, S. Patil, K. K. Chaubey, R. K. Thakur, P. Goyel, Clinical evaluation of hydroxyapatite and β-tricalcium phosphate composite graft in the treatment of intrabony periodontal defect: A clinico-radiographic study, *Journal of Indian Society of Periodontology*. **18**, 610–617 (2014), doi:10.4103/0972-124X.142455.

54. F. Poncin-Epaillard *et al.,* Surface Treatment of Polymeric Materials Controlling the Adhesion of Biomolecules, *JFB*. **3**, 528–543 (2012), doi:10.3390/jfb3030528.

55. U. Maus *et al.,* BMP-2 incorporated in a tricalcium phosphate bone substitute enhances bone remodeling in sheep, *Journal of biomaterials applications*. **22**, 559–576 (2008), doi:10.1177/0885328207083311.

56. L. Moore, M. Gatica, H. Kim, E. Osawa, D. Ho, Multi-protein Delivery by Nanodiamonds Promotes Bone Formation, *Journal of Dental Research*. **92**, 976–981 (2013), doi:10.1177/0022034513504952.

57. C. Mücksch, H. M. Urbassek, Adsorption of BMP-2 on a hydrophobic graphite surface: A molecular dynamics study, *Chemical Physics Letters*. **510**, 252–256 (2011), doi:10.1016/j.cplett.2011.05.036.

58. J. J. Patel, C. L. Flanagan, S. J. Hollister, Bone Morphogenetic Protein-2 Adsorption onto Poly-ε-caprolactone Better Preserves Bioactivity In Vitro and Produces More Bone In Vivo than Conjugation Under Clinically Relevant Loading Scenarios, *Tissue Engineering Part C: Methods*. **21**, 489–498 (2015), doi:10.1089/ten.tec.2014.0377.

59. R. D. Welch *et al.,* Effect of Recombinant Human Bone Morphogenetic Protein-2 on Fracture Healing in a Goat Tibial Fracture Model, *J Bone Miner Res*. **13**, 1483–1490 (1998), doi:10.1359/jbmr.1998.13.9.1483.

60. H. S. Yang *et al.,* Comparison between heparin-conjugated fibrin and collagen sponge as bone morphogenetic protein-2 carriers for bone regeneration, *Exp Mol Med*. **44**, 350 (2012), doi:10.3858/emm.2012.44.5.039.

61. D. Steinmüller-Nethl *et al.,* Strong binding of bioactive BMP-2 to nanocrystalline diamond by physisorption, *Biomaterials*. **27**, 4547–4556 (2006), doi:10.1016/j.biomaterials.2006.04.036.

62. F. R. Kloss *et al.,* The role of oxygen termination of nanocrystalline diamond on immobilisation of BMP-2 and subsequent bone formation, *Biomaterials*. **29**, 2433–2442 (2008), doi:10.1016/j.biomaterials.2008.01.036.

63. Y.-P. Yun *et al.,* Improving Osteogenesis Activity on BMP-2-Immobilized PCL Fibers Modified by the γ-Ray Irradiation Technique, *BioMed research international*. **2015**, 302820 (2015), doi:10.1155/2015/302820.

64. X. Yu, D. Suárez-González, A. S. Khalil, W. L. Murphy, How does the pathophysiological context influence delivery of bone growth factors?, *Advanced drug delivery reviews*. **84**, 68–84 (2015), doi:10.1016/j.addr.2014.10.010.

65. Kirby, Giles T. S. *et al.,* PLGA-Based Microparticles for the Sustained Release of BMP-2, *Polymers*. **3**, 571–586 (2011), doi:10.3390/polym3010571.

66. X. B. Yang *et al.,* Human Osteoprogenitor Bone Formation Using Encapsulated Bone Morphogenetic Protein 2 in Porous Polymer Scaffolds, *Tissue Engineering*. **10**, 1037–1045 (2004), doi:10.1089/ten.2004.10.1037.

67. Z. S. Patel, M. Yamamoto, H. Ueda, Y. Tabata, A. G. Mikos, Biodegradable gelatin microparticles as delivery systems for the controlled release of bone morphogenetic protein-2, *Acta Biomaterialia*. **4**, 1126–1138 (2008), doi:10.1016/j.actbio.2008.04.002.

68. Z. Wang *et al.,* BMP-2 encapsulated polysaccharide nanoparticle modified biphasic calcium phosphate scaffolds for bone tissue regeneration, *J. Biomed. Mater. Res.* **103**, 1520–1532 (2015), doi:10.1002/jbm.a.35282.

69. N. S. Gandhi, R. L. Mancera, Prediction of heparin binding sites in bone morphogenetic proteins (BMPs), *Biochimica et biophysica acta*. **1824**, 1374–1381 (2012), doi:10.1016/j.bbapap.2012.07.002.

70. Y.-P. Yun *et al.,* The effect of bone morphogenic protein-2 (BMP-2)-immobilizing heparinized-chitosan scaffolds for enhanced osteoblast activity, *Tissue Eng Regen Med*. **10**, 122–130 (2013), doi:10.1007/s13770-013-0386-4.

71. G. Hannink, P. J. Geutjes, W. F. Daamen, P. Buma, Evaluation of collagen/heparin coated TCP/HA granules for long-term delivery of BMP-2, *Journal of materials science. Materials in medicine*. **24**, 325–332 (2013), doi:10.1007/s10856-012-4802-4.

72. K.-H. Koo *et al.,* Controlled delivery of low-dose bone morphogenetic protein-2 using heparin-conjugated fibrin in the posterolateral lumbar fusion of rabbits, *Artificial organs*. **37**, 487–494 (2013), doi:10.1111/j.1525-1594.2012.01578.x.

73. K. H. Koo *et al.,* Lumbar posterolateral fusion using heparin-conjugated fibrin for sustained delivery of bone morphogenic protein-2 in a rabbit model, *Artificial organs*. **36**, 629–634 (2012), doi:10.1111/j.1525-1594.2012.01444.x.

74. T. Horbett, J. L. Brash, W. Norde, Eds., *Proteins at Interfaces III State of the Art 2012* (American Chemical Society, Washington, DC, 2012).

75. T.-H. Kim *et al.,* In vitro and in vivo evaluation of bone formation using solid freeform fabrication-based bone morphogenic protein-2 releasing PCL/PLGA scaffolds, *Biomedical materials (Bristol, England)*. **9**, 25008 (2014), doi:10.1088/1748-6041/9/2/025008.

76. E.-C. Kim, T.-H. Kim, J.-H. Jung, S. O. Hong, D.-W. Lee, Enhanced osteogenic differentiation of MC3T3-E1 on rhBMP-2-immobilized titanium via click reaction, *Carbohydrate polymers*. **103**, 170–178 (2014), doi:10.1016/j.carbpol.2013.12.023.

77. K. Hauff *et al.,* Matrix-Immobilized BMP-2 on Microcontact Printed Fibronectin as an in vitro Tool to Study BMP-Mediated Signaling and Cell Migration, *Frontiers in bioengineering and biotechnology*. **3**, 62 (2015), doi:10.3389/fbioe.2015.00062.

78. H. P. Jennissen, M. Laub, Development of an universal affinity fusion tag (Poly-DOPA) for immobilizing recombinant proteins on biomaterials, *Mat.-wiss. u. Werkstofftech.* **38**, 1035–1039 (2007), doi:10.1002/mawe.200700247.

79. Z. Shi, K. G. Neoh, E. T. Kang, C. K. Poh, W. Wang, Surface functionalization of titanium with carboxymethyl chitosan and immobilized bone morphogenetic protein-2 for enhanced osseointegration, *Biomacromolecules.* **10**, 1603–1611 (2009), doi:10.1021/bm900203w.

80. Y.-W. Du *et al.,* In vitro and in vivo evaluation of bone morphogenetic protein-2 (BMP-2) immobilized collagen-coated polyetheretherketone (PEEK), *Front. Mater. Sci.* **9**, 38–50 (2015), doi:10.1007/s11706-015-0276-x.

81. D. A. Puleo, R. A. Kissling, M. S. Sheu, A technique to immobilize bioactive proteins, including bone morphogenetic protein-4 (BMP-4), on titanium alloy, *Biomaterials.* **23**, 2079–2087 (2002).

82. R. Luxenhofer, R. Jordan, Click Chemistry with Poly(2-oxazoline)s, *Macromolecules.* **39**, 3509–3516 (2006), doi:10.1021/ma052515m.

83. K. Heinecke *et al.,* Receptor oligomerization and beyond: a case study in bone morphogenetic proteins, *BMC biology.* **7**, 59 (2009), doi:10.1186/1741-7007-7-59.

84. J. V. Holtje, Lysozyme substrates, *EXS.* **75**, 105–110 (1996).

85. R. Ruppert, E. Hoffmann, W. Sebald, Human bone morphogenetic protein 2 contains a heparin-binding site which modifies its biological activity, *European journal of biochemistry / FEBS.* **237**, 295–302 (1996).

86. K. K. Würzler *et al.,* Evaluation der osteoinduktiven Potenz von gentechnisch modifizierten BMP-2-Varianten, *Mund-, Kiefer- und Gesichtschirurgie : MKG.* **8**, 83–92 (2004), doi:10.1007/s10006-004-0528-x.

87. S. I. Presolski, V. P. Hong, M. G. Finn, Copper-Catalyzed Azide-Alkyne Click Chemistry for Bioconjugation, *Current protocols in chemical biology.* **3**, 153–162 (2011), doi:10.1002/9780470559277.ch110148.

88. T. Kirsch, J. Nickel, W. Sebald, BMP-2 antagonists emerge from alterations in the low-affinity binding epitope for receptor BMPR-II, *The EMBO journal.* **19**, 3314–3324 (2000), doi:10.1093/emboj/19.13.3314.

89. L. Polo-Corrales, M. Latorre-Esteves, J. E. Ramirez-Vick, Scaffold design for bone regeneration, *Journal of nanoscience and nanotechnology.* **14**, 15–56 (2014).

90. M. Bohner, Calcium orthophosphates in medicine: from ceramics to calcium phosphate cements, *Injury.* **31 Suppl 4**, 37–47 (2000).

91. H. S. Byrd, P. C. Hobar, K. Shewmake, Augmentation of the craniofacial skeleton with porous hydroxyapatite granules, *Plastic and reconstructive surgery*. **91**, 15-22; discussion 23-6 (1993).

92. R. R. Bos *et al.,* Degradation of and tissue reaction to biodegradable poly(L-lactide) for use as internal fixation of fractures: a study in rats, *Biomaterials*. **12**, 32–36 (1991).

93. E. R. Balmayor, M. van Griensven, Gene therapy for bone engineering, *Frontiers in bioengineering and biotechnology*. **3**, 9 (2015), doi:10.3389/fbioe.2015.00009.

94. K. A. Partridge, Oreffo, Richard O C, Gene delivery in bone tissue engineering: progress and prospects using viral and nonviral strategies, *Tissue Engineering*. **10**, 295–307 (2004), doi:10.1089/107632704322791934.

95. J. Shao, W. Zhang, T. Yang, Using mesenchymal stem cells as a therapy for bone regeneration and repairing, *Biological research*. **48**, 62 (2015), doi:10.1186/s40659-015-0053-4.

96. K. Hayashi *et al.,* Transplantation of human-induced pluripotent stem cells carried by self-assembling peptide nanofiber hydrogel improves bone regeneration in rat calvarial bone defects, *BDJ Open*. **2**, 15007 (2016), doi:10.1038/bdjopen.2015.7.

97. X. Sun *et al.,* Modeling vascularized bone regeneration within a porous biodegradable CaP scaffold loaded with growth factors, *Biomaterials*. **34**, 4971–4981 (2013), doi:10.1016/j.biomaterials.2013.03.015.

98. W. Zhang *et al.,* Porous silk scaffolds for delivery of growth factors and stem cells to enhance bone regeneration, *PloS one*. **9**, e102371 (2014), doi:10.1371/journal.pone.0102371.

99. K. L. Ong *et al.,* Off-label use of bone morphogenetic proteins in the United States using administrative data, *Spine*. **35**, 1794–1800 (2010), doi:10.1097/BRS.0b013e3181ecf6e4.

100. Center for Devices and Radiological Health Food and Drug Administration, *FDA letter to Healthcare Practitioners* (July 1, 2008).

101. Z. S. Haidar, R. C. Hamdy, M. Tabrizian, Delivery of recombinant bone morphogenetic proteins for bone regeneration and repair. Part A: Current challenges in BMP delivery, *Biotechnology letters*. **31**, 1817–1824 (2009), doi:10.1007/s10529-009-0099-x.

102. Wyeth Pharmaceuticals, *SUMMARY OF SAFETY AND EFFECTIVENESS DATA; INFUSE® Bone Graft; Premarket Approval Application (PMA) Number: P000054* (Date of Panel Rec6mmendation: November 21, 2002; Date of Notice of Approval to Applicant: April30, 2004)).

103. K. Minier *et al.,* BMP-2 delivered from a self-crosslinkable CaP/hydrogel construct promotes bone regeneration in a critical-size segmental defect model of non-union in dogs, *Veterinary and comparative orthopaedics and traumatology : V.C.O.T*. **27**, 411–421 (2014), doi:10.3415/VCOT-14-03-0036.

104. L. B. Priddy *et al.,* Oxidized alginate hydrogels for bone morphogenetic protein-2 delivery in long bone defects, *Acta Biomaterialia*. **10**, 4390–4399 (2014), doi:10.1016/j.actbio.2014.06.015.

105. M. Kisiel *et al.,* Improving the osteogenic potential of BMP-2 with hyaluronic acid hydrogel modified with integrin-specific fibronectin fragment, *Biomaterials*. **34**, 704–712 (2013), doi:10.1016/j.biomaterials.2012.10.015.

106. C. Scheufler, W. Sebald, M. Hülsmeyer, Crystal structure of human bone morphogenetic protein-2 at 2.7 A resolution, *Journal of Molecular Biology*. **287**, 103–115 (1999), doi:10.1006/jmbi.1999.2590.

107. S. D. Boden, J. Kang, H. Sandhu, J. G. Heller, Use of recombinant human bone morphogenetic protein-2 to achieve posterolateral lumbar spine fusion in humans: a prospective, randomized clinical pilot trial: 2002 Volvo Award in clinical studies, *Spine*. **27**, 2662–2673 (2002), doi:10.1097/01.BRS.0000035320.82533.06.

108. T. Smoljanović *et al.,* Regeneration of the skeleton by recombinant human bone morphogenetic proteins, *Collegium antropologicum*. **31**, 923–932 (2007).

109. S. D. Boden, G. J. Martin, W. C. Horton, T. L. Truss, H. S. Sandhu, Laparoscopic anterior spinal arthrodesis with rhBMP-2 in a titanium interbody threaded cage, *Journal of spinal disorders*. **11**, 95–101 (1998).

110. H. S. Sandhu *et al.,* Histologic evaluation of the efficacy of rhBMP-2 compared with autograft bone in sheep spinal anterior interbody fusion, *Spine*. **27**, 567–575 (2002).

111. E. H. Schwab *et al.,* Nanoscale control of surface immobilized BMP-2: toward a quantitative assessment of BMP-mediated signaling events, *Nano letters*. **15**, 1526–1534 (2015), doi:10.1021/acs.nanolett.5b00315.

112. F. Rusmini, Z. Zhong, J. Feijen, Protein immobilization strategies for protein biochips, *Biomacromolecules*. **8**, 1775–1789 (2007), doi:10.1021/bm061197b.

113. G. Bhakta *et al.,* The influence of collagen and hyaluronan matrices on the delivery and bioactivity of bone morphogenetic protein-2 and ectopic bone formation, *Acta Biomaterialia*. **9**, 9098–9106 (2013), doi:10.1016/j.actbio.2013.07.008.

114. K. V. Brown *et al.,* Improving bone formation in a rat femur segmental defect by controlling bone morphogenetic protein-2 release, *Tissue engineering. Part A*. **17**, 1735–1746 (2011), doi:10.1089/ten.tea.2010.0446.

115. S. Eger, M. Scheffner, A. Marx, M. Rubini, Formation of ubiquitin dimers via azide-alkyne click reaction, *Methods in molecular biology (Clifton, N.J.)*. **832**, 589–596 (2012), doi:10.1007/978-1-61779-474-2_41.

116. T. Fekner, X. Li, M. K. Chan, Pyrrolysine Analogs for Translational Incorporation into Proteins, *Eur. J. Org. Chem.* **2010**, 4171–4179 (2010), doi:10.1002/ejoc.201000204.

117. D. P. Nguyen *et al.,* Genetic encoding and labeling of aliphatic azides and alkynes in recombinant proteins via a pyrrolysyl-tRNA Synthetase/tRNA(CUA) pair and click chemistry, *Journal of the American Chemical Society*. **131**, 8720–8721 (2009), doi:10.1021/ja900553w.

118. A. Deiters, T. A. Cropp, D. Summerer, M. Mukherji, P. G. Schultz, Site-specific PEGylation of proteins containing unnatural amino acids, *Bioorganic & medicinal chemistry letters*. **14**, 5743–5745 (2004), doi:10.1016/j.bmcl.2004.09.059.

119. Y. Ryu, P. G. Schultz, Efficient incorporation of unnatural amino acids into proteins in Escherichia coli, *Nature methods*. **3**, 263–265 (2006), doi:10.1038/nmeth864.

120. T. Lühmann *et al.,* Bio-orthogonal Immobilization of Fibroblast Growth Factor 2 for Spatial Controlled Cell Proliferation, *ACS Biomater. Sci. Eng.* **1**, 740–746 (2015), doi:10.1021/acsbiomaterials.5b00236.

121. E. F. GALE, The assimilation of amino-acids by bacteria; the passage of certain amino-acids across the cell wall and their concentration in the internal environment of Streptococcus faecalis, *Journal of general microbiology*. **1**, 53–76 (1947), doi:10.1099/00221287-1-1-53.

122. T. Katagiri *et al.,* Bone morphogenetic protein-2 converts the differentiation pathway of C2C12 myoblasts into the osteoblast lineage, *The Journal of cell biology*. **127**, 1755–1766 (1994).

123. T. Kirsch, J. Nickel, W. Sebald, Isolation of recombinant BMP receptor IA ectodomain and its 2:1 complex with BMP-2, *FEBS letters*. **468**, 215–219 (2000).

124. J. E. Hein, V. V. Fokin, Copper-catalyzed azide-alkyne cycloaddition (CuAAC) and beyond: new reactivity of copper(I) acetylides, *Chemical Society reviews*. **39**, 1302–1315 (2010), doi:10.1039/b904091a.

125. S. Chang, S. H. Lamm, Human Health Effects of Sodium Azide Exposure: A Literature Review and Analysis, *International Journal of Toxicology*. **22**, 175–186 (2003), doi:10.1080/10915810305109.

126. J. A. Prescher, C. R. Bertozzi, Chemistry in living systems, *Nature chemical biology*. **1**, 13–21 (2005), doi:10.1038/nchembio0605-13.

127. Ahmad Fuaad, Abdullah A H, F. Azmi, M. Skwarczynski, I. Toth, Peptide conjugation via CuAAC 'click' chemistry, *Molecules (Basel, Switzerland)*. **18**, 13148–13174 (2013), doi:10.3390/molecules181113148.

128. N. M. Green, Avidin, *Advances in protein chemistry*. **29**, 85–133 (1975).

129. H. Alborzinia *et al.,* Quantitative kinetics analysis of BMP2 uptake into cells and its modulation by BMP antagonists, *Journal of cell science*. **126**, 117–127 (2013), doi:10.1242/jcs.109777.

130. Pohl, Theresa L M, J. H. Boergermann, G. K. Schwaerzer, P. Knaus, E. A. Cavalcanti-Adam, Surface immobilization of bone morphogenetic protein 2 via a self-assembled monolayer formation induces cell differentiation, *Acta Biomaterialia*. **8**, 772–780 (2012), doi:10.1016/j.actbio.2011.10.019.

131. H. Zhang, F. Migneco, C.-Y. Lin, S. J. Hollister, Chemically-conjugated bone morphogenetic protein-2 on three-dimensional polycaprolactone scaffolds stimulates osteogenic activity in bone marrow stromal cells, *Tissue engineering. Part A*. **16**, 3441–3448 (2010), doi:10.1089/ten.TEA.2010.0132.

132. H.-W. Liu, C.-H. Chen, C.-L. Tsai, I.-H. Lin, G.-H. Hsiue, Heterobifunctional poly(ethylene glycol)-tethered bone morphogenetic protein-2-stimulated bone marrow mesenchymal stromal cell differentiation and osteogenesis, *Tissue Engineering*. **13**, 1113–1124 (2007), doi:10.1089/ten.2006.0209.

133. J. E. Leslie-Barbick, J. E. Saik, D. J. Gould, M. E. Dickinson, J. L. West, The promotion of microvasculature formation in poly(ethylene glycol) diacrylate hydrogels by an immobilized VEGF-mimetic peptide, *Biomaterials*. **32**, 5782–5789 (2011), doi:10.1016/j.biomaterials.2011.04.060.

134. L. Wang *et al.,* "Click" immobilization of a VEGF-mimetic peptide on decellularized endothelial extracellular matrix to enhance angiogenesis, *ACS applied materials & interfaces*. **6**, 8401–8406 (2014), doi:10.1021/am501309d.

135. P. R. Kuhl, L. G. Griffith-Cima, Tethered epidermal growth factor as a paradigm for growth factor–induced stimulation from the solid phase, *Nat Med*. **2**, 1022–1027 (1996), doi:10.1038/nm0996-1022.

Acknowledgments

Affidavit

I hereby confirm that my thesis entitled 'Site-specific immobilization of BMP-2 as a tool for improved regeneration of bone defects' is the result of my own work. I did not receive any help or support from commercial consultants. All sources and materials applied are listed and specified in the thesis.

Furthermore, I confirm that this thesis has not yet been submitted as part of another examination process neither in identical nor in similar form.

Place, Date   Signature

Hiermit erkläre ich an Eides statt, die Dissertation 'Gerichtete Immobilisierung von BMP-2: Zwei Ansätze zur Herstellung osteogener Trägerstrukturen' eigenständig, d.h. insbesondere selbständig und ohne Hilfe eines kommerziellen Promotionsberaters, angefertigt und keine anderen als die von mir angegebenen Quellen und Hilfsmittel verwendet zu haben.

Ich erkläre außerdem, dass die Dissertation weder in gleicher noch in ähnlicher Form bereits in einem anderen Prüfungsverfahren vorgelegen hat.

Ort, Datum   Unterschrift

This work has been presented at the following conferences:

International Bone & Mineral Society (IBMS) conference - 2nd Herbert Fleisch Workshop (28.02 – 1.03.2016, Brugge)

Strategies in Tissue Engineering (WITE) (10-12.06.2015, Wuerzburg)

Eureka (9th International Symposium Organized by the Students of the GSLS) (14-15.10.2014, Wuerzburg)

10th International BMP Conference (16-20.09.2014, Berlin)

Cells, Proteins and Bioprocessing (17-19.06.2014, London)